DESIGN, CONSTRUCTION AND OPTIMIZATION STUDIES OF A HYDRIDE GENERATION LASER-INDUCED BREAKDOWN SPECTROMETRIC SYSTEM, (HG-LIBS), FOR THE DETERMINATION OF TOXIC ELEMENTS IN AQUEOUS SAMPLES

A Thesis Submitted to
the Graduate School of Engineering and Sciences of
İzmir Institute of Technology
in Partial Fulfillment of the Requirements of the Degree of

DOCTOR OF PHILOSOPHY

in Chemistry

by
Semira ÜNAL YEŞİLLER

May 2013
İZMİR

We approve the thesis of **Semira ÜNAL YEŞİLLER**

Examining Committee Members:

_____
Prof. Dr. Emür HENDEN
Department of Chemistry, Ege University

_____
Prof. Dr. Doğan ABUKAY
Department of Physics, İzmir Institute of Technology

_____
Prof. Dr. Kadriye ERTEKİN
Department of Chemistry, Dokuz Eylül University

_____
Prof. Dr. Durmuş ÖZDEMİR
Department of Chemistry, İzmir Institute of Technology

_____
Prof. Dr. Şerife H. YALÇIN
Department of Chemistry, İzmir Institute of Technology

28 May 2013

_____
Prof. Dr. Şerife H. YALÇIN
Supervisor, Department of Chemistry
İzmir Institute of Technology

_____   _____
Prof. Dr. Durmuş ÖZDEMİR   **Prof. Dr. R. Tuğrul SENGER**
Head of the Department of Chemistry   Dean of the Graduate School of
                                                       Engineering and Sciences

ACKNOWLEDGEMENTS

mates Nadir ARAS and Deniz BÖLEK, also to my former lab mate Dilek ARICA ATEŞ for their friendship and support.

Last, but by no means least, I ought to thank to my family: my parents Hatice and Selman ÜNAL, my brothers: Ali and Besim ÜNAL, my sister-in-law Özlem ÜNAL, my sister Bedia ÜNAL and my husband Gürcan YEŞİLLER, for their deepest love, invaluable patience, understanding, support and encouragements all throughout my life. No words can express, no act of gratitude can relay, no gift can represent what your love and support have meant to me.

ABSTRACT

DESIGN, CONSTRUCTION AND OPTIMIZATION STUDIES OF A HYDRIDE GENERATION LASER-INDUCED BREAKDOWN SPECTROMETRIC SYSTEM, (HG-LIBS), FOR THE DETERMINATION OF TOXIC ELEMENTS IN AQUEOUS SAMPLES

In this thesis study, design, construction and optimization of a continuous flow *hydride generation laser-induced breakdown spectroscopic system, HG-LIBS*, for the determination toxic and environmentally important elements: arsenic, selenium, lead, antimony, tin, bismuth, germanium and tellurium, has been performed.

The HG-LIBS system, which has been constructed from its commercially available components, consisted of four main parts: a laser source, a hydride generation unit, a sample/plasma cell and a detection unit. In order to maximize LIBS emission signal, some instrumental parameters such as laser energy and detector gating parameters were investigated. Some chemical parameters such as acid/reductant concentration and flow rate, carrier gas type and flow rate, presence of pre-reducing/oxidizing agent that effect hydride generation efficiency and transportation of hydrides were also studied.

Under optimized conditions detection limits of 0.2 mg L^{-1}, 1.1 mg L^{-1}, 1.0 mg L^{-1}, 1.3 mg L^{-1} and 0.2 mg L^{-1} were obtained for Sn, As, Sb, Pb and Ge, respectively. No analytical signal could be detected from Se and Te elements with the system developed. The applicability of the HG-LIBS system for the determination of As, Sb, Pb and Ge in aqueous environments has been tested on several real water samples including tap water, drinking water and reference river water standard.

Temporal variation of electron temperature and electron density values for tin and germanium hydride plasma was determined under argon and nitrogen environment. Electron temperatures were calculated by making use of neutral atomic lines in Boltzmann equation. Plasma electron density was evaluated from the Stark-broadened line shapes of H_α line at 656.3 nm. In order to investigate the main cause of increase in germanium signal under argon environment, physical plasma parameters were evaluated in argon and nitrogen gas mixtures.

With this thesis study, the applicability of the HG-LIBS system for on-line monitoring of environmental pollutants has been shown.

ÖZET

SULU ORTAMLARDA BULUNAN ZEHİRLİ ELEMENTLERİN TAYİNİ İÇİN BİR HİDRÜR OLUŞTURMALI LAZER PLAZMA SPEKTROSKOPİSİNİN, (HG-LIBS), TASARIM, KURULUM VE OPTİMİZASYON ÇALIŞMALARI

Bu çalışmada arsenik, selenyum, kurşun, antimon, bizmut, germanyum, tellür ve kalay gibi zehirli ve çevresel önem taşıyan elementlerin tayini için bir *Hidrür Oluşturmalı-Lazer Plazma Spektroskopi, (HG-LIBS),* sisteminin tasarım, kurulum ve optimizasyon çalışmaları gerçekleştirilmiştir.

Sistem lazer kaynağı, hidrür oluşturma ünitesi, örnek/plazma hücresi ve detektörden oluşmaktadır. Hidrür oluşturma ünitesi, peristaltik pompa, gaz-sıvı ayırıcı ve membran kurutucu parçalarından oluşturulmuştur. LIBS emisyon sinyalini optimize etmek amacı ile lazer enerjisi, detektör zamanlama parametreleri gibi bazı enstrümental parametreler incelenmiştir. Bunun yanı sıra hidrür bileşiklerinin oluşumunu ve plazma hücresine etkin bir şekilde taşınmasını etkileyen asit ve indirgen derişimi ve hızı, taşıyıcı gaz çeşidi ve hızı, ön-indirgen/yükseltgen madde varlığı gibi bazı kimyasal koşullar da sistematik bir şekilde incelenmiştir.

Optimum koşullar altında Sn, As, Sb, Pb ve Ge için kalibrasyon grafikleri oluşturulmuş ve gözlenebilirlik sınırları sırasıyla 0,2 mg L^{-1}, 1,1 mg L^{-1}, 1,0 mg L^{-1}, 1,3 mg L^{-1} ve 0,2 mg L^{-1} olarak belirlenmiştir. Çalışılan koşullarda, Se ve Te elementlerinden HG-LIBS sinyali gözlenememiştir. Metodun gerçek sularda uygulanabilirliği referans nehir suyu, içme suyu ve çeşme suyu kullanılarak dışarıdan katım yöntemiyle test edilmiştir.

Ayrıca, kalay ve germanyum hidrür plazmaların sıcaklık ve elektron yoğunluğu gibi bazı fiziksel parametreleri azot ve argon atmosferi altında irdelenmiştir. Germanyum plazmanın fiziksel parametrelerindeki değişim değişik oranlarda karıştırılan azot ve argon gazları varlığında irdelenmiş ve germanyum sinyalinin argon varlığında artış göstermesinin sebepleri tartışılmıştır.

Bu tez çalışması ile HG-LIBS sisteminin çevresel öneme sahip toksik elementlerden doğan kirliliğin yerinde izlenmesi için taşınabilir LIBS sensörleri geliştirilmesine uygunluğu gösterilmiştir.

Dedicated to:

"Assist. Prof. Dr. Ritchie C. EANES"

TABLE OF CONTENTS

LIST OF FIGURES

LIST OF TABLES

LIST OF ABBREVIATIONS AND SYMBOLS

LIBS	Laser-Induced Breakdown Spectroscopy
HG	Hydride Generation
ICCD	Intensified Charge Coupled Detector
Nd:YAG	Neodymium-Yttrium Aluminum Garnet
GLS	Gas-liquid Separator
MDU	Membrane Drying Unit
PMT	Photomultiplier Tube
NIST	National Institute of Standards and Technology
LE	Laser Energy
LTE	Local Thermodynamic Equilibrium
Ne	Number of Electron Density
T	Electron Temperature
$NaBH_4$	Sodium borohydride
HCl	Hydrochloric acid
LOD	Limit of Detection
DL	Detection Limit
SD	Standard Deviation
RSD	Relative Standard Deviation
S/N	Signal-to-Noise Ratio
BG	Background
FWHM	Full Width at Half Maximum
OD	Outer Diameter
i.d	Inner Diameter
rpm	revolution per minute
ppb	parts per billion
ppm	parts per million
t_d	Delay time
t_g	Gate width
SnH_4	Stannane
AsH_3	Arsine
SbH_3	Stibine

PbH_4	Plumbane
GeH_4	Germane
BiH_3	Bismuthine
H_2Se	Selenium hydride
H_2Te	Tellurium hydride
λ	Wavelength
Hz	Hertz
μs	microsecond
μm	micrometer
mJ	milli-Joule
nm	nanometer
ns	nanosecond
K	Kelvin
k	Boltzmann constant
eV	Electron volt
MW	Mega Watt
TW	Tera Watt

CHAPTER 1

INTRODUCTION

1.1. Laser-Induced Breakdown Spectroscopy

1.1.1. General Information

Laser-induced breakdown spectroscopy, (LIBS), (Cremers and Radziemski, 2006, Miziolek *et al.,* 2006), also called laser-induced plasma spectroscopy is an optical atomic emission spectroscopy technique. LIBS technique utilizes plasma for vaporization, atomization, ionization, and excitation of a sample, similar to the techniques of inductively coupled of plasma optical emission spectroscopy (ICP-OES), direct current plasma (DCP)-OES, arc-atomic emission spectroscopy (arc-AES), spark-AES and microwave-induced plasma (MIP)-AES. However, unlike these techniques it is not required to transport the sample in to the plasma; instead plasma is formed inside or on the surface of the sample.

In LIBS technique a high powered pulse of laser is focused on the sample by means of a lens and luminous plasma is created. The light emitted by excited atomic ions and neutral atoms in plasma is collected by suitable optics and detected by a spectrograph.

LIBS has many advantages over other atomic spectrometric techniques. There is no limitation on the type of sample to be analyzed. The sample can be in the form of a solid, liquid, gas or aerosol. Whether the sample is conductive, semi conductive or insulator, it can be analyzed easily. Likewise sample preparation is minimized. A small amount of material on the orders of nanograms to femtograms is consumed. The spot size of the laser can be as small as a few micrometers and hence, it is possible to perform spatially and depth-resolved analysis with μm range of resolution. One of the main advantages is that it is a very suitable technique to be used as a portable instrument for remote analysis. However, due to the difficulty in obtaining suitable calibration standards, relatively high detection limits (high ppb - low ppm) and variation

in laser pulse energy results in low analytical performance (Cremers and Radziemski, 2006).

LIBS has been used in many fields of application including, elemental analysis (Fichet *et al.,* 2001), analysis of liquids (Samek *et al.,* 2000; Cahoon *et al.,* 2012), quality control in steel manufacturing (Barette and Turmel, 2001), characterization of jewelry products (Garcia-Ayuso *et al.,* 2002), soil investigation (Senesi *et al.,* 2009), quality control of pharmaceutical products (St-Onge *et al.,* 2009), classification and automatical separation of Al cast and wrought alloys (Werheit *et al.,* 2011), surface cleaning (Kleina *et al.,* 2000), forensic application (Dockery and Good, 2003; Taschuk , *et al.,* 2006), detection of explosives (Gottfried *et al.,* 2009; Harmon *et al.,* 2006), space exploration (Lasue *et al.,* 2011), cultural heritage (Brysbaert *et al.,* 2006), and bio-medical application (Kasem *et al.,* 2011; Anzano and Lasheras, 2009). Several interesting applications of LIBS have been reviewed in many publications (Fortes *et al.,* 2013; Michel, 2010; Gaudiuso *et al.,* 2010; Giakoumaki *et al.,* 2007, Fantoni *et al.,* 2006, Sneddon and Lee, 1999; Rusak *et al.,* 1997, Song *et al.,* 1997).

1.1.2. Theory

When a highly energetic laser pulse is focused in a gas, spark plasma which has a bright flash of intense light appearance is formed at the focal point. This light is accompanied by a loud sound due to the shock waves coming from the focal volume (Cremers and Radziemski, 1987).

There are two main mechanisms leading to breakdown of a gas by a laser pulse. The first step is multiphoton ionization (MPI) which involves the simultaneous absorption by an atom or molecule of a sufficient number of photons to cause its ionization (Cremers and Radziemski, 2006). MPI is described by the following reaction:

$$M + mhv \longrightarrow M^+ + e^- \tag{1.1}$$
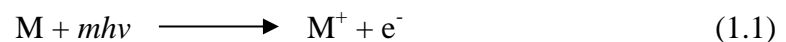
Where, M is the atom or molecule, *m* is the number of photons and M^+ is the ionized atom or molecule.

MPI is important only at a short wavelengths ($< 1\mu m$), and at low gas pressures (Weyl, 1989). The initial electrons are produced by MPI of atoms, molecules, or even dust particles in the focal point (Cremers and Radziemski, 1987).

The second mechanism is cascade/avalanche ionization. In this step the electrons absorbs the laser radiation when they collide with neutrals. This is called *inverse Bremsstrahlung*. If the electrons gain sufficient energy, they can impact ionize the gas or solid through the reaction (Weyl, 1989).

$$e^- + M \longrightarrow 2e^- + M^+ \tag{1.2}$$

This step produces other free electrons that gain energy from the electric fields and causes further ionization. This process of electron multiplication continues during the laser pulse and results in the ionization of the gas and breakdown (Cremers and Radziemski, 2006). Cascade ionization dominates at long wavelength and at moderate to high pressures (Weyl, 1989).

After breakdown of the sample, the plasma expands outward in all directions from the focal volume. Since the laser plasma is a pulsed source, the formation, evolution and the decay of the LIBS plasma are time dependent processes. The schematic illustration of the temporal evolution of a LIBS plasma is given in Figure 1.1. Plasma formation starts as soon as the laser pulse hits the sample and grows while the laser pulse is on (about several nanoseconds). In the strong electric field of the laser, a strong "white light" continuum emission, *(bremsstrahlung radiation)* (Cremers and Radziemski, 2006), due to collisions of two charged particles is observed. When the laser pulse is off, plasma decay starts. At the earlier stages of plasma formation, spectra are mostly dominated by ionic lines and at later stages neutral lines start to appear, due to ion-electron collisions. Use of time-resolved detectors allows one to monitor the spectral evolution of the plasma with respect to laser pulse. The two important parameters for time resolved detection are the delay time, t_d, and the detector gate width, t_b or t_g. Delay time is the time between the onset of the laser pulse and start of the observation of the plasma emission. Gate width is the time interval during with signal acquisition is performed.

The elemental composition of the plasma produced using LIBS technique should be the same with that of the sample. As well, the plasma also should be in local thermodynamic equilibrium (LTE) and optically thin. When these conditions are

satisfied, then observed line emission intensities can be related to the concentration of the elements present in the sample. In practical, these conditions are only met approximately. These two terms; plasma opacity and local thermodynamic equilibrium, are discussed below.
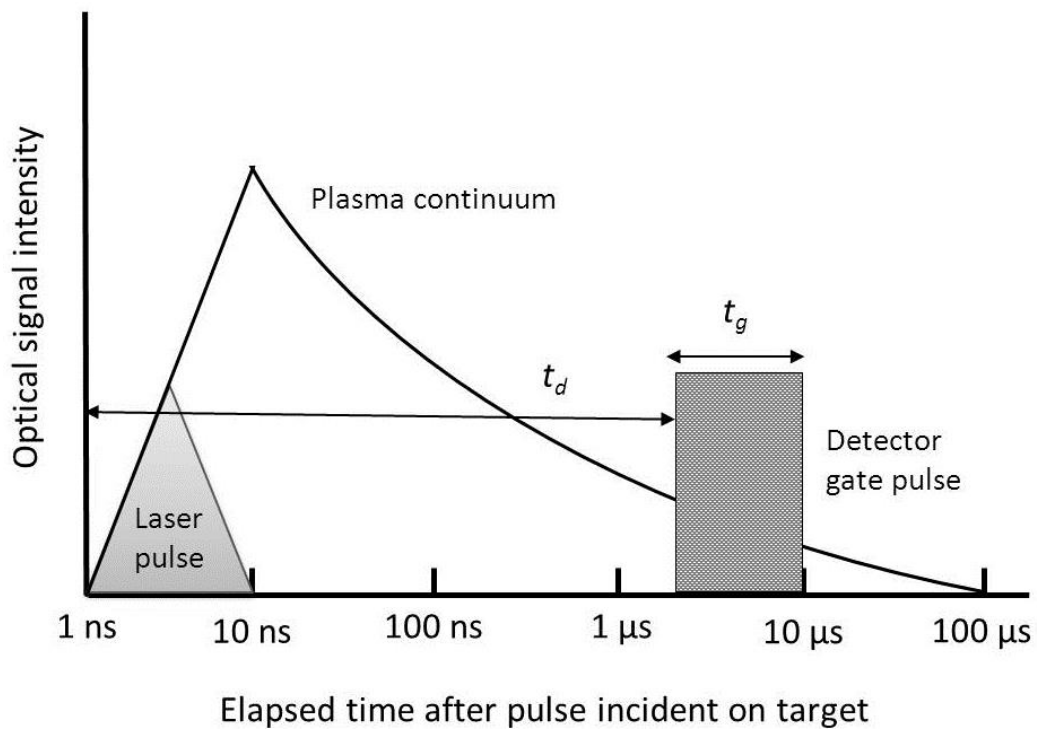
Figure 1.1. Schematic overview of the temporal evolution of a LIBS plasma.
(Source: Cremers and Radziemski; 2006)

1.1.2.1. Plasma Opacity

If the emitted radiation traverses and escapes from the plasma without significant absorption or scattering, the plasma is called optically thin (Cremers and Radziemski, 2006). When re-absorption becomes noticeable, the observed intensities, especially the most intense lines, will deviate from the expected value. Moreover, these lines approach a flat-topped profile and they become self-absorbed. In more extreme cases, a single line will appear to have a dip at the central frequency. In such a case the line is said to be self-reversed.

There are some ways for checking the optical thickness of the plasma. First one is as described by Radziemski *et al.,* to compare the relative intensity of lines belonging to N(I) triplet (414.3 nm, 414.5 nm and 4115.1 nm) with statistical weight of the upper level (Radziemski *et al.,* 1983). A similar verification can be done for other elements such as the three O(I) emission lines at 777.19 nm, 777.42 nm and 777.64 nm (Siemonsson and Miziolek, 1993). Other method is to use a spherical mirror behind the plasma and compare the intensity of a given line with and without the mirror in place (Bekefi, 1976). Another one described by Aragon *et al.,* is based on the calculation of the curve of growth, that is, the intensity versus concentration curve (Aragon *et al.,* 2001).

1.1.2.2. Local Thermodynamic Equilibrium

Thermodynamic equilibrium (TE) is a state where all electrons, ions, and neutrals have the same energy. In this case, the velocity distributions of all kind of free particles (molecules, ions, atoms, and electrons) have a Maxwellian form defined by the temperature of the system. The relative population of excited levels in an atom/ion is described by the Boltzmann distribution. Under TE, the population of different ionization stages, under typical LIBS conditions, is described by the Saha–Boltzmann equation. Finally, the photon energy is described by the Planck function at temperature T. In fact, thermodynamic equilibrium is rarely complete, so it is assumed that the plasma is in local thermodynamic equilibrium (LTE) where thermodynamic equilibration occurs in small regions of plasma although it may be different from region to region (Cremers and Radziemski, 2006).

One of the methods for confirming the LTE is to use McWhirter criterion (Miziolek *et al.,* 2006).

$$Ne(cm^{-3}) \geq 1.6x10^{12}T^{1/2}(\Delta E)^3 \qquad (1.3)$$

Where,

N_e is the number of electron density in cm^{-3},

T is the plasma temperature in K,

ΔE in eV is the highest energy difference between upper and lower energy levels populated according to LTE conditions and between which a transition is possible.

In other words ΔE is the energy difference between upper and lower level of the smallest wavelength used in temperature calculations. N_e is the lower limit of the electron density necessary to maintain the populations of the energy levels at 10% of the LTE by collisions.

1.1.3. Physical Plasma Parameters

Plasma electron temperature and electron number density are some important parameters that give valuable information about the elemental composition and emissivity of the plasma. The incident energy given by the laser is used to produce plasma species: electrons, neutral and ionized atoms. The extent of the laser energy affects the number density of these species and hence the plasma temperature. There is a strong correlation between the plasma temperature and emission intensity. Spatially and temporally integrated emission intensities of the spectral lines in the plasma are used for the calculation of the plasma electron temperature. While performing temperature and electron density calculations the plasma is assumed to be optically thin and under local thermodynamic equilibrium.

1.1.3.1. Plasma Electron Temperature Calculations

There are mainly two methods for determination of plasma temperatures using optical emission spectroscopy. These are based on the use of the Boltzmann equation and the Saha-Boltzmann equation.

1.1.3.1.1. The Boltzmann Equation

The oldest method to determine the plasma temperature by optical spectroscopy is the Boltzmann equation method which is based on the measurement of the relative line intensities from the same element and ionization stage e.g. N(I) lines. This method based on the assumption that the population of ions and molecules at different energy levels follow Boltzmann distribution with an equation given below (Griem, 1964),

$$N_k = N_o\left(\frac{g_k}{Z}\right)\exp\left(\frac{-E_k}{kT}\right) \quad \text{With respect to the ground state or,} \quad (1.4)$$

$$N_k = N_i\left(\frac{g_k}{g_i}\right)\exp\left(\frac{-E_k}{kT}\right) \quad \text{For relative populations} \quad (1.5)$$

Where k and i subscripts refer to excited and ground level, respectively. N_0 is the total atom population, Z is the partition function usually taken as the statistical weight of the ground state. N_k and N_i are the number of atoms in corresponding states, g_k and g_i statistical weight of k and i levels, E_k is the energy of upper level, k is the Boltzmann constant, and T is the temperature.

The spectral line intensity originating from the transition between the energy levels k to i is given by (Griem, 1964),

$$I_{ki} = h\nu_{ki}.g_k.A_{ki}.N_k / 4\pi \quad (1.6)$$

Where h is Planck constant and v *is* frequency corresponding to this line transition, and A_{ki} is the transition probability (Einstein A coefficient) in s^{-1}. If equation (1.6) is inserted in to the equation (1.4), the intensity of an emission become as

$$I_{ki} = \left(\frac{hcN_o g_k A_{ki}}{4\pi\lambda Z}\right)\exp\left(\frac{-E_k}{kT}\right) \quad (1.7)$$

Where, λ is the wavelength of the transition. The ratio of two lines is:

$$\frac{I_1}{I_2} = \frac{g_1 A_1}{g_2 A_2} \cdot \frac{\lambda_2}{\lambda_1}\exp\left(-\frac{|E_1 - E_2|}{kT}\right) \quad (1.8)$$

In two line method, two emission lines having precise *g*, *A* and *E* values are selected and temperature is calculated using their line intensities and wavelengths.

Relative intensities cannot be measured precisely. A way to improve temperature values is to use many lines simultaneously and to perform a graphical analysis. If the equation (1.7) is rearranged by taking its logarithm:

$$\ln(I\lambda / gA) = -E_k / kT - \ln(4\pi Z / hcN_0) \qquad (1.9)$$

A graph of $\ln(I\lambda / gA)$ against E_k (energy of the upper state for emission) results in a straight line with a slope of *(-1/kT)*. The reliable temperature calculation depends on the accuracy of line intensities, transition probabilities and a good separation between the upper levels (Griem, 1964).

1.1.3.1.2. The Saha-Boltzmann Equation

In this method, relative line intensities of the same element but different ionization stage are used e.g. N(I) and N(II) lines or N(II) and N(III). The Saha-Boltzmann equation is given by the following equation (Griem, 1964).

$$\frac{I_1}{I_2} = 2 \frac{g_1 A_1 \lambda_2}{g_2 A_2 \lambda_1} \frac{(2\pi mk)^{3/2}}{h^3} \frac{1}{N_e} T^{3/2} \, exp\left[-\frac{(E_1 + E_\infty - E_2 - \Delta E_\infty)}{kT} \right] \qquad (1.10)$$

Where

I: relative line intensity $\qquad\qquad$ g: statistical weight

A: transition probabilities $\qquad\qquad$ λ: spectral wavelength

m: mass of an electron $\qquad\qquad$ k: Boltzmann constant

h: Planck constant $\qquad\qquad$ N_e: number of electron density

T: temperature $\qquad\qquad$ E: excited states upper energy level

E_∞: ionization potential $\qquad\qquad$ ΔE_∞: the reduction in ionization potential

In order to apply the Saha-Boltzmann equation the electron density of the plasma should be known. The plasma temperature can be obtained by an iterative computation technique. In these techniques the energy difference is larger than the

energy spread available within a single ionization stage. As a result, the temperature is less sensitive to measurement errors than in single level case.

1.1.3.2. Plasma Electron Density Calculations

Spectral lines emitted in laser generated plasma are strongly broadened due to several broadening mechanisms. This property is used for the calculation of the electron number density of the plasma.

1.1.3.2.1. Atomic Line Broadening Mechanisms

Various types of line broadening have been observed in the plasma emission (Singh and Thakur, 2007). These are natural broadening, the Doppler broadening and the Stark broadening.

Natural broadening occurs due to the finite life time of excited states and results in a Lorentz profiles (Griem, 1974).

The Doppler broadening occurs due to the thermal or directed motion of the emitting ions and has a Gaussian line shape with a width proportional to the square root of the emitter temperature.

$$\Delta \lambda_D = 7.2 \times 10^{-7} (T/M)^{1/2} \lambda_0 \qquad (1.11)$$

Where M is the atomic mass of the element and λ_o is the central wavelength of the spectral line. The Doppler broadening is dominant at low electron densities.

1.1.3.2.2. Stark Broadening

Stark broadening is observed because the emitting ions experience an electric field due to the presence of plasma electrons and ions around them. The profiles for Stark-broadened lines are well described by a Lorentz function (Griem, 1974).

In the LIBS experiments the electron density is very high ($N_e \sim 10^{15}\text{-}10^{18}$ cm^{-3}) during the early times of the plasma. As a result, the lines profiles are dominated by Stark broadening for a considerable period of time. Over time the plasma cools and the electron density become lower, the Stark broadening reduces and Doppler broadening becomes dominant.

Under normal LIBS conditions, the most important contributions to the line width are the Doppler width and the Stark effect. Natural line broadening can be neglected. The theory of line broadening is described in detail by Griem (Griem, 1974).

The measured line profiles normally also contain contribution from instrument resolution width. Thus, before plasma parameters are evaluated, the instrument width needs to be measured experimentally for a given spectrometer. Instrumental broadening depends on the slit width, the grating dispersion, and the dynamic behavior of the photon detector (Samek *et al.,* 2000). The total line width observed for a given line is

$$\Delta\lambda_{total} = \Delta\lambda_{line} + \Delta\lambda_{spectrometer} \tag{1.12}$$

This shows that the actual line width can be easily extracted from the measured line width by simply subtracting the instrument width.

Stark-broadened line width can be used to calculate the electron density (N_e) in plasma since the width of these spectral lines depends on N_e. In spectroscopy both the linear and the quadratic Stark effect are encountered. However, only the hydrogen atom having one electron and H-like ions exhibit the linear Stark effect; all other atoms exhibit the quadratic Stark effect. For the linear Stark effect the electron density and the line width are related by the simple formula (Griem, 1964),

$$N_e = C(N_e, T)\Delta\lambda_{FWHM}^{3/2} \tag{1.13}$$

Where $\Delta\lambda$ is the full width at half maximum (FWHM) and the parameter *C* is a constant depends only weakly on *N_e* and *T*. The constant *C* for the H Balmer lines is tabulated in the literature (Griem, 1964).

Due to the fact that, H$_\beta$ (486.1 nm) line is an intense line, sufficiently broadened for precise measurements, in a very accessible region of the spectrum, and has low

tendency to become self-absorbed this line can be used for electron density calculation. Owing to these properties H_β line should be the first choice for N_e calculation of LIBS plasma containing hydrogen. Among the Balmer series H_γ line (434.1 nm) is the next best choice. In cases where the electron density is not too high (less than about 10^{17} cm^{-3}) the H_α line (656.3 nm) is suitable for N_e calculations since at higher electron densities this strong line have a tendency to self-absorption (Samek *et al.*, 2000).

In literature another equation was reported for electron density calculation using stark-broadened H_α line (El Sherbini *et al.*, 2006).

$$N_e\,(H_\alpha) = 8.02 \times 10^{12}\left(\Delta\lambda_{1/2}\,/\alpha_{1/2}\right)^{3/2}\,cm^{-3} \qquad (1.14)$$

Where, $\Delta\lambda_{1/2}$ is the FWHM of the line in Å, and $\alpha_{1/2}$ is the half width of the reduced Stark profiles in Å. Precise values of $\alpha_{1/2}$ for the Balmer series can be found in literature (Griem, 1974).

For non-H-like lines the quadratic Stark effect (two- and more-electron atoms) is encountered and the electron density and the line width are related by

$$\Delta\lambda_{FWHM} = 2\left[2 + 1.75 \times 10^{-4}N_e^{1/4}\alpha\left(1 - 0.068N_e^{1/6}T^{-1/2}\right)\right] \times 10^{-16}wN_e \qquad (1.15)$$

In this equation, the first term in the brackets represents the contribution from electron broadening, and the second term originates from ion broadening. In that equation w is the electron impact parameter at $Ne=10^{16}$ cm^{-3}, and α is the ion broadening parameter. The parameters w and α can be found from the reference (Griem, 1964). Since the second term in equation 1.15 is normally small, the expression reduces to

$$\Delta\lambda_{FWHM} = 2\omega\left(\frac{N_e}{10^{16}}\right) \qquad (1.16)$$

1.1.3.3. Effect of Ambient Gas on Plasma Parameters

As soon as the plasma formed on/inside the sample it expands away from the target. The expansion of the plasma (Kurniawan *et al.,* 1997; Harilal *et al.,* 2006; Garrelia *et al.,* 1999, Cristoforetti *et al.,* 2005), the amount of sample loss (Knight *et al.,* 2000; Iida, 1990), crater formation (Bogaerts *et al.,* 2006, Mateo *et al.,* 2012) plasma emission intensity (Mateo *et al.,* 2012; Kim *et al.,* 1997, Kagawa *et al.,* 1984; Iida, 1989; Iida, 1990; Cristoforetti *et al.,* 2004; Salle *et al.,* 2005), temperature and electron density of plasma (Yalçın *et al.,* 1996; Yalçın *et al.,* 1999; Aguilera and Aragon, 1999; Iida, 1990; Park *et al.,* 2005; Kagawa *et al.,* 1984) are strongly dependent on the type and pressure of the ambient gas. A more detailed publication list on this issue can be found in two review papers of De Giacomo *et al.,* 2012; Effenberger et al, 2010).

Iida investigated the effect of different ambient gases (argon, air and helium) and pressure on the plasma emission and ablated mass of various metal and ceramic samples using a nanosecond Nd:YAG laser (Iida, 1990). It was found that at atmospheric pressure (760 torr) helium provided higher emission intensity while at 100 torr argon gave higher signal. At 100 torr lower temperatures and a faster cooling were obtained in the presence of He compared to Ar. The amount of ablated mass was lower in the presence of argon.

Harilal *et al.* performed a similar study and investigated the effect Ar, He and air with pressures varied from 1 mbar to 10^{-3} bar on the temperature and electron density of laser produced carbon plasma (Harilal *et al.,* 1998). Studies showed that electron density decreased with an increase in pressure irrespective of the gas type while higher plasma temperature was obtained at argon environment compared to that of helium and air. It is claimed that since argon has more capacity to absorb energy, plasma temperature in argon will be higher than helium. It is also stated that as the pressure increases the confinement of the plasma will increase and result in an increase in collisions of electrons with background gas atoms. That's why lower electron densities were obtained under high pressures.

Kim *et al.* also observed higher emission intensity and slower cooling thus longer plasma life time in argon environment compared to air (Kim *et al.,* 1997). These behaviors attributed to smaller conductivity (0.037 cal cm^{-1} s^{-1} deg^{-1} at 760 Torr and 20 °C) and a smaller specific heat capacity (0.0763 cal g^{-1} deg^{-1} at 760 torr and 20 °C) of

argon gas than that of air values. Additional result of this study was that as the pressure of ambient buffer gas increases emission intensity also increases. They explained that electrons and ions cannot escape easily from the target due to confinement of plasma by the ambient gas. Thus the atomization of the droplets and particles will be facilitated leading to higher emission at high pressure.

In another study, Aguilera and Aragon studied the temporal evolution of the electron density and temperature of laser produced plasmas generated in air, argon, and helium at atmospheric pressure (Aguilera and Aragon, 1999). In this study a pulsed Nd:YAG laser at fundamental wavelength (1064 nm) was focused below the surface of the low alloyed steel sample to obtain a more stable plasma with higher emission intensities. The finding of this study revealed that Ar environment provides the highest initial temperature and the slowest temporal decay. The same temporal behavior was observed for air but lower temperature values are obtained at all delay times. In regard to air and argon, He produces lower initial temperature value with a faster decay. At atmospheric conditions in the presence of He a rapid reduction of the electron density takes place having smallest value at each delay time compared to corresponding values of air and Ar. Although air and Ar provide same initial electron number density, at later times air provided lower values with a faster decay.

1.1.4. Instrumentation

A typical LIBS instrument basically consists of three main parts: a *pulsed laser source* to create plasma, *optical components* for focusing the laser beam and collection of the plasma emission and a *detection system* comprising of a spectrograph to disperse the light and a detector to record the light (Figure 1.2). Depending on the specific application and the type of the samples, a target holder or sample container may also be needed. The details of each component are discussed in the following parts.
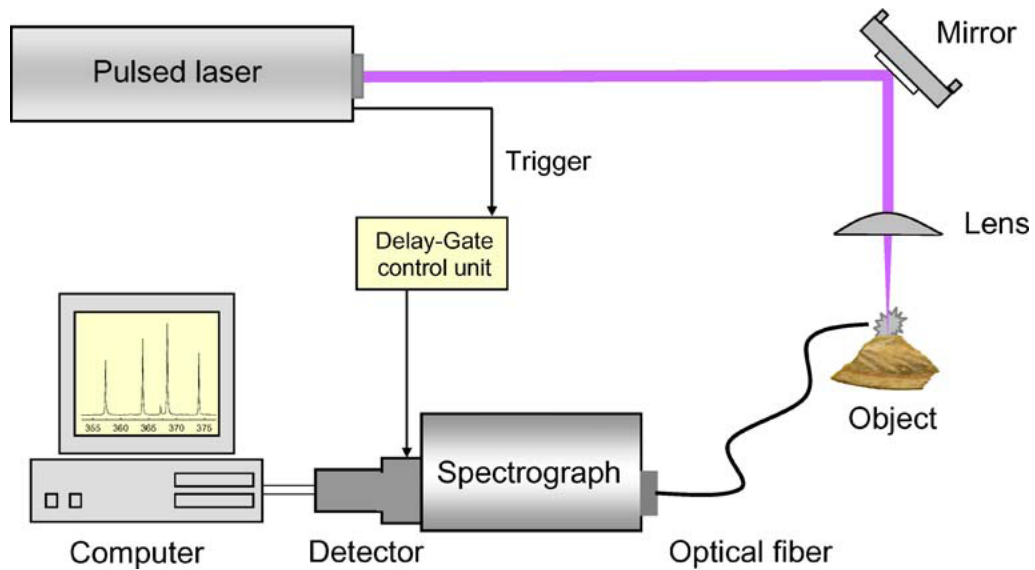
Figure 1.2. A schematic diagram of a simple apparatus for laser-induced breakdown spectroscopy. (Source: Giakoumaki *et al.,* 2007)

1.1.4.1. Laser Sources

The acronym LASER stands for **L**ight **A**mplification by **S**timulated **E**mission of **R**adiation. As the acronym suggest laser radiation involves an amplifications process and gaining intensity when photons having same frequency passes through a medium (Telle *et al.*, 2007). Since the light is amplified a laser produce narrow and extremely intense coherent radiation.

Figure 1.3 shows the main components of a laser source consisting of active medium, optical resonator and pumping. The core of the laser is active medium and pumped by an external radiation or electrical source to become excited to higher energy levels by absorption of energy from the source. When the population of excited state particles exceeds the number in lower states, *population inversion* is developed. Therefore the light is amplified by stimulated emission (Skoog *et al.,* 2007).

The optical resonator composed of a pair of mirrors (high reflective, HR, and output coupler) placed on either end of the active medium. The light is reflected back and forth between these mirrors, passing through the active medium and amplified each time. The output laser beam is emitted through output coupler that is partially transparent (Skoog *et al.,* 2007).

14
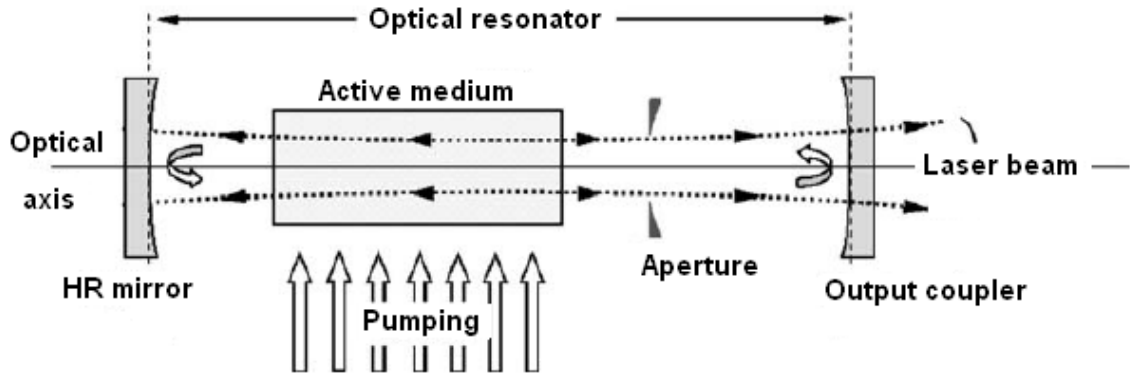
Figure 1.3. A schematic representation of laser components.
(Source: Telle *et al.*, 2007)

Lasers can be operated in either continuous wave (CW) or pulsed mode. The laser having a power on the order of 5 MW is needed for LIBS application in order to produce the plasma when focused to a small spot (Cremers and Radziemski, 2006). Such a high power can be easily accomplished using pulsed and Q-switched lasers. *Q*-switching is a mode of operating a laser in which energy is stored in the laser active material during pumping, In that mode an electro optic Q-switch shutter is placed between HR resonant mirror and active medium. When the shutter is closed the HR mirror is blocked to prevent feedback of the light and very strong laser action is developed inducing population inversion. Then Q-switch is activated to become transparent and now feedback is allowed leading to stimulated emission and giant pulses are produced (Telle *et al.,* 2007).

The classification of the laser generally is made by the type of the active medium. These are gas lasers (HeNe, Ar^+, CO_2), excimer lasers (KrF, XeCl, ArF), solid state lasers (ruby, Nd:YAG, Ti:Sapphire, Er:YAG), semi-conductor diode lasers (silicon diode, AlGaAs, GaAs) and dye lasers (Skoog *et al.*, 2007). Among these flash lamp pumped Q-switched Nd:YAG lasers are mostly used in LIBS application since they are reliable and convenient source of the powerful pulses. In addition the fundamental wavelength (1064 nm) can be easily shifted to shorter wavelengths (532 nm, 355 nm and 255 nm) using non-linear crystal thus allowing to be used at fixed wavelength laser sources ranging from near infrared to the near UV spectral region (Cremers and Radziemski, 2006).

1.1.4.2. Optical Components

In LIBS some optical components are required for focusing the laser beam and collection of the plasma emission. Focusing of the laser beam can be accomplished using lenses or mirrors. Usually a single lens that will be sufficient to focus the laser beam where the lens to distance is not changing. Some important parameters for selecting lenses are the focal length, diameter and construction material. They should be transparent to the laser wavelength (Cremers and Radziemski, 2006).

Plasma collection can be made in several approaches depending on the apparatus. In some cases a lens system consisting of two lenses is used, first one is to make the emission parallel and the second one is to focus to the plasma emission on to the slit of the spectrograph or fiber optic cable that is connected to a detection system (Cremers and Radziemski, 2006).

1.1.4.3. Detection Systems

LIBS detection systems consist of a dispersing element, a detector, signal processing electronics and a computer for data processing (Singh and Thakur, 2007).

The type of the dispersing element that provides spectral resolution can be narrow-bandpass spectral filter, acousto optic tunable filter (AOTF), grating monochromator, polychromator or spectrograph (Cremers and Radziemski, 2006). In the case of narrow bandpass filter and AOTF only a single narrow wavelength band is passed through the dispersing element, then transmitted light is detected by a photon type detector. Similarly grating monochromator and detector combination provides single element detection.

The simultaneous emission of multiple lines should be recorded by using a polychromator or a spectrograph combined with a photon detector which is the most common configuration used in LIBS measurements. A polychromator contains a series of photomultiplier tubes or array type detectors for detection while a spectrograph uses two dimensional detectors (Skoog *et al.,* 2007).

In recent years use of echelle spectrograph has gained popularity and several compact versions have become available (Bauer *et al.,* 1998). The echelle spectrograph provides large wavelength range (from 180 nm to 800 nm) with a reasonable resolution

(Miziolek *et al.,* 2006). A schematic diagram of an echelle spectrograph is provided in Figure 1.4. It contains both a grating and a prism. The echelle grating is a diffraction grating that has spaced grooves. A series of overlapping spectra with high resolution are produced when the light is diffracted at normal incidence to the face of these grooves. The prism, placed perpendicular to the echelle is used for separating out the overlapping spectra (Skoog *et al.,* 1997).

For LIBS measurements the spectrally resolved signal can be detected with photon type detector such as photomultiplier tube (PMT), photo diode (PD), photodiode array (PDA), charged injection device (CID) or charged-coupled device (CCD). PMT and PD detectors consist of a photosensitive material that produce signal linearly with the amount of incoming light. These type detectors can be used in combination of filters or AOTF's and monochromators while array type detectors (PDA, CID and CCD) are used with spectrographs (Miziolek *et al.,* 2006).
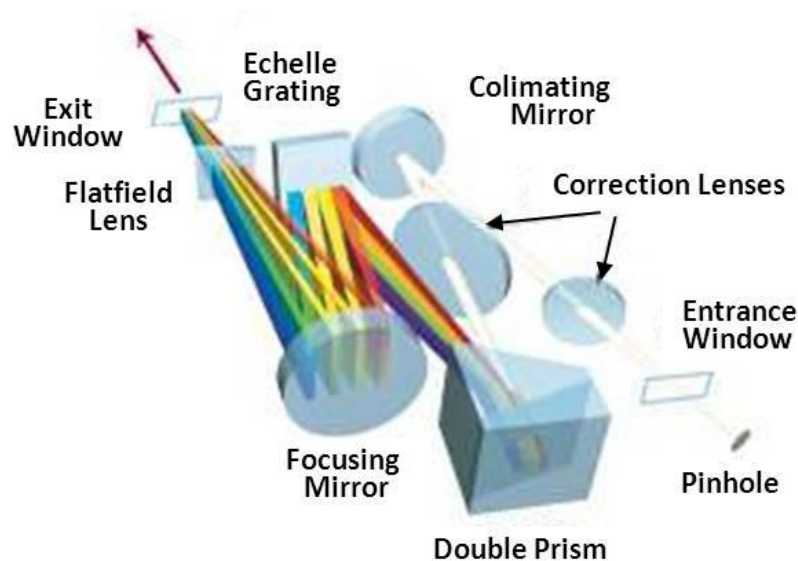
Figure 1.4. A schematic diagram of an echelle spectrograph.
(Source: Andor Technology, 2013)

For LIBS measurements the spectrally resolved signal can be detected with photon type detector such as photomultiplier tube (PMT), photo diode (PD), photodiode array (PDA), charged injection device (CID) or charged-coupled device (CCD). PMT and PD detectors consist of a photosensitive material that produce signal linearly with

the amount of incoming light. These type detectors can be used in combination of filters or AOTF's and monochromators while array type detectors (PDA, CID and CCD) are used with spectrographs (Miziolek *et al.,* 2006).

An intensified CCD (ICCD) detector is a type of CCD detector that consists of three parts: a photocathode, a micro channel plate (MCP) and a phosphor screen as shown in Figure 1.5. The dispersed light coming from the spectrograph reaches the photocathode and ejects electrons. Ejected electrons are accelerated toward the MCP by applying voltage and they are multiplied here. These multiplied electrons are converted back into photons in phosphor screen. Therefore the light is intensified and guided to a CCD chip using an optical fiber or a lens system (Linden *et al.,* 2012).

Spectrograph-ICCD combination is used widely in LIBS applications since it provides multi element analysis capability and allows to record time resolved spectra (Miziolek *et al.,* 2006).
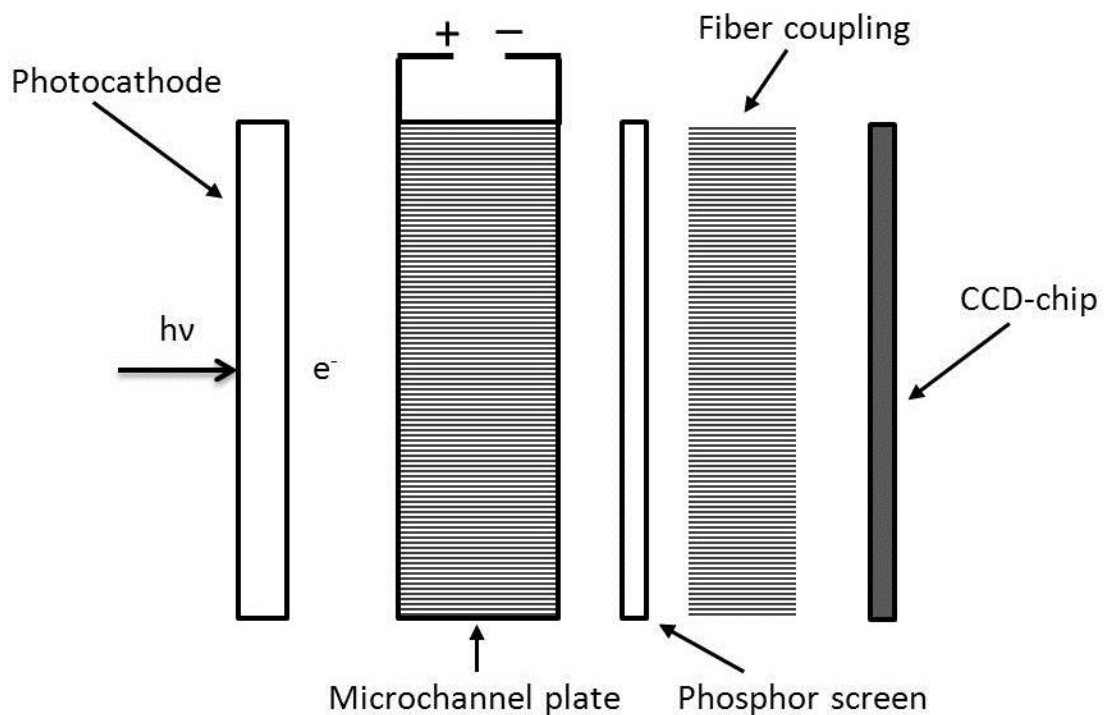
Figure 1.5. A schematic diagram of an ICCD detector.
(Source: Linden *et al.,* 2012)

1.2. Liquid Analysis by LIBS

1.2.1. Direct Analysis

Applications of LIBS on direct analysis of liquids (Cremers *et al.,* 1984; Koch *et al.,* 2004; De Giacomo *et al.,* 2004; Knopp *et al.,* 1996) are not as many as the ones on solids due to the difficulties experienced during analysis. Those difficulties are splashing, bubble formation and shock wave formation after focusing the laser beam on liquids. Liquid analysis by LIBS also suffers from poor signal quality, reduced plasma emission and low limits of detection due to shot to shot signal fluctuations. Some approaches to overcome these difficulties encountered in bulk liquid analysis include formation of the plasma; on liquid surfaces (Yaroshchyk *et al.,* 2005a; Fichet *et al.,* 2001; Gruber *et al.,*2001; Berman *et al.,* 1998), on single isolated droplets (Groh *et al.,* 2010; Cahoon and Almirall, 2012; Archontaki and Crouch, 1988) on flowing-jet liquids (Rai and Rai, 2008; Samek *et al.,* 2000; Ho *et al.,* 1997, Yaroshchyk *et al.,* 2005a) and in cavitation bubbles (Koch *et al.,* 2005).

Electrospray ionization technique was also used as an alternative method for the liquid analysis by LIBS (Huang *et al.,* 2007; Huang and Lin, 2005).

Some authors also describe a method in which the liquid solution is converted to solid either by freezing in liquid nitrogen (Caceres *et al.,* 2001) or making pellets of calcium hydroxide by mixing with CaO (Diaz Pace *et al.,* 2006). Use of filter paper (Yaroshchyk *et al.,* 2005b), wood-slice (Chen *et al.,* 2008) and graphite (Sarkar *et al.,* 2010) substrate for analysis of trace metals in aqueous solution has been reported.

Another approach is using double-pulse (DP) technique instead of single pulse-LIBS (Babushok *et al.,* 2006; Burakov *et al.,* 2009; Gottfried *et al.,* 2007). This technique has been successfully applied for the analysis of aqueous samples in a flowing cell (Rifai *et al.,* 2012), or underwater samples (De Giacomo *et al.,* 2005) in which the first laser pulse is used to create a gaseous atmosphere and the second pulse to produce plasma with reduced background emission and longer lifetimes. Therefore, double pulse LIBS approach presents higher sensitivity over single pulse LIBS experiments and the analytical capability of the technique increases. Pu and Cheung showed the applicability of DP-LIBS method for the analysis of lead in aqueous samples using flowing-jet technique (Pu and Cheung, 2003).

1.2.2. Sample Introduction Techniques in Liquids Analysis

Pneumatic and ultrasonic nebulization techniques are also widely employed to introduce liquid samples in the form of an aerosol in order to overcome the difficulties that have been encountered in direct analysis of liquid by LIBS.

The first reported study on the analysis of liquids in the form of an aerosol was performed by Radziemski *et al.,* in 1983. In this study, aqueous solutions of beryllium, sodium, arsenic and mercury were introduced into a sample cell after passing the nebulizer-heating chamber. A linear calibration range over 4 orders of magnitude has been declared for Na in air. Detection limits were calculated and compared with that of obtained by ICP-OES. They stated that detection limits obtained with ICP-OES are much lower than the ones obtained by LIBS.

Essien and co-workers showed the applicability of the LIBS system for the analysis of cadmium (Cd), lead (Pb) and zinc (Zn) using pneumatic nebulizer (Essien *et al.,* 1988). Their detection system included a monochromator, PMT and a boxcar averager to provide amplification, averaging and time resolution. They reported a detection limit of 0.019, 0.21 and 0.24 $\mu g\ g^{-1}$ for Cd, Pb and Zn aerosols, respectively. They also investigated the effect of chemical form of lead (as acetate, chloride and nitrate salts) on the analytical signal and it was stated that Pb signal was constant within 10%. Effect of easily ionizable element (EIE) on lead signal was studied and concluded that in the presence of Na background continuum signal was lowered 30% at various delay times studied.

Fisher *et al.* described another example for use of pneumatic nebulization technique for detection of toxic metals by LIBS (Fisher at al., 2001). They investigated optimal temporal gating parameters for analysis of arsenic, beryllium, cadmium, chromium, lead, and mercury. It was found that for detection of As, Be, Cd, and Hg optimal gate time was 12 μs while for lead and chromium it was 50 μs. For arsenic and lead LOD value was found to be 400 $\mu g\ m^{-3}$ and 190 $\mu g\ m^{-3}$, respectively.

Panne *et al.* demonstrated an alternative method for analysis of aerosols (Panne *et al.,* 2001). In this study sample solutions converted to aerosols via nebulization and produced aerosols automatically filtered on a quartz fiber. Authors claimed that deposition of particles on filters would provide better detection limits since this method afford enrichment of the analyte. Optimum timing parameter, emission wavelength and

filter material were investigated. Several toxic elements including Cd, Ni, As, Co, Mn, Sb, Cr, Tl, Sn, V, Cu and Pb were analyzed and their detection limits were reported.

In 2012, Aras *et al.* reported a sample introduction system based on ultrasonic nebulization for analysis of toxic metals by LIBS (Aras *et al.,* 2012). The system consisted of an ultrasonic nebulizer, a desolvating unit and a membrane dryer connected to the sample cell. Particle size of the aerosols was estimated to be at sub-micron level. They obtained lower detection limit with use of membrane dryer for some elements.

Although nebulization techniques are reproducible and reliable, the main drawback is the poor sample introduction efficiency. Only 1-5% of the sample enters the atomizer while the rest is sent to the waste. Another alternative sample introduction technique that is commonly used in atomic spectrometry is hydride generation technique. Due to high sampling efficiency, hydride generation provide better sensitivity.

1.3. Hydride Generation Method

1.3.1. General Information

Hydride generation (HG) is a chemical derivatization technique in which some elements of the periodic table including arsenic (As), antimony (Sb), bismuth (Bi), germanium (Ge), lead (Pb), selenium (Se), tellurium (Te), and tin (Sn) form their volatile hydrides when they react with a strong reducing agent and an acid (Dedina and Tsalev, 1995). Although indium and thallium also have known to form hydrides no reliable methods of analysis has been reported in literature. Hydride generation term involves the complete process of:

a) Conversion of an analyte in an acidified sample to hydride and its transfer to the gaseous phase.

b) Transport of the released hydride by a flow of purge gas to an atomizer.

The hydride generation reaction can be performed using either a metal/acid or tetrahydroborate reduction (Dedina and Tsalev, 1995, Pohl, 2004). The first method used at early times is known as Marsh reaction that employs Zn/HCl system. In this method nascent hydrogen is obtained from the reaction of Zn metal and H^+ as shown below:

$$Zn + 2H^+ \rightarrow Zn^{2+} + 2H \tag{1.17}$$

The second and most commonly used reductant system is (BH_4^-)/acid reaction in which boric acid (H_3BO_3) and nascent hydrogen is produced:

$$BH_4^- + 3H_2O + H^+ \rightarrow H_3BO_3 + 8H \tag{1.18}$$
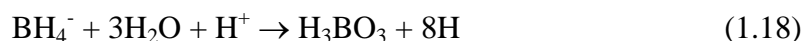
Sodium tetrahydroborate ($NaBH_4$) and hydrochloric acid (HCl) is the most employed (BH_4^-)/acid system. This reaction (1.18) is very fast and completed within a few microseconds at pH≤1 (Narsito *et al.,* 1990).

Nascent hydrogen produced in either way, then reacts with metal or metalloid and respective hydride is obtained according to following reaction:

$$8H + E^{+m} \rightarrow EH_n \uparrow + H_2 \text{ (excess)} \tag{1.19}$$

Here, E is the desired metal such as As, Sn, Sb, Pb etc., m is the oxidation state of the element in the sample solution, n is the oxidation state of the analyte in the hydride and EH_n is the volatile metal hydride. m and n are may or not equal. Table 1.1 summarizes the formula and name of volatile hydrides.

There are mainly two modes of hydride generation: collection and direct transfer methods. In the former method the hydrides are trapped in a collection medium until the evolution is completed and then transported to an atomizer. The direct mode can be performed in three ways: continuous flow (CF), flow injection and batch method (Dedina and Tsalev, 1995; Pohl, 2004).

A typical block diagram of continuous flow mode hydride generation system is given in Figure 1.6. Analyte, acid and reductant solutions are delivered to the gas liquid separator (GLS) by the help of a peristaltic pump. A gas liquid separator is used for separation of volatile hydrides from the waste solution. The drain of the waste solution is drawn from the bottom of the GLS while the volatile hydrides are transferred to the atomizer by a stream of carrier gas.

Table 1.1. Nomenclature and chemical formula of volatile hydrides.

Element	Systematic Name	Common Name	Formula
Se	Hydrogen selenide	-	H_2Se
	Selenium hydride		
Te	Hydrogen telluride	-	H_2Te
	Tellurium hydride		
As	Arsenic trihydride	Arsine	AsH_3
Sb	Antimony trihydride	Stibine	SbH_3
Bi	Bismuth trihydride	Bismuthine	BiH_3
Ge	Germanium tetrahydride	Germane	GeH_4
Sn	Tin tetrahydride	Stannane	SnH_4
Pb	Lead tetrahydride	Plumbane	PbH_4

Hydride generation not only provide high sampling efficiency but also high sensitivity. Elements are separated from other accompanying materials in the form of gaseous hydrides and are introduced to the sample cell for atomization, leaving the sample matrix in the liquid waste. Thus, spectral and chemical interferences can be eliminated. Therefore, a significant increase in sensitivity, by 10–100 folds, over commonly used liquid sample introduction techniques has been reported (Farias *et al.,* 2002, Lajunen and Perämäki, 2004, Krachler *et al.,* 2002).
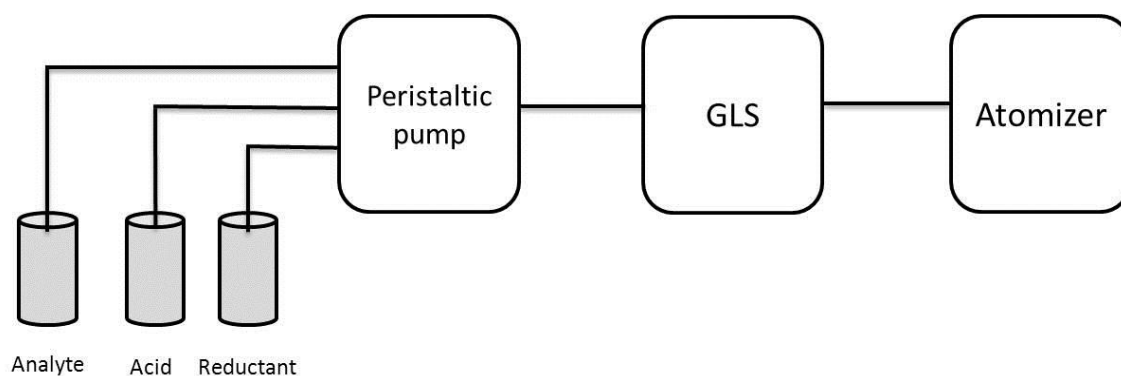
Figure 1.6. A typical block diagram of continuous flow mode hydride generation system.

1.3.2. Hyphenated Hydride Generation Techniques

The first analytical use of hydride generation technique in atomic spectrometry was reported by Holak in 1969 (Holak, 1969). Holak used Marsh reaction to produce arsine and then coupled to flame atomic absorption spectrometry (FAAS). In that early study, produced arsine was collected in a liquid nitrogen trap and transported to air acetylene flame after warming.

Braman *et al.,* contributed to a great improvement in HG with the use of sodium tetrahydroborate (NaBH$_4$) as a reducing agent in the reaction of arsine generation (Braman *et al.,* 1972). In this study the emission excitation source i.e. direct current (DC) arc discharge was also reported for the first time.

In 1972, the first study based on coupling of HG to plasma arc excitation source was described by Lichte and Skogerboe (Lichte and Skobergoe, 1972).

Eventually, Thompson and coworkers employed inductively coupled plasma atomic emission spectrometry (ICP-AES) for simultaneous determination of As, Sb, Bi, Se and Te using continuous flow hydride generation method (Thompson *et al.,* 1978).

Since 1978, there are enormous numbers of studies in literature specifically devoted to coupling of hydride generation, HG to:

- Atomic absorption spectrometric techniques such as flame atomic absorption spectrometry; FAAS (De Lima *et al.,* 2013; Musil and Dedina, 2013; Kula *et al.,* 2008; Kratzer and Dedina, 2008; Henden *et al.,* 2011; Elçi *et al.,* 2009; Berkkan and Ertaş, 2004; Korkmaz *et al.,* 2002), and electrothermal atomic absorption spectrometry; ETAAS (Yıldırım *et al.,* 2012; Tsalev *et al.,* 1992; Moreda-Pineiro *et al.,* 2001; Niedzielski *et al.,* 2002; Tyson *et al.,* 2000; Ni and Bin, 1995)
- Atomic fluorescence spectrometry; AFS (Deng *et al.,* 2013; DUlivo *et al.,* 1995; Karadjova *et al.,* 2007; Reyes *et al.,* 2009; Cava-Montesinos *et al.,* 2003),
- Atomic emission spectrometric techniques such as inductively-coupled plasma atomic emission spectrometry, ICP-AES (Kılınc and Aydın, 2012; Etxebarria *et al.,* 2005; Masson *et al.,* 2005; Carrion *et al.,* 2003; Farias *et al.,* 2002), microwave-induced plasma optic emission spectrometry, MIP-OES (Pohl and Jamroz, 2011; Matusiewicz and

Slachcinski, 2006; Pereiro *et al.,* 1994; Robbins *et al.,* 1979), direct-current plasma atomic emission spectrometry, DCP-AES (Brindle *et al.,* 1998; Ek *et al.,* 1995; Chen *et al.,* 1992) and glow discharge optic emission spectrometry, GD-OES (Orellana-Velado *et al.,* 2001; Broekaert *et al.,* 1993)

- Inductively coupled plasma mass spectrometry, ICP-MS (Yılmaz *et al.,* 2013; Forniles *et al.,* 2013; Chen *et al.,* 2002; Jin *et al.,* 1991; Li *et al.,* 2000; Hall *et al.,* 1997; Hosick *et al.,* 2002)

In addition, there is a great interest in the field of analytical chemistry in exploring the analytical capabilities of HG with respect to speciation analysis (Yalcin and Le, 1998, Karadjova *et al.,* 2005, Vinas *et al.,* 2004; Feng *et al.,* 1999), multi-element determinations (Le *et al.,* 1998, Li and Guo, 2005) and investigation of interferences (Henden *et al.,* 2011; Alp and Ertaş, 2010; Kumar and Riyazuddin, 2010; Kratzer *et al.,* 2011; Novotny and Kratzer, 2013; Erdem and Henden, 2004; Pohl and Zyrnicki; 2002) since its first use by Holak.

The generation of volatile hydrides followed by atomic spectroscopic detection is the most common method of choice for the determination of toxic metals at trace levels of concentration, (μg L^{-1} – ng L^{-1}). These techniques provide high sensitivity but require laborious and time consuming sample collection steps for analyses to be conducted in the laboratory. In addition, the chemical identity of the sample may change during its delivery from the field to the laboratory. For this reason, there is a growing demand for rapid, real time, *in situ* and sensitive analysis techniques for environmental research applications.

LIBS is a very suitable technique toward the development of portable sensors and the utilization of this technique for the determination of environmental pollutants is ever increasing (Cremers and Radziemski, 2006, Miziolek *et al.,* 2006, Singh and Thakur, 2007). There are several portable-LIBS sensors developed for environmental and industrial applications (Cunat *et al.,* 2009, Mosier-Boss and Lieberman, 2005, Cremers *et al.,* 1996).

1.3.3. HG-LIBS

HG coupled with atomic spectrometric detection (HG-AAS, HG-ICP-OES, HG-AFS), is among the most common method for decades for its higher sensitivity and is widely used for quantification of As, Se, Bi, Ge, Sb, Sn, Te and Pb in liquid samples. However, there are a few studies based on coupling of the hydride generation system to laser-induced breakdown detection.

The analytical capability of liquid analysis by LIBS, in terms of detection limits, may be improved by converting relevant metal species to their metal hydrides. To our knowledge, only one of the four studies in the literature on the chemical generation of volatile hydrides followed by LIBS detection was carried out by Singh *et al.,* (Singh *et al.,* 1996). They have used batch type hydride generation method. Acidified sample (in 1.0% HCl) and a reductant solution of 1.0% $NaBH_4$ in 1.0% NaOH were mixed in a three-armed glass flask. After the reaction was completed, the cell was opened to an evacuated cell, the hydrides were mixed with a carrier gas (He, N_2) of predetermined concentration and pressure. They investigated the effect of the type of the carrier gas and ambient pressure on temporal emission behavior of LIBS signal on tin (Sn) and arsenic (As) hydrides, observing that the neutral atomic emission of Sn at 284.0 nm decreases exponentially with time in a N_2 atmosphere while the signal increases logarithmically under identical experimental conditions in a He atmosphere. Authors report no quantitative data for the detection limit of the studied elements.

The second study on HG-LIBS is an MSc thesis by Kunati at Youngstown State University (Kunati, 2008). In this study, the HG-LIBS results for As, Sn and Te was compared with the results from HG-LIF (Laser-Induced Fluorescence) and HG-ICP-AES. They report the same detection limit of 1.0 mg L^{-1} for the three elements studied (As, Sn and Te) by an HG-LIBS system equipped with a Czerny-Turner monochromator using PMT detection. Another MSc thesis study at the same university was performed by Chari (Chari, 2008). Similarly in this study, HG-LIBS results for Sb and Se were compared with HG-LIF, HG-ICP-AES and HG-ICP-AES. Chari obtained limit of detections of 1.6 mg L^{-1} and 1.0 mg L^{-1} for Sb and Se, respectively. Both of these studies did not contain any optimization studies and there was no data reported on the applicability of the technique to real waters.

In a more recent study, same group published a study on spectroscopic characterization of arsine (AsH_3), stibine (SbH_3) and selenium hydride (H_2Se) plasma in Ar only and Ar/H_2 gas mixture (Simeonsson and Williamson, 2011). Plasma electron density determined through hydrogen emission measurements was found to vary from 4.5×10^{17} to 8.3×10^{15} cm^{-3} over time delays of 0.2-15 µs. Plasma temperatures determined through argon and arsenic emission measurements range from 8800 to 7700 K for Ar and from 8800 to 6500 K for As in HG-LIBS plasmas. Little difference in the excitation temperatures was observed. However, a significant reduction in the intensity and lifetime of Ar atomic emission lines in the HG-LIBS plasmas that appeared to be due to the presence of H_2 was shown. Work does not include optimization of the chemical and instrumental LIBS parameters; however, limit of detection values of 0.7, 0.2 and 0.6 mg L^{-1}, were reported for arsenic, antimony and selenium, respectively. Results were obtained with a single wavelength detector, photomultiplier tube (PMT) and a boxcar averaging.

Literature studies on the analysis of hydride-forming elements by liquid-LIBS and HG-LIBS with their detection limits are summarized in Table 1.2. As can be seen from the table, LOD values have not been determined for all hydride forming elements. Moreover, their limit of detection is not lower than the direct analysis of liquid, as expected.

1.4. Aim of the Study

Due to their high level of toxicity, arsenic, antimony, bismuth, germanium, lead, selenium, tellurium and tin are some elements that have environmental and technological importance. Quantification of these elements in environmental samples can be done by introducing aqueous solutions of these elements directly to atomic spectroscopic instruments, such as atomic absorption and inductively coupled plasma spectrometer. These elements can also be determined in the form of their volatile hydrides. HG coupled with atomic spectrometric detection (HG-AAS, HG-ICP-OES, HG-AFS), is among the most common method for decades for its higher sensitivity and is widely used for quantification of As, Se, Bi, Ge, Sb, Sn, Te and Pb in liquid samples. However, there are a few studies based on coupling of the hydride generation system to laser-induced breakdown detection. Laser Induced Breakdown Spectroscopy (LIBS), is

a very suitable technique to develop portable sensors and utilization of this technique for detection of the environmental pollutants is ever increasing. There are several portable-LIBS sensors developed for environmental and industrial applications.

In this thesis study, it has been aimed to construct a laser-induced breakdown spectrometry hyphenated with on-line continuous flow hydride generation sample introduction system, HG-LIBS, for the determination of toxic elements in aqueous environments. Optimum chemical and instrumental parameters governing chemical hydride generation, laser plasma formation and detection were investigated for each element under argon and nitrogen atmosphere. The effect of differing ambient gas, argon and nitrogen, on the sensitivity of the HG-LIBS signal has been investigated. The cause of higher signal intensity under argon environment has also been examined by performing plasma temperature and electron density calculations under both gases. Detection limits of the hydride forming elements have been determined and compared with that of obtained by the method of direct analysis of liquids. The suitability of the proposed system for analysis of tin, arsenic, antimony, lead and germanium in aqueous environment has been investigated through spiking experiments using real water samples.

This work is the first systematical investigation of the chemical and instrumental parameters of the HG-LIBS method for the analysis of Sn, As, Sb, Pb and Ge in aqueous environments.

Table 1.2. Literature studies on determination of hydride forming elements by liquid LIBS and HG-LIBS.

Element	Liquid LIBS			HG-LIBS	
	Method	LOD	Reference	LOD	Reference
As	Nebulization	0.5 mg g^{-1}	Radziemski *et al.,* 1983	Not reported	Singh *et al.,* 1996
	Pneumatic nebulization	400 μg m^{-3}	Fisher *et al.,* 2001	1.0 mg L^{-1}	Kunati, 2008
	Liquid evaporation on graphite	5.0 mg L^{-1}	Wal *et al.,* 1999	1.0 mg L^{-1}	Cheng *et al.,* 1991
	Aerosol on filer	2.73 μg m^{-3}	Panne *et al.,* 2001	0.7 mg L^{-1}	Simeonsson and Williamson, 2011
Bi	Liquid on filter	350 mg L^{-1}	Fichet *et al.,* 1999	-	-
Ge	-	-	-	-	-
Sb	-	-	-	1.6 mg L^{-1}	Chari, 2008
				0.2 mg L^{-1}	Simeonsson and Williamson, 2011
Se	-	-	-	1.0 mg L^{-1}	Chari, 2008
				0.6 mg L^{-1}	Simeonsson and Williamson, 2011
Sn	Direct liquid	100 mg L^{-1}	Fichet *et al.,* 2001	Not reported	Singh *et al.,* 1996
				0.9 mg L^{-1}	Kunati, 2008
Te	-		-	1.0 mg L^{-1}	Kunati, 2008

Table 1.2. **(Cont.)**

Element	Liquid LIBS			HG-LIBS	
	Method	**LOD**	**Reference**	**LOD**	**Reference**
Pb	Pneumatic nebulization	0.21 μg g^{-1}	Essien et. al. 1988	-	-
	Pneumatic nebulization	190 μg m^{-3}	Fisher *et al.,* 2001		
	Direct liquid	12.5 mg L^{-1}	Knopp *et al.,* 1996		
	Direct liquid	0.2 mg L^{-1}	Cremers *et al.,* 1984		
	Liquid-jet	0.3 mg L^{-1}	Lo and Cheung, 2002		
	Direct liquid	100 mg L^{-1}	Fichet *et al.,* 2001		
	Liquid evaporation on graphite	2.0 mg L^{-1}	Wal *et al.,* 1999		
	Aerosol on filer	0.17 μg m^{-3}	Panne *et al.,* 2001		
	Ultrasonic nebulization	13.6 mg L^{-1}	Aras *et al.,* 2012		
	Flowing cell	*6 ± 1 mg L^{-1} 74 ± 5 mg L^{-1}	Rifai *et al.,* 2012		
	Liquid-jet	*136 μg L^{-1} 2.02 mg L^{-1}, ArF laser 12.0 mg L^{-1}, Nd:YAG laser	Pu ve Cheung, 2003		
	Liquid-jet	40.0 mg L^{-1}	Samek *et al.,* 2000		
	Liquid on paper substrate	*3.0 mg L^{-1} 18.0 mg L^{-1}	Yaroshchyk *et al.*, 2005b		

*Double pulse LIBS technique was used.

CHAPTER 2

EXPERIMENTAL

In this thesis study, a continuous flow-hydride generation sample introduction system has been coupled to Laser Induced Breakdown Spectroscopic detection for liquids analysis. The system was constructed from its commercially available parts. The details of the system and functions of each component are given below.

2.1. HG-LIBS System

The experimental HG-LIBS system, as shown schematically and pictorially in Figure 2.1.(a) and (b), respectively, consisted of four main parts; a laser source, a hydride generation unit, a sample cell and a detection unit. Volatile hydrides produced in hydride generation unit are transferred to the sample/plasma cell through Teflon tubing. Laser source is directed to the sample cell with suitable optics where it interacts with hydrides to form luminous plasma. Plasma emission is collected and focused onto the tip of a fiber optic cable connected to the spectrograph.

2.1.1. Laser Source

A Q-switched Nd:YAG laser (*Spectra Physics, LAB 170-10, California-USA*) operating at the second harmonic (532 nm) wavelength with 10 ns pulse width and 10 Hz pulse repetition rate is used as the plasma source. The maximum laser pulse energy that can be attained is 460 mJ at its second harmonic wavelength and is measured by an energy/power meter (*Ophir Nova II, Israel*). The laser beam is focused inside the sample cell using 17.5 cm focal length Plano-convex lens (1″ OD, *NewFocus*).

2.1.2. Hydride Generation Unit

A schematic diagram of the hydride generation unit is presented in Figure 2.2. The acidified analyte and reductant solutions are delivered by means of a four-channel peristaltic pump (*Longer Precision Pump*) to a 3-way PTFE connector (*Supelco*) where hydride generation reaction starts. The reaction mixture is then passed to a U type gas-liquid separator (GLS) to separate volatile hydrides from the solution. Volatile hydrides are carried by an inert gas stream, (N_2 or Ar), to the Nafion membrane dryer unit (*Perma Pure, MD050*) where the moisture of hydrides is removed. The flow of the carrier gas and drying gas is controlled by two different flow meters (*Cole Parmer*). After passing the dryer unit, volatile hydrides are introduced into the sample cell via 80 mm long and 4 mm i.d Teflon tubing. In the case of no dryer used, 450 mm Teflon tubing was used to connect the GLS to the sample cell.

Waste solution is pumped from the GLS to drain by using a second peristaltic pump (*ISMATEC, Germany*).

The analyte, reductant and waste solutions are pumped with 0.85 mm, 1.42 mm and 1.85 mm i.d peristaltic pump tubing (*Cole Parmer, Germany*), respectively.

(a)

(b)
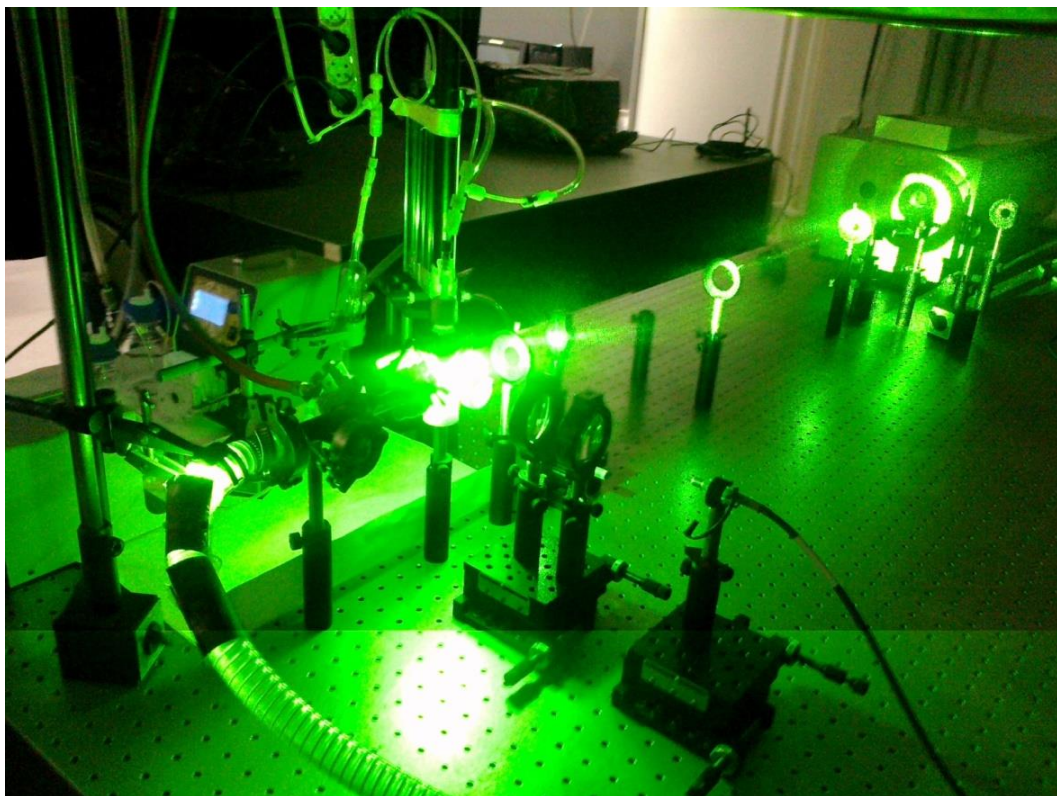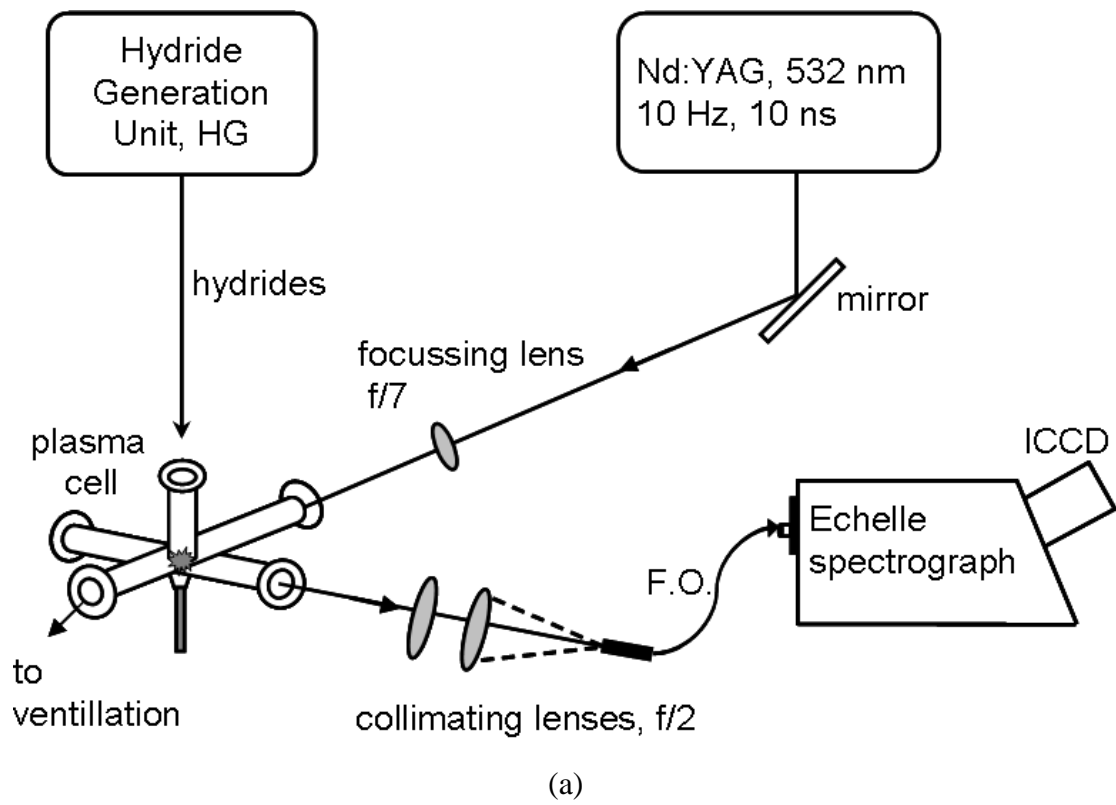
Figure 2.1. (a) Schematic diagram (b) actual view of the HG-LIBS set-up.
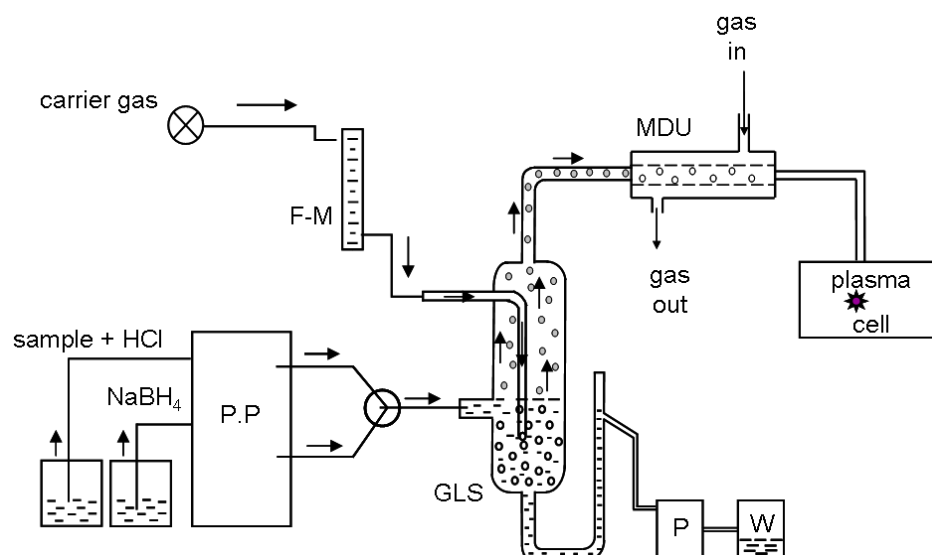
Figure 2.2. Schematic diagram of continuous flow Hydride Generation, HG, unit. P.P: Peristaltic Pump, GLS: Gas-Liquid Separator, HCl: Hydrochloric acid, NaBH$_4$: Sodium borohydride, F-M: Flow meter, MDU: Membrane Drying Unit, P: Pump, W: Waste.

2.1.3. Sample-Plasma Cell

Being as one of the most critical parts of the HG-LIBS system, several sample cell designs were used for optimal performance.

Initially, a six armed glass cell with 1" diameter was machined (Figure 2.3.a) in a local machine shop. Hydrides were introduced from the top arm and plasma emission was collected from the side arm at 90 degrees with respect to incoming laser beam. All other arms were kept open to ambient atmosphere, while a ventilating hood is located at the top of the entire HG-LIBS system to circulate the corrosive and toxic atmosphere. No emission signal was detected from the hydrides with this cell. The reason for that may be the dilution and quenching of the plasma emission by air entering into the cell since the cell arms were open to air. When the arms were closed, hydrogen flame was observed due to excess hydrogen produced from the hydride generation reaction. It was also inconvenient to work with this glass cell due to the scattering of the laser light from the transparent glass surfaces in all directions. Thus, another cell design was needed.

Secondly, rather than glass, a material opaque to the laser light was chosen to construct a plasma cell. Teflon was the best choice for that purpose in addition to its

chemical resistivity. A rectangular prism cell, shown in Figure 2.3.b, was machined from the Teflon material in which two 1 inch hole was opened on the two side faces that are at 90 degrees with respect to each other. One is used for incoming laser beam and the other is for collecting the plasma emission. Hydrides were introduced from the top face of the cell through Teflon tubing and another face is used for connecting to the ventilation. In this design, atomic signal was observed, however; plasma was very labile because of the condensation of hydrides on the cell walls. It was decided to connect the system to the vacuum pump but continuous flow could not be obtained.

These difficulties necessitated a more compact cell design. Then, a five-armed Teflon cell was constructed (Figure 2.3.c). It is a closed system and the two arms were equipped with quartz windows which are transparent to incoming laser beam and plasma emission. The inner diameter of the cell arms is 1 cm and the length of the one arm to another is 5 cm. The cell has a 21 cm^3 inner volume. One side arm of the cell was used for incoming laser beam another one situated at 90º was used for the collection of plasma emission. Hydrides were introduced from the top arm and the remaining two arms were closed by connecting one to a ventilation system through a vacuum pump (*Edwards*) and another one to a pressure gauge when needed to measure the pressure. Here, the reason for using vacuum pump was to obtain a directional and continuous flow. Since continuous flow was obtained, the pressure was measured as atmospheric pressure. The photos given in Figure 2.4 show the location of the cell in the system.

2.1.4. Detection Unit

The plasma emission from the volatile hydrides was collected at an angle of 90º with respect to incoming laser beam by a means of two 10.0 cm focal length plano convex lenses of 2 inch diameter, as shown in Figure 2.1. The collected light was launched onto the tip of an optical fiber (*Ocean Optics, 600 μm*) coupled to an Echelle type spectrograph (*ME5000, Andor Inc. f=195 mm*), equipped with a gated, image intensified charge coupled detector, ICCD (*iStar DH734, Andor Inc.*). Spectrograph has multi-element analysis capability between 200-850 nm spectral range and 0.08 nm resolution. The detector gain was kept at the setting of 100 out of 250 in most of the measurements. The spectral calibration of the detector was performed by using a Hg-Ar

line source (*HG-1, Mercury Argon Calibration Source, Ocean Optics*) and intensity calibration was performed by using a continuous source (NIST certified Deuterium-Tungsten Halogen lamp, *DHCal-2000, Ocean Optics*). A summary of the system specifications are listed in Table 2.1.

2.2. Chemicals and Reagents

Standard solutions of Sn (in 20% HCl), As^{3+} (in 2% HCl), Sb^{3+} (in 20% HCl), Pb (in 2% HCl), Te (in 20% HCl), Se (in 2% HCl), Bi (in 2% HCl) and Ge (in 1% HNO_3) were prepared daily from their stock solutions (1000 mg L^{-1}, *High-Purity Standards*) through appropriate dilutions with ultra-pure water. Samples were acidified with concentrated HCl (37%, *Riedel-de Haën*) to reach a desired acid concentration. All reagents were of analytical grade or higher purity. Reductant solution, sodium borohydride, were prepared by dissolving appropriate amounts of $NaBH_4$ powder (*Sigma- Aldrich*) in NaOH (*Riedel-de Haën*) for stabilization and used without filtration. Reductant solution was made alkaline with 1.0% NaOH for tin and antimony, with 0.2% NaOH for germanium and arsenic, and with 0.4% NaOH for bismuth. L-cysteine (*Aldrich*) was used as a pre-reducing agent for antimony, and potassium hexacyanoferrate(III), $K_3[Fe(CN)_6]$ (*Sigma-Aldrich*), was used as a pre-oxidizing agent for lead. Since in the presence of HCl and $K_3[Fe(CN)_6]$, a highly toxic product, "HCN", is formed, this substance should be handled carefully. Iron(III) nitrate, $Fe(NO_3)_3$ (*Merck*), or potassium thiocyanate, KSCN (*Merck*) was used as an additive in order to eliminate the formation of black precipitates of metallic bismuth, Bi°. Sample and reductant solution flow rate was investigated in detail. Unless otherwise stated, acidified standards/samples and reductant solutions were delivered to the GLS at a flow rate of 2.5 mL min^{-1} and 5.0 mL min^{-1}, respectively.

River Water Reference Material for trace metals, *SLRS-4*, (*NRC, Canada*), tap water from the İzmir-Urla municipal water supply and bottled spring water *(Pınar)* from Aydın, Turkey were used without dilution in the analysis of real water samples.
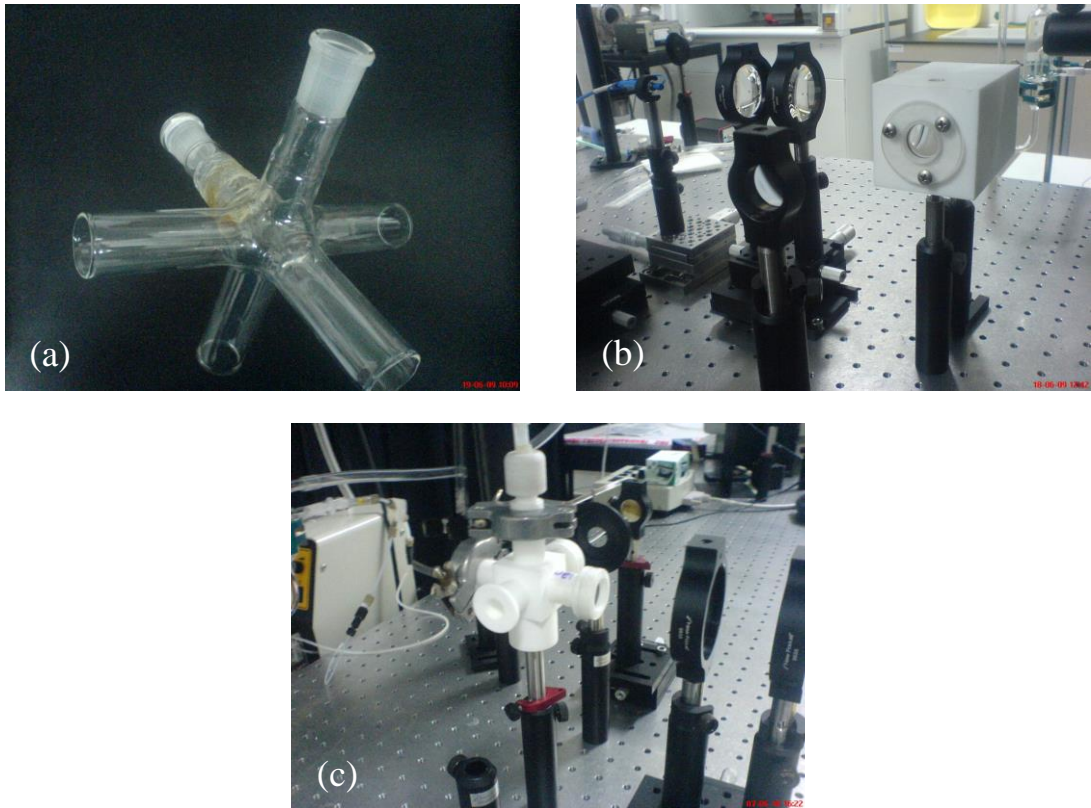
Figure 2.3. (a) Six-armed glass cell (b) rectangular Teflon cell and (c) five-armed Teflon cell.
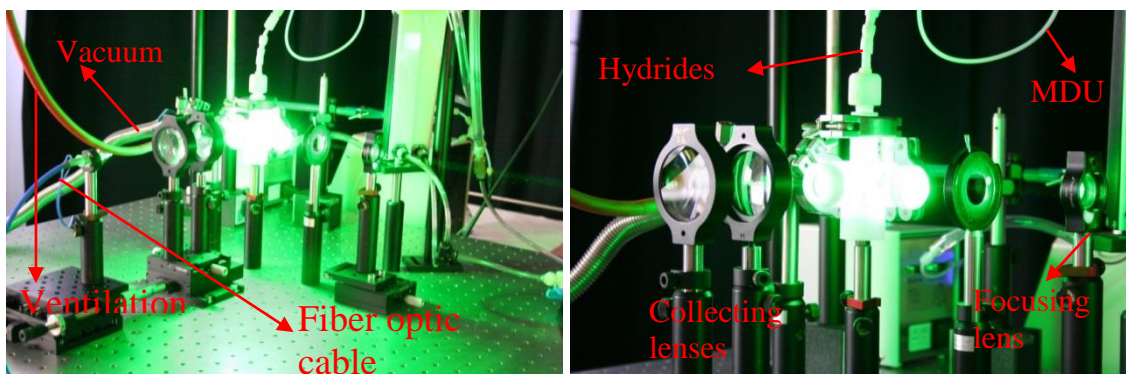
Figure 2.4. Photos showing the location of the five armed Teflon cell in the set-up

Table 2.1. HG-LIBS System Specifications

Q-Switched Nd:YAG laser	Quanta-Ray Lab-170, Spectra Physics (California-USA)
Power meter	PE50BB-DIF-V2, Nova II, Ophir (Israel)
Focusing lens	17.5 cm, 1″ OD, 245-335 nm coated silica, NewFocus (Darmstad-Germany)
Collimating lenses	10.0 cm, 2″ OD, fused silica, CVI, (Bensheim-Germany) 10.0 cm, 2″ OD, LA4545, uncoated UV fused silica, Thorlabs
Echelle spectrograph	Mechelle 5000, Andor Inc., f/7 (European)
ICCD detector	iStar DH734, Andor Inc. (European)
Fiber optic cable	600μm, QP600-2-SR, Ocean Optics Inc.
Mercury Argon Calibration source	HG-1, Ocean Optics Inc.
Deuterium-Tungsten Halogen lamp	DHCal-2000, Ocean Optics Inc.
Gas liquid separator	Borosilicate glass
Flow Meters	Cole Parmer
Peristaltic pumps	Sample: 4-way, Longer Precision Waste: 4-way, Ismatec (Germany)
Vacuum pump	Edward
Vacuum controller	PKG 020 Pirani-Cold Cathode Gauge Control, Gauge Head TPR 010, Balzers
Membrane dryer	Nafion, MD-050, PermaPure
Sample cell	Handmade, Teflon
Quartz widows	1″ OD, 1 mm thickness, WFS-2501, Quartz, UQG Optics

2.3. Instrumental LIBS Parameters

Time resolution experiments are crucial in laser-induced breakdown spectrometric measurements in order to maximize the signal for each laser pulse. Strong background emission can be eliminated from the spectral line measurements by using time gated detectors. The two important parameters for time resolved detection are the delay time, t_d, and the detector gate width, t_g. Delay time is the time between the onset of the laser pulse and start of the observation of the plasma emission. Gate width is the time interval during which the signal acquisition is performed.

In the HG-LIBS system for hydride forming element detection, important detector parameters such as delay time and gate width were investigated separately for each element. For this purpose, stannane plasma was formed from 5.0 mg L^{-1} standard solutions with laser pulses of 100 mJ pulse[-1] energy under argon atmosphere. Plasma emission was collected at various delay times from 1.0 μs to 10.0 μs. The same procedure was applied for gate width measurements between 0.075 ms - 2.0 ms at a fixed delay time of 5.0 μs. In order to investigate the effect of delay time on arsenic signal, arsine, AsH_3, plasma emission was collected at 130 mJ pulse[-1] energy and argon atmosphere at a delay time ranging from 0.5 μs to 6.0 μs. Gate width measurements between 0.075 ms – 1.0 ms were performed at a delay time of 3.0 μs. For antimony analysis, delay time and gate width were scanned between 0.3 μs -6.0 μs and 10.0 μs-200.0 μs; respectively. For lead analysis plasma emission was collected at various delay times ranging between 2.0 μs and 7.0 μs under nitrogen environment. For gate time measurements plasma emission recorded at a laser energy of 150 mJ pulse[-1] and a delay time of 5.0 μs while gate width varied between 50 μs – 200 μs. In the case of germanium, germane, GeH_4 plasma emission was collected at a delay time ranging from 0.2 μs to 6.0 μs. In order to find optimum t_g, plasma emission were scanned between 25 μs – 200 μs were performed at a delay time of 1.0 μs.

In order to investigate the effect of laser energy on emission signal intensity, plasma emission produced from 5.0 mg L^{-1} Sn, 20.0 mg L^{-1} As, 40.0 mg L^{-1} Sb, 20.0 mg L^{-1} Pb and 20.0 mg L^{-1} Ge solutions were analyzed at laser energies ranging from 60.0 mJ pulse[-1] to 160 mJ pulse[-1].

2.4. Parameters that Affect the Efficiency of Hydride Generation

Hydride generation and transportation efficiency is dependent on some certain parameters like reductant / acid concentration and flow rate, sample and carrier gas flow rate, and the presence of pre-oxidizing or reducing agent. These parameters were all optimized in order to obtain maximum signal intensity.

It is known that the types and concentration of acid plays an important role in hydride generation reactions. Various acid types have been used such as hydrochloric acid, nitric acid, sulfuric acid, tartaric acid, acetic acid and hydrofluoric acid (Farias *et al.,* 2002). Among these the most widely used one is HCl. In this study HCl was also used. In order to maximize acid concentration, analyte solutions were prepared in the presence of HCl solutions at a range of 0.1% − 3.0% (v/v) and plasma emission was recorded as a function acid concentration.

The effect of $NaBH_4$ concentration on LIBS emission signal was also investigated. For this purpose, analyte solutions were prepared in the presence of hydrochloric acid and they were allowed to react with $NaBH_4$ solutions. Hydrides formed at the end of this reaction were transferred to the plasma cell and plasma emission was collected.

The possibility of increasing Sb(3+) signal by the addition of L-cysteine was investigated. 100.0 mg L^{-1} Sb^{3+} solutions containing 2.0% HCl (v/v) were prepared in in the presence of L-cysteine in 0.2%, 0.5%, 1.0%, 2.0%, and 5.0% (w/v) and plasma emission from stibine plasma was collected. A solution of 1.0% $NaBH_4$ in 1.0% NaOH and laser energy of 100 mJ was used.

$K_3[Fe(CN)_6]$ was used as an oxidizing agent for the analysis of lead by HG-LIBS. In order to find optimum oxidizing agent concentration, 20.0 mg L^{-1} Pb solutions containing 2.0% HCl were prepared in the presence of 1.0%, 2.0%, 3.0%, and 4.0% (w/v) potassium hexacyanoferrate(III).

The acidified sample to the reductant flow rate was kept at a ratio of 1:2 by selecting an appropriate tubing size. Sample flow rate was adjusted to a desired flow rate by controlling pump rate. Three sample flow rate 1.0 mL min^{-1}, 2.5 mL min^{-1} and 4.0 mL min^{-1} were studied.

A stream of nitrogen or argon gas was used to transport hydride gases from GLS to sample cell. In order to study the effect of carrier gas flow rate, analyte signal from

each element at their maximum emission wavelength was recorded as a function of carrier gas flow rate.

CHAPTER 3

RESULTS AND DISCUSSION

3.1. Signal Optimization

After construction of the HG-LIBS system, optimization of instrumental and chemical parameters was performed for selective analysis of the elements considered: tin, arsenic, antimony, lead and germanium. Optimizations were done separately for each element as each shows differing sensitivities at different conditions. The effect of membrane dryer, ambient gas type, instrumental and chemical parameters are some of the points investigated in detail through optimization of the LIBS signal studies.

3.1.1. The Effect of Membrane Dryer

Volatile hydrides produced by a chemical reaction in GLS are transported to the sample cell for plasma formation by a flow of purge gas. At this stage, volatile hydrides are separated from the solution, but are still wet. In order to improve the sensitivity of the analytical technique, removal of this moisture is required. Several desolvation techniques, such as, chemical desiccants ($CaSO_4$, silica gel, $CaCl_2$), physical moisture traps and membrane desolvating unit can be used for the removal of the moisture. Among these use of membrane desolvating unit, MDU, for the removal of humidity is recently becoming more popular. In this technique, a dry purge gas, N_2 or Ar flows over the exterior surface of the membrane tubing, while wet gas (hydrides in this case) flows in a counter current direction inside the tubing (Figure 2.2). The water from the gaseous hydrides was extracted by the humidity gradient between the inside and outside of the tubing. N_2 was used as a purge gas at flow rates less than the carrier gas flow rate. Spectra recorded from the stannane plasma in the presence and absences of a drying unit were shown Figure 3.1, as dotted and solid line, respectively. Also %RSD values of the analyte and the background signal with and without MDU were given in Table 3.1. It can be easily seen that 50% decrease in RSD value of the signal was obtained with the

use of a membrane desolvating unit while RSD of the background, BG, does not change much. This enhancement in RSD of the signal corresponds to 30% enhancement in signal to noise ratio. In this study, data were obtained from eight single laser shots of 150 mJ pulse^{-1} energy. Signal is defined as the peak area under 284.0 nm Sn(I) line minus the background intensity. Noise was defined as three times the standard deviation of the background intensity.
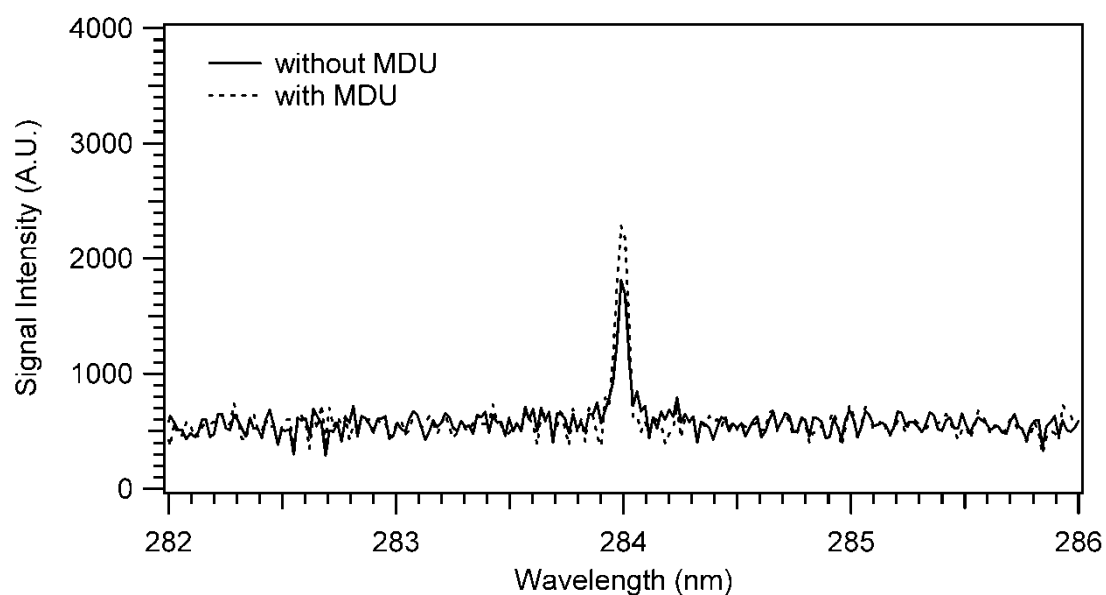
Figure 3.1. The effect of membrane drying unit on Sn(I) signal intensity at 284.0 nm, under nitrogen gas and optimum hydride generation conditions.

Table 3.1. Effect of using membrane desolvating unit on Sn LIBS Signal.

	S/N	% RSD	
		BG	Signal
Without Dryer	24.37	22.98	43.29
With Dryer	31.61	24.38	19.24
Enhancement	30 %		

3.1.2. Effect of Ambient Gas Type

The type of the ambient gas is known to have significant effect on physical plasma parameters and the expansion of laser-induced plasmas. There are several reports in literature on this issue (Aguilera and Aragon, 1999, Harrilal *et al.,* 1998). In this thesis work, HG-LIBS signal variation with respect to type of the carrier gas was studied in the presence of nitrogen and argon. Work will be discussed in the following parts, in detail, however, in this section only the effect of gas type on the HG-LIBS signal intensity is given.

To investigate the effect of carrier gas type on HGLIBS signal, continuous flow of argon and nitrogen gas was used to carry SnH_4, AsH_3, SbH_3, PbH_4 and GeH_4 from the gas-liquid separator into the plasma cell. Same analyte concentrations and identical instrumental and chemical conditions were used for recording a signal from the two different carrier gases. Figure 3.2 shows relative signal strength of each element under nitrogen and argon atmosphere. Solid lines represent signal in Ar and dotted lines represent signal in N_2 atmosphere. As can be seen from the figure, arsenic signal at 278.0 nm could only be observed under argon atmosphere, however tin signal at 284.0 nm, lead signal at 405.8 nm, antimony signal at 259.8 and germanium signal at 265.1 nm were observed in the presence of both gases. Strong enhancement in Sn(I), Ge(I) and Sb(I) signal is observed under Ar atmosphere compared to nitrogen while Pb(I) signal intensity does not seem to be dependent on the type of the carrier gas. The same behaviour was also observed for other emission lines of Sn(I), As(I), Sb(I) Pb(I) and Ge(I) within the full spectra.

Based on these observations optimization studies of arsenic, antimony and germanium were performed under argon environment while signal optimizations for lead were performed in the presence of nitrogen due to its lower cost. Optimization studies of tin were performed under both argon and nitrogen gas and the detection limits calculated for each gas type are compared.
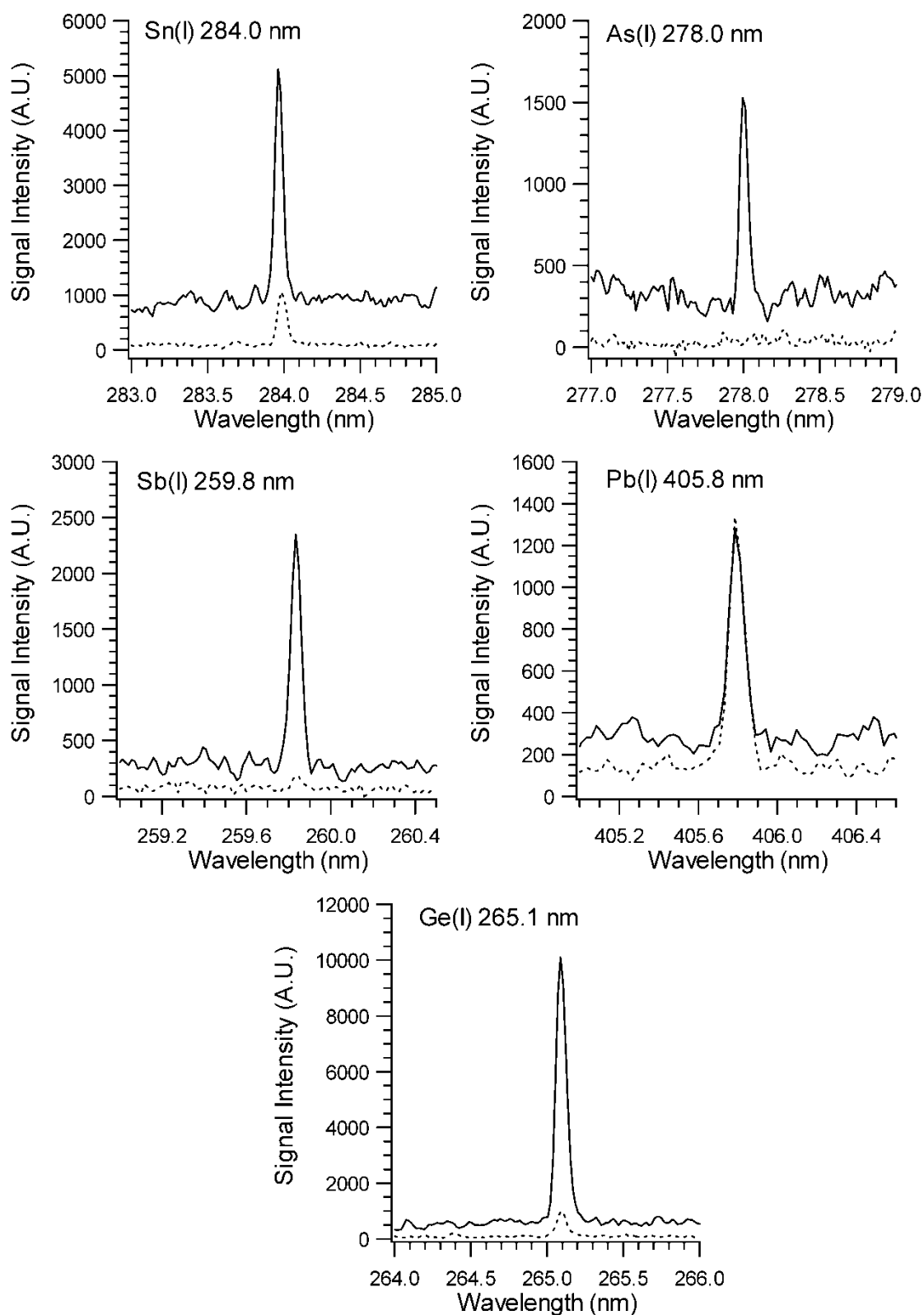
Figure 3.2. Effect of ambient gas type on Sn(I) 284.0 nm, As(I) 278.0 nm, Sb(I) 259.8 nm, Pb(I) 405.8 nm and Ge (I) 265.1 nm signal intensity. Spectra recorded from, 10.0 mg L^{-1} Sn, 20.0 mg L^{-1} As^{3+}, 40.0 mg L^{-1} Sb^{3+}, 20.0 mg L^{-1} Pb, and 20.0 mg L^{-1} Ge. Solid line represents hydride signal under Ar environment and dotted line represents hydride signal under N$_2$.

3.1.3. Instrumental Parameters Optimizations

In order to maximize LIBS signal some of the key parameters, like laser energy, detector delay time, gate width and detector gain was studied first. In all experiments detector gain was kept at 100 in order to avoid saturation of the ICCD detector.

3.1.3.1. Delay Time

It is known that the spectral evolution of the LIBS plasma with respect to laser pulse is a time dependent process that occurs in various stages. The ionic and atomic emissions dominate at different stages of the plasma. In order to examine different stages of the plasma, time resolution experiments need to be performed. Time resolution experiments are also crucial for establishment of the highest emission signal since quantitative analysis should be performed at the stage where the signal is at its maximum level.

In order to investigate the effect of delay time, t_d, on LIBS signal variation, plasma emission signal from chemically generated hydrides was recorded at various detector delay times with respect to the laser pulse. The variation of signal intensity with respect to delay time, for each element under consideration, was provided in Figure 3.3. In the same figure signal to noise ratio (S/N) values were also given with empty circles and scaled on the right side of each graph. Here, signal is defined as the average peak height from five sequential measurements and the noise is defined as three times the standard deviation of the background in a region near the signal for the same number of measurements.

In general, at early times of the plasma relative signal intensity is higher and decreases as delay time increases. However, due to the presence of higher level of the background at early delay times, the S/N ratio consideration would be more accurate for the determination of optimal delay time.

Figure 3.3(a) represents the effect of delay time on neutral Sn signal at 284.0 nm under argon environment. As delay time increases Sn signal was also increased. Optimum t_d was determined to be 4.0 µs.

As seen from Figure 3.3(b), while arsenic signal decreases from 5.0 µs to 6.0 µs delay time, signal to noise ratio was increased from 0.5 µs to 3.5 µs and S/N ratio

started to decrease beyond this value. For this reason 3.0 μs was selected as an optimum value for arsenic.

Investigation of the signal intensity for antimony with respect to delay time was performed using 100.0 mg L^{-1} Sb^{3+} (in 2.0% HCl) solution and 1.0% NaBH$_4$ stabilized with 1.0% NaOH was used. Stibin, SbH$_3$, plasma emission was collected at a laser energy of 100 mJ pulse^{-1} at various delay times. The effect of delay time on antimony signal strength is given in Figure 3.3(c). Optimum t_d was determined to be 2.0 μs since the background level is low with compared to 0.2 and 0.5 μs.

In the case of lead, when the delay time is changed from 1.0 μs to 5.0 μs, lead emission signal at 405.8 nm did not change significantly, whereas at 6.0 μs and 7.0 μs signal decreased (Figure 3.3(d)). Either 3.0 μs or 5.0 μs can be used as an optimum value for Pb since both signal intensity and S/N ratio are high. In this study 5.0 μs was used as an optimum value.

As it is clearly seen in Figure 3.3(e), signal intensity of germanium decreased from 0.2 μs to 6.0 μs delay time while signal to noise ratio increased from 0.2 μs to 1.0 μs and S/N remained nearly unchanged at higher delay times. Therefore optimum t_d value is selected to be 1.0 μs, for Ge.

Figure 3.3. Variation of LIBS signal intensity with respect to detector delay time, t_d, for (a) Sn(I) 284.0 nm, (b) As(I) 278.0 nm, (c) Sb(I) 259.8 nm, (d) Pb(I) 405.8 nm and (e) Ge (I) 265.1 nm. Closed circles indicate relative signal intensity and open circles indicate S/N ratio. Spectra recorded from, 5.0 mg L^{-1} Sn, 100.0 mg L^{-1} As^{3+}, 100.0 mg L^{-1} Sb^{3+}, 20.0 mg L^{-1} Pb, and 20.0 mg L^{-1} Ge.

48

3.1.3.2. Gate Width

Investigation of optimum gate width was performed at optimum delay times for each element. The effect of gate width on Sn(I) 284.0 nm, As(I) 278.0 nm, Sb(I) 259.8 nm, Pb(I) 405.8 nm and Ge(I) 265.1 nm line intensity can be seen in Figure 3.4(a-e), respectively.

In order to investigate the effect of gate width on Sn plasma emission signal was recorded at a t_g range of 75 μs – 100 μs and resulting graph can be seen in Figure 3.4(a). Optimum gate time was selected to be 750 μs.

For As, plasma emission was collected as a function of gate width varying from 75 to 1000 μs. A value of 750 μs was found to be an optimum value at which As(I) signal at 278.0 nm is at maximum level (Figure 3.4(b)) .

For antimony, gate width measurements were performed at a fixed delay time of 2.0 μs and gate width was scanned between 10 μs and 200 μs. As seen from the Figure 3.4(c) antimony signal increased from 10 μs to 50 μs and while signal was decreased at 75 μs t_g value and remained constant up to 200 μs. Thus optimum gate width was obtained to be 50 microsecond.

Gate width optimization studies for lead was performed using 20.0 mg L^{-1} Pb in 2.0% HCl and 2.0% $K_3[Fe(CN)_6]$ and 1.0% $NaBH_4$ in 0.1% NaOH. Plasma emission was recorded at laser energy of 150 mJ pulse^{-1} and a delay time of 5.0 μs while gate widths were scanned between 50 μs and 200 μs. Variation of lead signal at 405.8 nm with respect to gate width is provided in Figure 3.4(d). It was seen that gate width had no important effect on Pb signal. So, optimum gate width was determined as 100 μs for lead.

The change in germanium signal with respect to gate width is given in Figure 3.4(e). When gate width varied from 25 μs to 200 μs, highest germanium signal was obtained at 100 μs. This value is selected to be an optimum value for Ge.

Time resolution experiments were also performed for Sn under nitrogen environment and provided in Appendix A. Optimum delay and gate time were determined to be 10.0 μs and 3.0 ms, respectively.
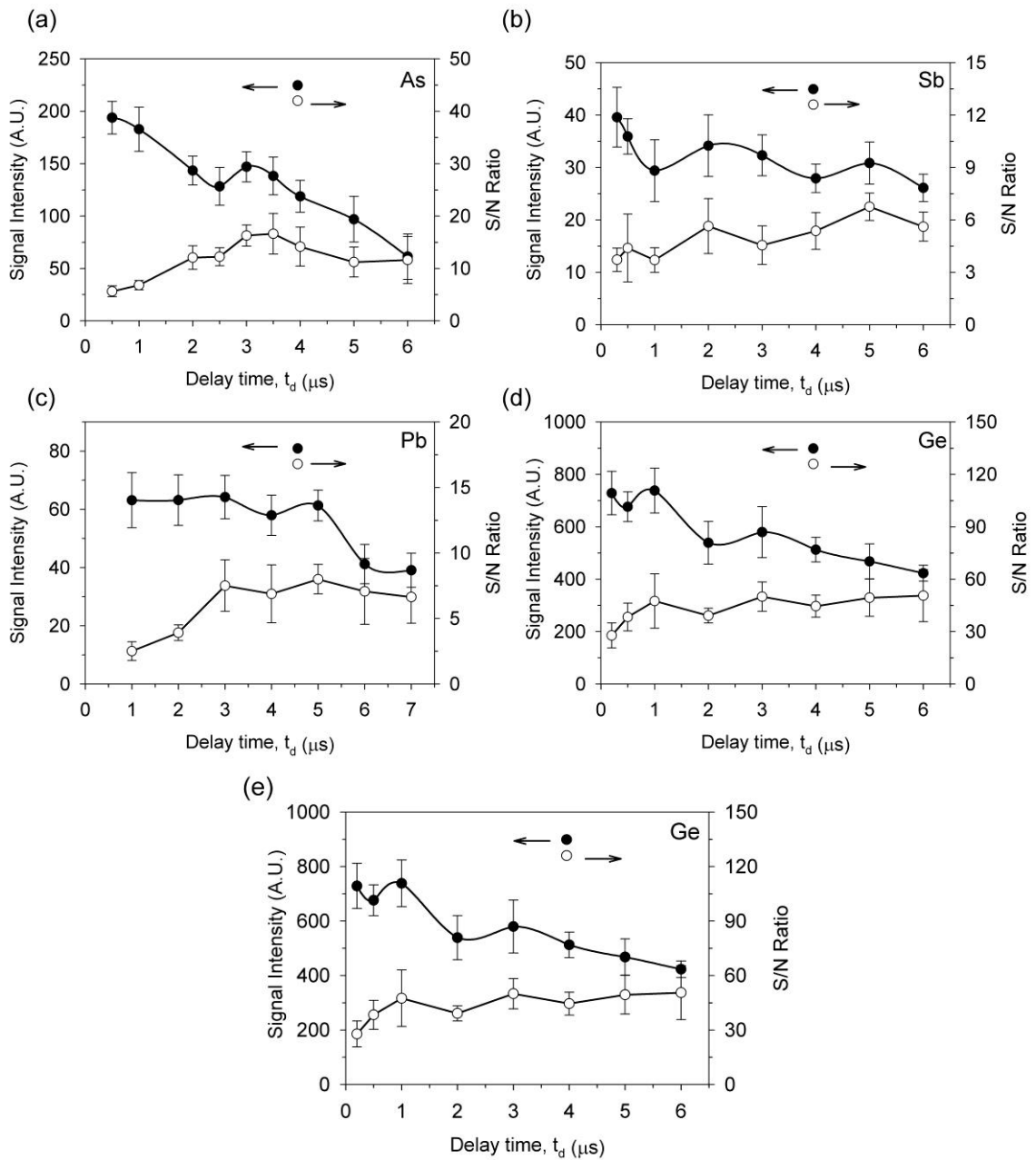
Figure 3.4. Variation of LIBS signal intensity with respect to detector gate width, t_g, for (a) Sn(I) 284.0 nm, (b) As(I) 278.0 nm, (c) Sb(I) 259.8 nm, (d) Pb(I) 405.8 nm and (e) Ge (I) 265.1 nm. Spectra recorded from, 5.0 mg L^{-1} Sn, 20.0 mg L^{-1} As^{3+}, 100.0 mg L^{-1} Sb^{3+}, 20.0 mg L^{-1} Pb, and 20.0 mg L^{-1} Ge.

3.1.3.3. Laser Energy

Another important instrumental parameter that needs to be optimized in laser induced plasmas is the laser pulse energy (J pulse^{-1}) or the fluence (J cm^{-2}). A certain amount of energy needs to be transferred to the sample in order to exceed the breakdown threshold of the sample. This threshold level may vary with the type of the sample and the optics used to form the plasma. Once this specific threshold is exceeded, excess energy is used to enlarge the plasma.

Figure 3.5(a) exhibits the percentage absorption of laser energy by the SnH_4 plasma in nitrogen environment. The percentage of the pulse energy deposited into stannane plasma was quantified from pulse energy measurements between 80 and 175 mJ pulse^{-1} laser energy range. This energy range corresponds to average power density of 1.9–4.2 TW cm^{-2} for a diffraction limited beam size of 23 μm. As it is shown in Figure 3.5(a), the plasma absorbs 65% of the input pulse energy when 80 mJ pulse^{-1} laser energy is applied. Increasing input laser energy to 175 mJ pulse^{-1}, percentage absorption increases only up to 76%. This so called 'saturation effect' has been observed previously by some other researchers (Carranza and Hahn, 2002; Radziemski *et al.*, 1983). It can be explained that, after sufficient energy is deposited for ionization, excess energy is used to enlarge the size of the plasma rather than increasing the plasma temperature or electron density.

Effect of laser energy on Sn signal intensity inN_2 environment is provided in Figure 3.5(b). From 80 mJ to 100 mJ pulse^{-1} energy, LIBS signal intensity was increased more than two times. However, after 100 mJ pulse^{-1} energy, no significant change in LIBS signal intensity was observed. Also, at high laser energies, RSD of the signal calculated for seven sequential measurements was quite high, ranging from 20% to 25%, due to increased shot to shot variation. However, experiments were performed at 150 mJ pulse^{-1} laser energies, to ensure complete breakdown for all laser shots.
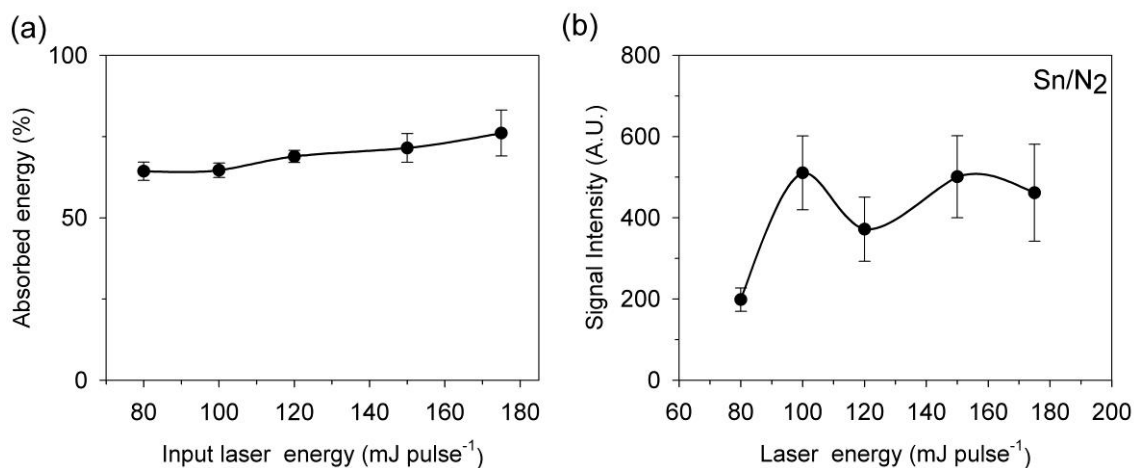
Figure 3.5. (a) Absorbed energy by the tin plasma under nitrogen gas with respect to input pulse energy. (b) Variation of Sn(I) line intensity at 284.0 nm as a function of laser pulse energy.(t_d: 10 μs, t_g: 3 ms, 10.0 mg L^{-1} Sn, 155 mL min^{-1} N$_2$, n=7).

In order to investigate the effect of laser energy on Sn under argon environment, plasma emission collected with 5.0 mL of Sn solution at laser energies from 60 to 175 mJ pulse^{-1}. Gate width and delay time was kept at 4.0 μs and 750.0 μs, respectively. In general, signal intensity of Sn(I) 284.0 nm line increases with increasing laser energy, however, no important change was observed between 60 – 80 mJ, while 40% increase was observed from 80 – 90 mJ (Figure 3.6(a)). This behaviour shows that the breakdown threshold of tin hydride plasma under argon is around 60 mJ per pulse. Signal intensity is continued to increase between 90 – 130 mJ and beyond 130 mJ no significant increase was observed. Therefore measurements were performed at laser energy of 130 mJ per pulse.

In the case of As, Sb and Ge, increasing laser pulse energy increases the emission intensity for all elements (Figure 3.6). After 100 mJ pulse^{-1} laser energy, deviation from the linearity could be attributed to the plasma shielding effect that was observed for arsenic, antimony and germanium. For arsenic and antimony optimum energy was selected to be 130 mJ pulse^{-1} and for germanium 160 mJ pulse^{-1} was used.

The variation of lead signal at 405.8 nm line intensity with respect to laser energy is given in Figure 3.6(d). Increasing laser energy from 60 mJ to 160 mJ lead emission signal also increases. Thus, the optimum laser energy is determined to be 150 mJ pulse^{-1}.
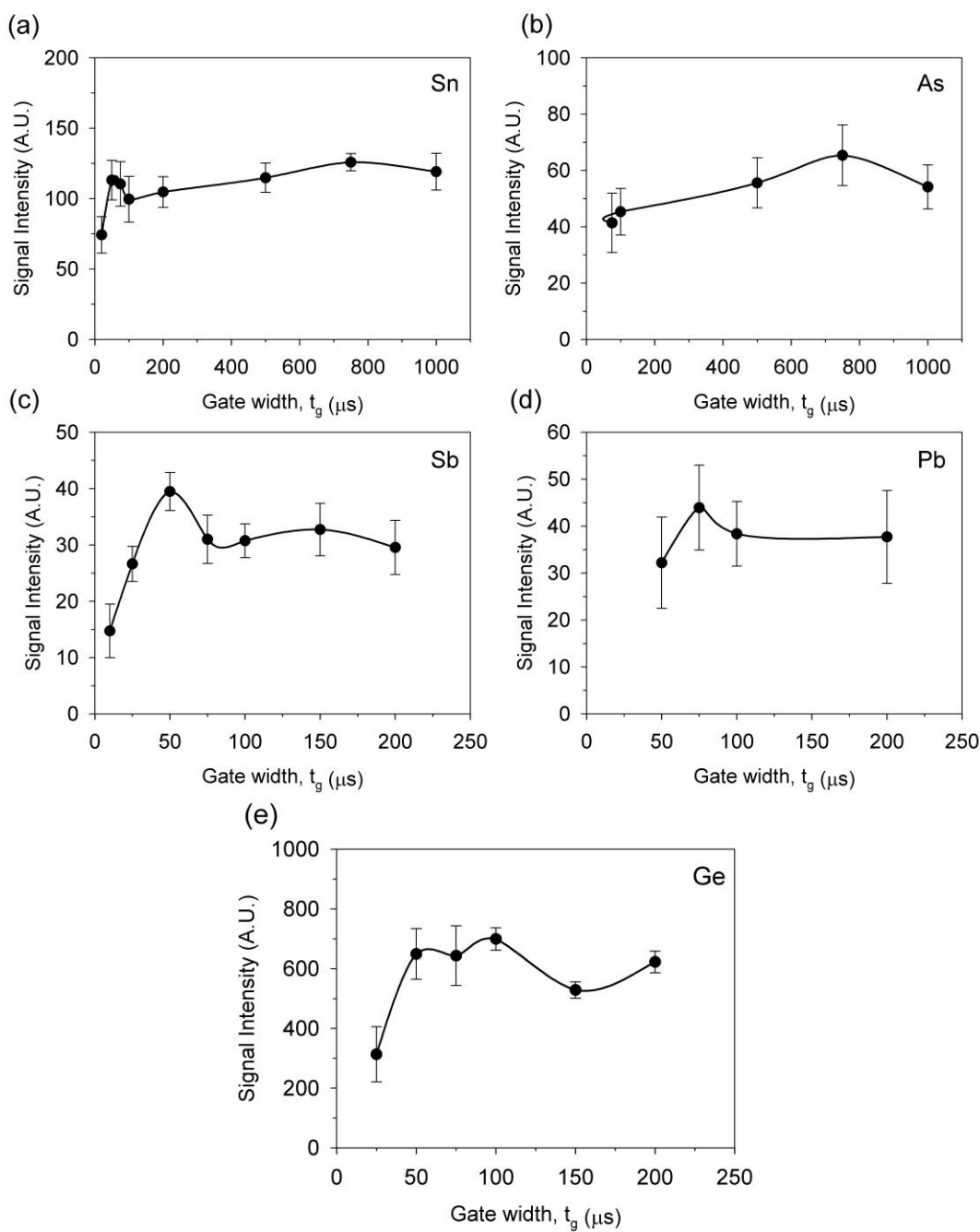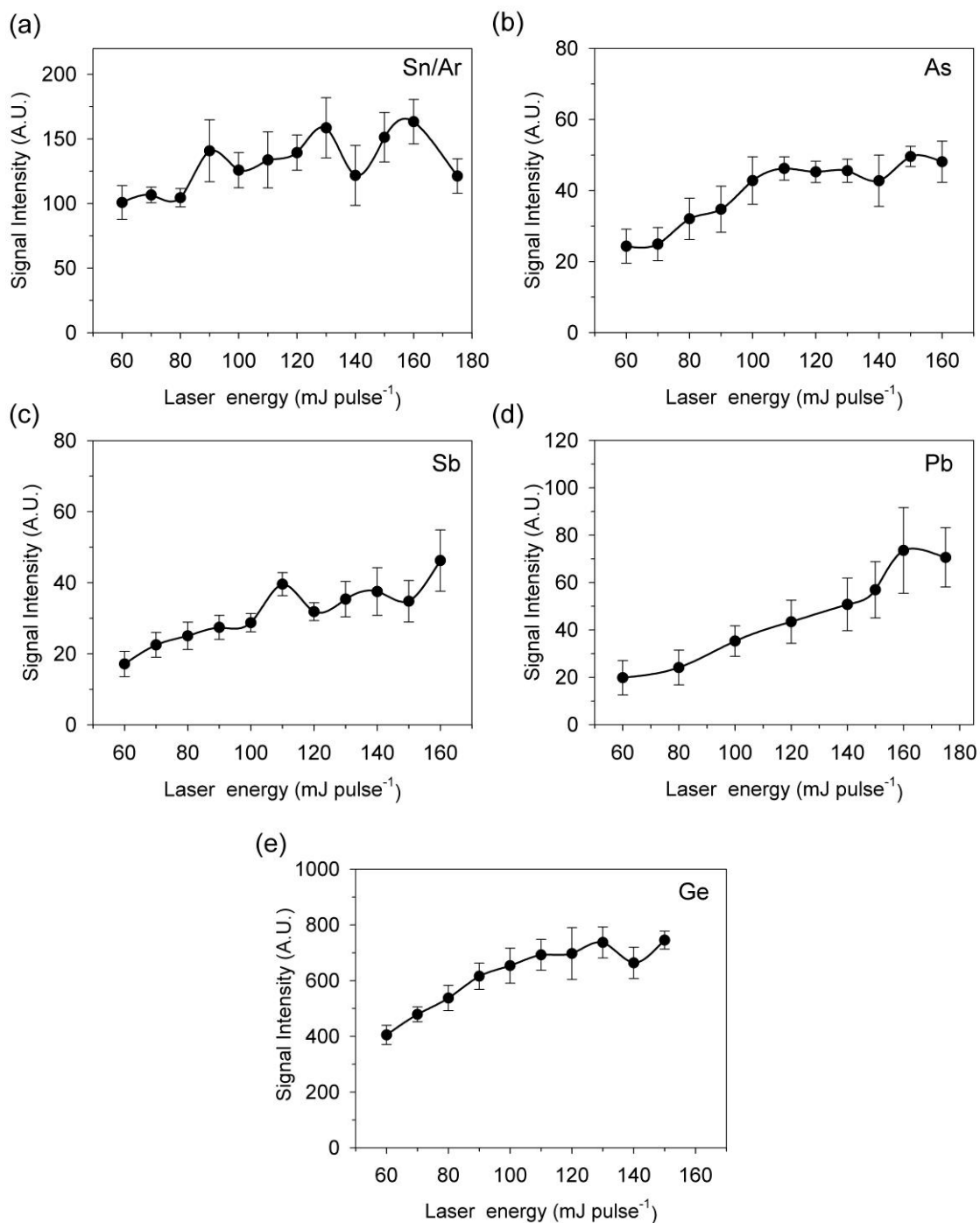
Figure 3.6. Variation of LIBS signal intensity with respect to laser energy for (a) Sn(I) 284.0 nm, (b) As(I) 278.0 nm, (c) Sb(I) 259.8 nm, (d) Pb(I) 405.8 nm and (e) Ge (I) 265.1 nm. Spectra recorded from, 5.0 mg L^{-1}, Sn, 20.0 mg L^{-1} As^{3+}, 100.0 mg L^{-1} Sb^{3+}, 20.0 mg L^{-1} Pb, and 20.0 mg L^{-1} Ge (n=5).

3.1.4. Chemical Parameters

It is very well known for decades that generation and transport of the volatile hydrides are very much dependent on some chemical parameters, such as acid and reductant concentration, presence of pre-reducing or oxidizing agent, acid and reductant flow rate, sample and carrier gas flow rate. For this purpose not only instrumental conditions, but also chemical parameters were also systematically investigated in order to maximize HG-LIBS signal.

3.1.4.1. Effect Oxidizing Agent Concentration on Lead Signal

Lead determination by hydride generation is known to be difficult due to the low yield and instability of plumbane (PbH_4). It was shown that the reaction rate and signal sensitivity could be increased by adding an oxidizing agent in the presence of acidic environment (Dedina and Tsalev, 1995).

Enhancement of lead signal by the addition of $K_3[Fe(CN)_6]$ has been reported (Tyson *et al*, 2000; D'Ulivo *et al.,* 2008; Brindle *et al.,* 1998). In this study, $K_3[Fe(CN)_6]$ was also used as an oxidizing agent for the analysis of lead by HG-LIBS.

In order to find optimum oxidizing agent concentration, 20.0 mg L^{-1} Pb solutions containing 2.0% HCl were prepared in the presence of 1.0%, 2.0%, 3.0%, and 4.0% (w/v) potassium hexacyanoferrate(III). A solution of 1.0% (w/v) $NaBH_4$ in 0.1% NaOH was used. As shown in Figure 3.7 the highest LIBS signal intensity at 405.8 nm Pb emission was obtained at 2.0% $K_3[Fe(CN)_6]$ containing solution.

However, during analysis of lead by HG-LIBS some problems have been encountered. It has been experimentally observed that, during plumbane generation, a vigorous reaction that occur between acid and $NaBH_4$ results with a visible foam formation and liquid carry over from the GLS due to excessive bubbling, which in turn negatively affect the reproducibility of the LIBS signal. Produced foam and bubbles are adsorbed on the walls of GLS and Teflon tubing that connects the GLS and membrane drying unit and a black deposition was observed after certain times of flow. For this reason in order to reduce the liquid carry over, the liquid level inside the GLS was kept below the tip of the gas flow so that the carrier gas blowing on the liquid surface rather than bubbling inside the liquid. At the end of the experiment the walls of waste pump

tubing and membrane dryer was covered with Prussian blue complex and this complex is also observed by other authors (Brindle *et al.,* 1998) and is identified as $(Fe_7(CN)_{18})$.
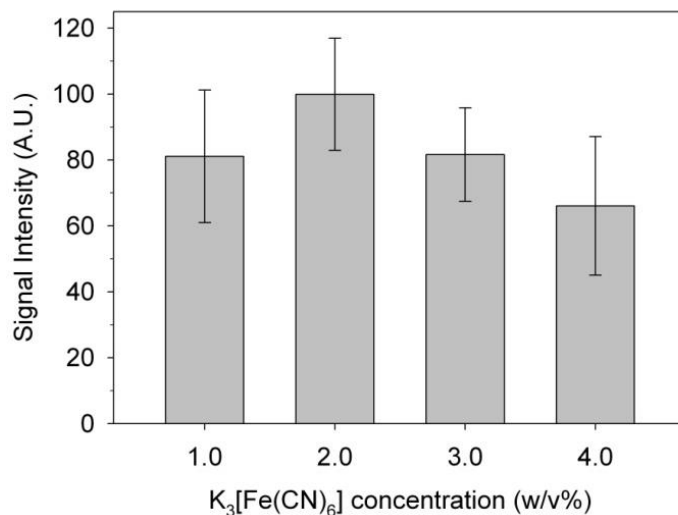
Figure 3.7. Effect of concentration of oxidizing agent on Pb(I) signal at 405.8 nm. 20.0 mg L^{-1} Pb in 2.0% HCl, 1.0% $NaBH_4$ in 0.1% NaOH, t_d: 5 μs, t_g: 100 μs, Carrier gas: 155 mL min^{-1} N_2, LE: 150 mJ $pulse^{-1}$.

3.1.4.2. Effect of L-cysteine Concentration on Antimony Signal

Instrumental parameters optimizations were performed using 100 mg L^{-1} Sb^{3+} solutions. Since this value is not a practical concentration we tried to maximize the signal intensity by adding a pre-reducing agent. In atomic spectroscopy, for the determination of antimony by hydride generation technique use of various pre-reducing agents namely KI, KI + ascorbic acid, thiourea, thiourea + ascorbic acid, L-cystine, and L-cysteine, have been shown (Moreda-Pineiro *et al.,* 2001; Cava-Montesinos *et al.,* 2003; Kratzer and Dedina, 2008; Matusiewicz and Mariusz, 2006; Feng and Fu, 19988; Feng *et al.,* 1999; D'Ulivo *et al.,* 1995). Although the main purpose of using pre-reducing agent is to reduce Sb(3+) to Sb(5+), it has been demonstrated that Sb(3+) signal is also increased significantly by adding L-cysteine in the presence of some mineral acid mixtures (D'Ulivo *et al.,* 1995). In this study, the possibility of increasing Sb(3+) signal by the addition of L-cysteine was investigated. In literature the common concentration range of L-cysteine is 0.3% - 2.0% (w/v). As a starting point, 100.0

mg L^{-1} Sb^{3+} prepared in the presence of 2.0% L-cysteine and plasma emission from stibine plasma was collected. As seen from the Figure 3.8(a), in the presence of 2.0% L-cysteine Sb^{3+} signal was increased two times.

After this observation a detailed study was performed in order to optimize L-cysteine concentration. Solutions of 100.0 mg L^{-1} Sb^{3+} were prepared in the presence of L-cysteine at a concentration range of 0.2%-5.0% (w/v). 100.0 mg L^{-1} Sb^{3+} solutions contained 2.0% HCl and reducing solutions of 1.0% NaBH4 in 1.0% NaOH were used. Carrier gas and sample flow rate, delay time, gate time and laser pulse energy was optimized as 160 mL min^{-1}, 2.5 mL min^{-1}, 2 μs, 50 μs and 100 mJ; respectively. Increasing L-cysteine concentration from 0.2% to 0.5% increased the Sb(I) signal by more than two times, while from 1.0% to 5.0% Sb signal started to decrease linearly (Figure 3.8(b)). Optimum value was obtained as 0.5% L-cysteine.
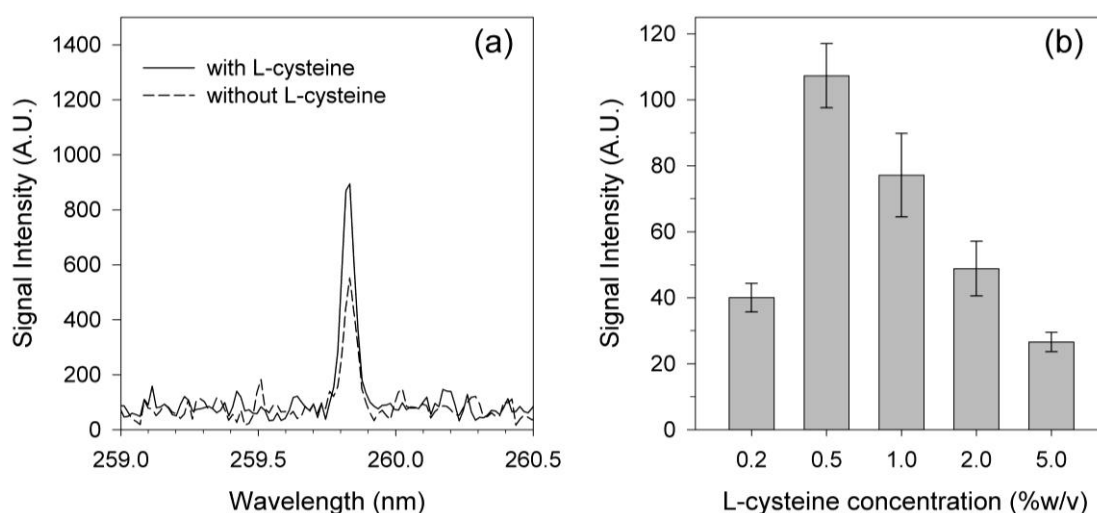
Figure 3.8. Effect of (a) presence and (b) concentration of L-cysteine on Sb(I) signal at 259.8 nm. 100.0 mg L^{-1} Sb^{3+} in 2.0% HCl, 1.0% $NaBH_4$ in 1.0% NaOH, t_d: 2.0 μs, t_g:50 μs, carrier gas: 160 mL min^{-1} Ar, LE: 100 mJ $pulse^{-1}$.

3.1.4.3. HCl and $NaBH_4$ Concentration

In this study, most widely used acid, hydrochloric acid, was employed for acid optimization studies. In order to investigate effect of HCl concentration, hydride forming element solutions were prepared in the presence of various acid concentrations

and plasma emission signal was collected from each element under optimum instrumental conditions. Variation of Sn, As, Sb, Pb and Ge signal emission in relation to acid concentration is provided in Figure 3.9. Each data point indicates an average of 10 replicate measurements with 10 shot accumulation.

In order to examine effect of acid concentration on tin signal, Sn solutions containing 0.1%, 0.2%, 0.5%, 1.0%, 1.5%, 2.0% and 2.5% (v/v) HCl were prepared and reacted with sodium borohydride solution. Figure 3.9(a) and (b) shows the effect of HCl concentration on tin signal in nitrogen and argon environment. In the presence of nitrogen, Sn signal increased up to 1.0% HCl and showed a little variation between 1.0% and 2.5% concentration. In the presence of argon, increasing HCl concentration from 0.2% to 1.0%, Sn signal increased by 60% while acid concentration higher than 1.0% decreased the signal intensity. Thus for Sn analysis 1.0% HCl was used in the presence of both gases.

Acid optimization studies for arsenic was performed using 20.0 mg L^{-1} As^{3+} solution containing various concentrations of HCl in the range of %0.1 - %2.5 (v/v). These solutions and 2.0% $NaBH_4$ solution in 0.2% sodium hydroxide were delivered to the T-connector where the reaction started by means of pump at a flow rate of 2.5 mL min^{-1} and 5.0 mL min^{-1}; respectively. Produced AsH_3 gas was transported with an argon carrier gas at a flow rate of 126 mL min^{-1} to the membrane dryer and then to the plasma/sample cell. The arsine gas interacted with the incoming laser beam at 130 mJ per pulse energy and plasma emissions were collected at 3.0 μs delay time, and 0.75 ms gate width. Arsenic signal intensity with respect to acid concentration is provided in Figure 3.9(c). It was seen that arsenic signal is not affected significantly by increasing acid concentration from 0.2% to 1.0% while at higher concentration signal was decreased. As an optimum value 1.0% HCl was used for the rest of the study.

The graph of HCl concentration with respect to antimony LIBS signal is given in Figure 3.9(c). The signal was obtained from 40.0 mg L^{-1} Sb^{3+} in 0.5% L-cysteine. Antimony signal decreased when acid concentration was changed from 0.8% to 1.0% while an increase was observed from 1.0% to 2.0% and beyond this value the signal started to decrease again. Therefore 2.0% HCl was determined as an optimum acid concentration.

For the investigation of the effect of acid concentration on LIBS signal, 20.0 mg L^{-1} lead containing solution in 2.0 (w/v %) $K_3[Fe(CN)_6]$ was prepared in various HCl concentrations ranging from 1.0% to 3.0% (v/v). Emission spectra were collected

at laser energy of 150 mJ, at 5.0 μs delay time and 100 μs gate width. In this study a solution of 1.0% $NaBH_4$ was used. Figure 3.9(e) shows the variation of Pb signal at 405.8 nm with respect to acid concentration. Pb signal increases with increasing HCl concentration from 1.0% to 2.5% while the signal decreases at 3.0% acid concentration. Thus, optimum acid concentration was selected as 2.5% HCl.

The effect of acid concentration was investigated using 20.0 mg L^{-1} Ge in differing concentration of HCl solution and 1.0% $NaBH_4$ solution prepared in 0.2% sodium hydroxide. Germanium signal intensity with respect to acid concentration is provided in Figure 3.9(f). Increasing HCl concentration from 0.2% to 1.0% resulted in a sharp increase in germanium signal and at 1.5% HCl concentration signal decreased drastically and continued to decrease slowly up to 3.0%. Thus 1.0% HCl was selected as an optimum acid concentration for germanium.

Other parameter that affects the efficiency of hydride generation is the concentration of reductant solution. In order optimize concentration of reductant solutions, sodium borohydride solutions with different strength were prepared and made alkaline with sodium hydroxide for stability. These reductant solutions and analyte solutions prepared in HCl were reacted and delivered to the GLS. Plasma emissions were collected as a function of concentrations of $NaBH_4$ solutions. Signal intensity evaluated from peak area against concentration of sodium borohydride presented in Figure 3.10(a–f).

Figure 3.10(a) shows the effect of reductant concentration on the efficiency of tin hydride generation under nitrogen environment. As seen from the figure there is a marked increase in hydride production with increasing $NaBH_4$ concentration up to 2.0% and maximum LIBS signal was obtained at 5.0% $NaBH_4$ concentration. In cases where better detection limits are not required, 2.0% $NaBH_4$ with slightly lower sensitivity was employed in order to reduce $NaBH_4$ consumption. HCl concentration was kept at 1.0% and N_2, as a carrier gas, with a flow rate of 155 mL per min was used.

Variation of Sn signal under argon environment with respect to reductant solutions ranging from 0.05% − 2.5% (w/v) exhibited in Figure 3.10(b). There was approximately three times increase in signal intensity when $NaBH_4$ concentration was increased from 0.05% to 0.5%. Since there is no significant difference from 0.5% to 2.0% $NaBH_4$, 1.0% was selected as an optimum concentration.

The optimization studies for arsenic were performed using 20.0 mg L^{-1} As^{3+} in 1.0% HCl, 130 mJ laser energy, 3.0 μs delay time, 0.75 ms gate width and 126 mL

min^{-1} argon. NaBH$_4$ concentration was varied from 0.05% to 2.5% (w/v) and As signal intensity at 278.0 nm versus reductant concentration was evaluated. The plot of signal intensity against NaBH$_4$ concentration is given in Figure 3.10(c). Increasing NBH$_4$ concentration from 0.05% to 0.5% increases arsenic signal two times. At higher concentrations signal was decreased. Thus remaining studies were performed with 0.5% NaBH$_4$.

In order to optimize reductant concentration for antimony analysis, 0.1%, 0.2%, 0.5%, 1.0%, 1.5%, 2.0%, and 2.5% (w/v) NaBH$_4$ were prepared in 1.0% NaOH and delivered to the GLS at a flow rate of 5.0 mL min^{-1}. A solution of 40.0 mg L^{-1} Sb^{3+} in 2.0% HCl and 0.5% L-cysteine was prepared from the stock solution and introduced at a flow rate of 2.5 mL min^{-1}. SbH$_3$ resulting from the hydrides reaction was purged with 160 mL min^{-1} Ar, and then interacted with 100 mJ laser pulse energy. Signal intensity at 259.8 nm versus NaBH$_4$ concentration is represented in Figure 3.10(d). As seen from the figure, there was a sharp increase in signal intensity when NaBH$_4$ concentration was increased from 0.1% to 1.0% while the signal was decreased slowly from 1.0% to 2.5%. A concentration of 1.0% NaBH$_4$ was selected as an optimum value.

For the investigation effect of NaBH$_4$ concentration on Pb signal, five different NaBH$_4$ solutions were prepared at a range of 0.05% - 4.0% (w/v) and made alkaline with 0.1% NaOH for stability. This study was performed using 20.0 mg L^{-1} Pb in 2.0% K$_3$[Fe(CN)$_6$] and 2.5% HCl, laser energy and carrier gas (nitrogen) flow rate were kept at 150 mJ and 155 mL per min, respectively Increasing reductant concentration from 0.5% to 1.0%, Pb signal at 405.8 nm also increased and beyond 1.0%, Pb signal decreased drastically and remained unchanged for 3 and 4% (Figure 3.10(e)). Optimum reductant concentration was found to be 1.0% for lead.

The effect of NaBH$_4$ concentration on Ge signal at 265.1 nm can be seen in Figure 3.10(f). In this study spectra were recorded from 20.0 mg L^{-1} Ge in 1.0% HCl, 130 mJ laser energy, 1.0 μs delay time, 100 μs gate width and 126 mL min^{-1} argon gas. Increasing of NaBH$_4$ concentration from 0.05% to 0.2% resulted in an increase in germanium signal while after 0.2% signal started to decrease. Thus, study of effect of sodium borohydride concentration on germanium signal showed that maximum signal could be obtained with 0.2% NaBH$_4$ solution.
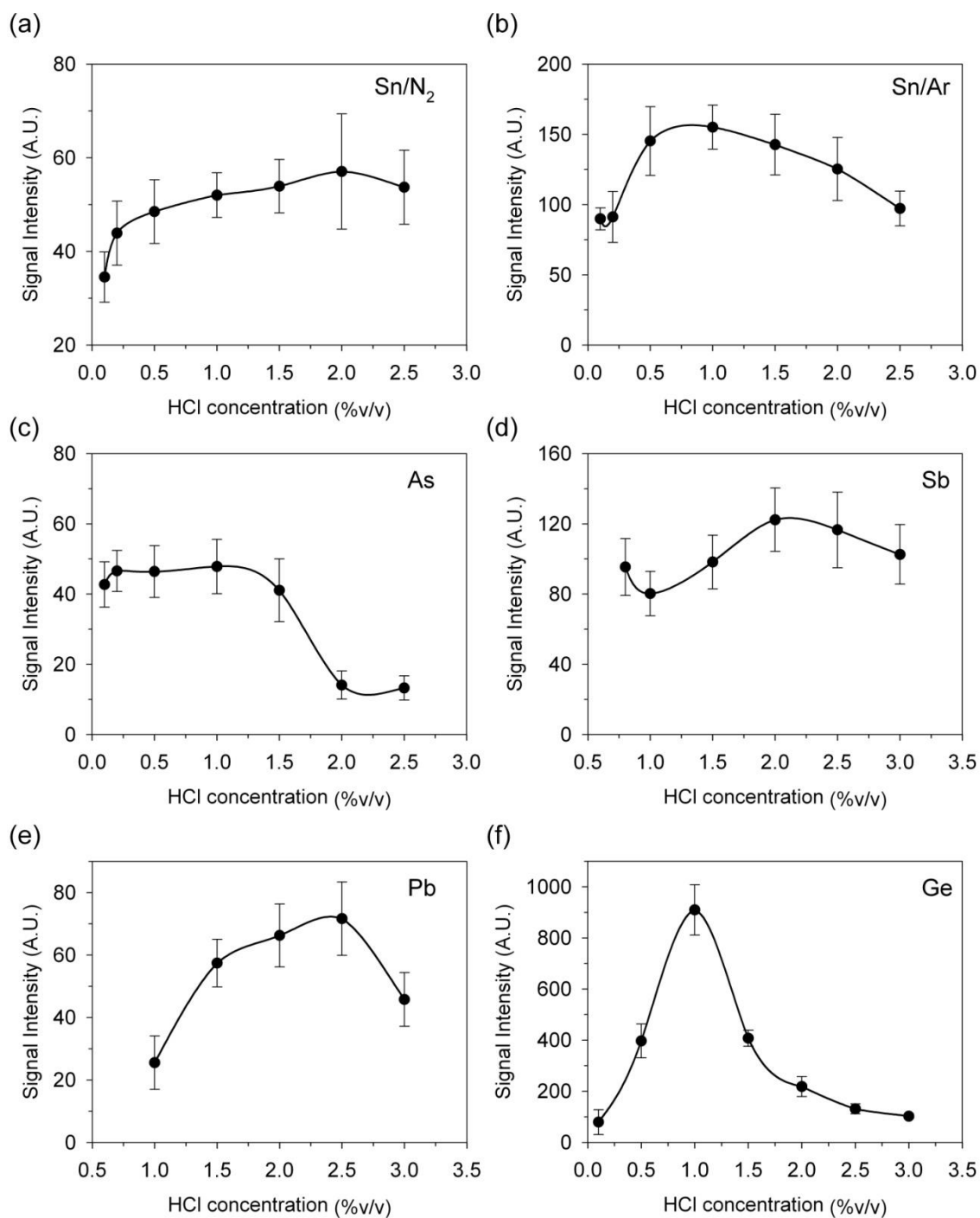
Figure 3.9. Variation of LIBS signal intensity with respect to hydrochloric acid concentration for (a) Sn(I) 284.0 nm under N_2, (b) Sn(I) 284.0 nm under Ar, (c) As(I) 278.0 nm, (d) Sb(I) 259.8 nm, (e) Pb(I) 405.8 nm and (f) Ge(I) 265.1 nm. Spectra recorded from, 5.0 mg L^{-1} Sn, 20.0 mg L^{-1} As^{3+}, 40.0 mg L^{-1} Sb^{3+}, 20.0 mg L^{-1} Pb, and 20.0 mg L^{-1} Ge (n=10).
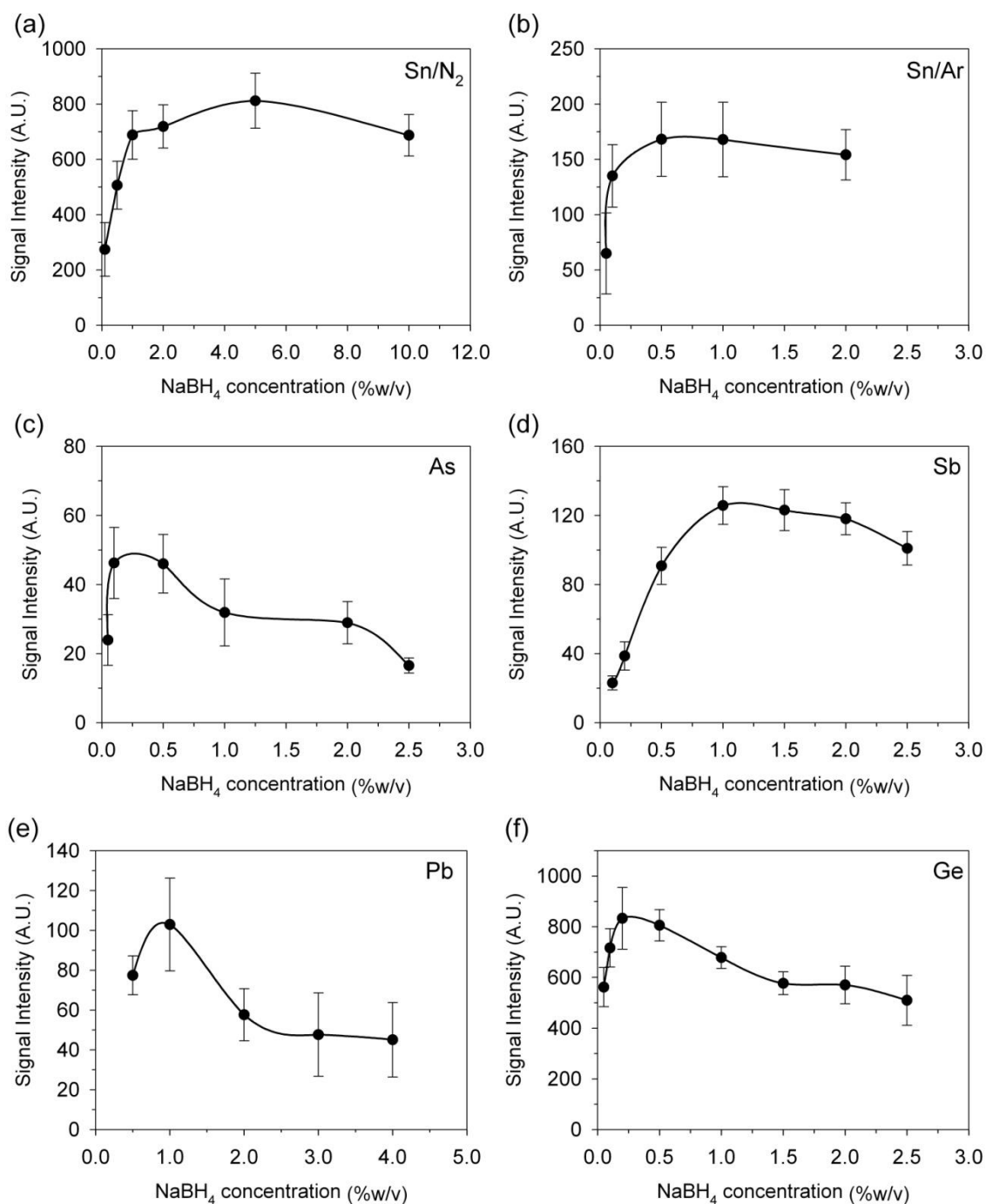
Figure 3.10. Variation of LIBS signal intensity with respect to reductant (NaBH$_4$) concentration for (a) Sn(I) 284.0 nm under N$_2$, (b) Sn(I) 284.0 nm under Ar, (c) As(I) 278.0 nm, (d) Sb(I) 259.8 nm, (e) Pb(I) 405.8 nm and (f) Ge (I) 265.1 nm. Spectra recorded from 20.0 mg L^{-1} As^{3+}, 40.0 mg L^{-1} Sb^{3+}, 20.0 mg L^{-1} Pb, and 20.0 mg L^{-1} Ge (n=10).

3.1.4.4. Sample and Carrier Gas Flow Rates

Other investigated parameters were sample and carrier gas flow rates. Acidified sample and reductant solutions were delivered to the GLS by means of a peristaltic pump in a continuous flow. Optimization of sample and reductant flow rates is essential for efficient hydride reaction.

Analyte solutions and reagents were introduced to the GLS continuously by using a peristaltic pump. The ratio of acidified sample to the reductant flow rate was kept at 1:2 by selecting an appropriate tubing size. Sample flow rate was adjusted to a desired flow rate by controlling the rpm of the pump. The variation of analyte signal was evaluated at a flow rate of 1.0 mL min^{-1} (3.673 rpm), 2.5 mL min^{-1} (9.054 rpm) and 4.0 mL min^{-1} (14.82 rpm). Resulting graph is presented in Figure 3.11(a-f). Typically, increasing sample flow rate increases the signal strength due to the increased amount of analyte loading into the GLS. A sharp increase in tin, lead and germanium signal from 1.0 mL min^{-1} to 2.5 mL min^{-1} was observed, however at 4.0 mL min^{-1} no noticeable increase could be seen (Figure 3.11(a, b and e)). In the case of arsenic signal increased linearly with increasing sample flow rate (Figure 3.11(c)). For antimony signal no important change is obtained with varying sample rate. In order to eliminate condensation of hydrides and prevent over consumption of sample and reagent 2.5 mL min^{-1} sample flow rate was selected as optimum for all elements.

Although they are volatile, fast and efficient transport of the hydrides from reaction medium to the sample cell is necessary for obtaining highly sensitive measurements. Both the type and the flow rate of the carrier gas have significant influence on the signal strength. As discussed in Section 3.1.2 transportation of volatile SnH_4, AsH_3, SbH_3 and GeH_4 was performed by using argon, for SnH_4, and PbH_4 nitrogen gas was used. In order to study the effect of carrier gas flow rate, analyte signal from each element at their maximum emission wavelength was recorded as a function of carrier gas flow rates. The Sn, As, Pb, Sb and Ge signal strength variation with respect to carrier gas flow rates is shown in Figure 3.12(a-f). Maximum signal was obtained at 155 mL min^{-1} N_2 for tin and lead. For Sn, As, Sb and Ge flow rates of 95.4 mL min^{-1}, 126 mL min^{-1}, 160 mL min^{-1} and 126 mL min^{-1} Ar was determined as optimum value, respectively.
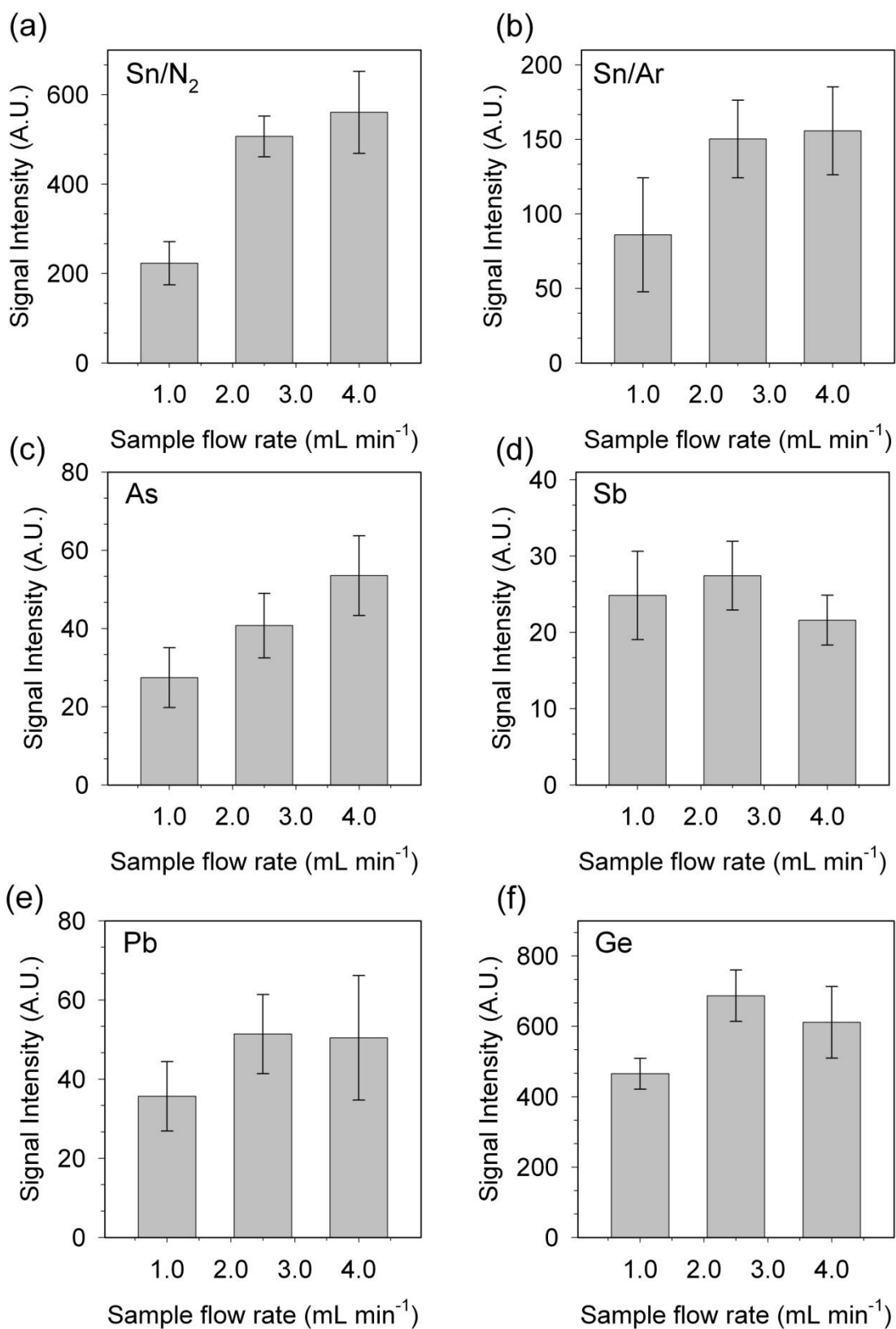
Figure 3.11. Effect of sample flow rate on (a) Sn(I) 284.0 nm under N_2, (b) Sn(I) 284.0 nm under Ar, (c) As(I) 278.0 nm, (d) Sb(I) 259.8 nm, (e) Pb(I) 405.8 nm and (f) Ge (I) 265.1 nm signal intensity.
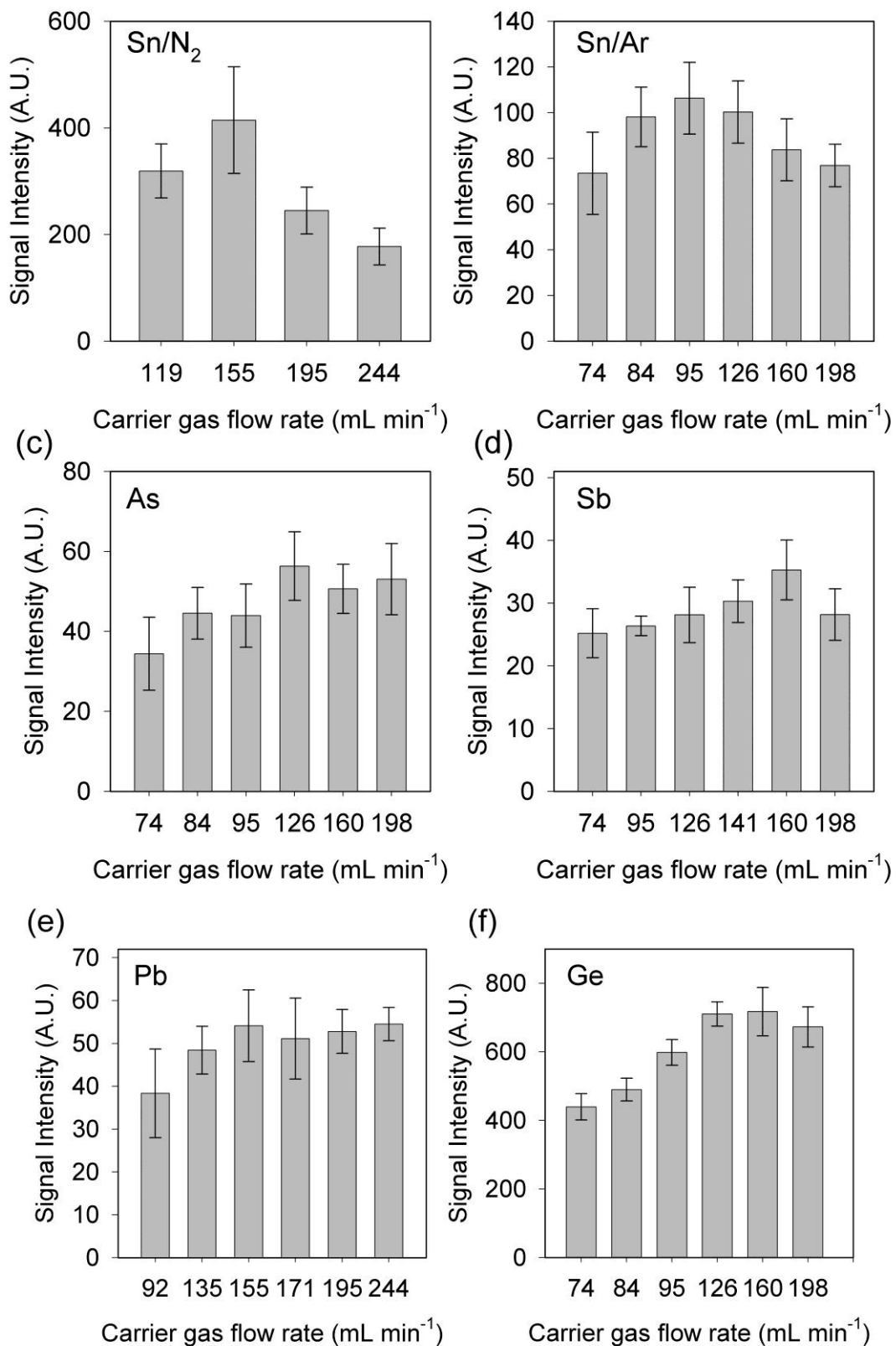
Figure 3.12. Effect of carrier gas flow rate on (a) Sn(I) 284.0 nm under N$_2$, (b) Sn(I) 284.0 nm under Ar, (c) As(I) 278.0 nm, (d) Sb(I) 259.8 nm, (e) Pb(I) 405.8 nm and (f) Ge (I) 265.1 nm signal intensity.

Optimum instrumental and chemical parameters for determination of Sn, As, Sb, Pb and Ge by HG-LIBS are summarized in Table 3.2.

Table 3.2. Optimum instrumental and chemical conditions of HG-LIBS system for Sn, As, Sb, Pb and Ge analysis.

	Sn		As	Sb	Pb	Ge
Carrier Gas type	N_2	Ar	Ar	Ar	N_2	Ar
Spectral line (nm)	284.0	284.0	278.0	259.8	405.8	265.1
Laser energy (mJ pulse^{-1})	150	130	130	160	150	130
Delay time, t_d (µs)	10.0	4.0	3.0	2.0	5.0	1.0
Gate width, t_g (µs)	3000	750	750	50	100	100
$NaBH_4$ conc. (w/v, %)	2.0	1.0	0.5	1.0	1.0	0.2
$NaBH_4$ flow rate (mL min^{-1})	5.0	5.0	5.0	5.0	5.0	5.0
HCl conc. (v/v, %)	1.0	1.0	1.0	2.0	2.5	1.0
Sample flow rate (mL min^{-1})	2.5	2.5	2.5	2.5	2.5	2.5
Pre-reducing/oxidizing agent conc. (w/v, %)	-	-	-	0.5[†]	2.0[‡]	-
Carrier gas flow rate (mL min^{-1})	155	95.4	126	160	155	126

[†] L-cysteine was used as a pre-reducing agent.
[‡] $K_3[Fe(CN)_6]$ was used as an oxidizing agent.

3.1.4.5. Hydride Conversion Efficiency

After optimization of chemical parameters hydride conversion efficiency was investigated. For this purpose 10.0 mg L^{-1} Sn in 1.0% (v/v) HCl and 2.0% (w/v) $NaBH_4$ in 1.0% (w/v) solutions were delivered to the GLS at a flow rate of 2.5 mL min^{-1} and 5.0 mL min^{-1}, respectively. After that, liquid waste was collected and analyzed with ICP-MS in order to find the concentration of tin in the waste solution. It was found that 99% of the analyte was transported into the gaseous phase while lower than 1% of the analyte remained in the waste liquid.

3.2. Representative LIBS Spectra under Optimum Conditions

Representative LIBS spectra from stannane, arsine, stibine, plumbane and germane plasma obtained under optimal instrumental and chemical conditions between 200 and 850 nm spectral intervals are given in Figure 13, 14, 15, 16 and 17, respectively. Each spectrum acquired from the accumulation of 10 laser shots. For almost all elements analyzed, several neutral emission lines could be observed, but no ionic lines were detected. The reason for that could be the use of large gate width, in which ionic lines disappear due to ion electron recombination process. Detailed spectra representing neutral atomic emission lines of interests are provided as insets of each figure.

Figure 3.13 indicates a representative spectrum from stannane plasma in argon environment. The peaks given in the figure (242.2 nm, 242.9 nm, 270.6, 284.0 nm, 300.9 nm, 303.4 nm, 317.5 nm, and 326.3 nm) correspond to the neutral emission lines of Sn(I) and well consistent with NIST atomic spectral database. Typical spectrum obtained from stannane plasma under nitrogen environment is provided in Appendix B.

In Figure 3.14, neutral As(I) lines at 228.8 nm, 235.0 nm, 274.5 nm, 278.0 nm, and 286.0 nm are given.

Representative spectrum from SbH_3 is shown in Figure 3.15 shows four neutral emission lines of Sb(I) at 252.8 nm, 259.8 nm, 277.0 nm, and 287.8 nm.

Three neutral emission lines of Pb(I) at 280.2 nm, 368.4 and 405.8 nm were provided in Figure 3.16. Besides, a well resolved sodium doublet emission at 589.0 and 589.6 nm and potassium doublet at 766.5 nm and 769.9 nm were also observed. Presence of these lines in the spectra indicates Na and K transport from GLS to the Teflon plasma cell along with the gaseous hydrides.

Figure 3.17 include seven neutral emission lines of germanium at 259.2 nm, 265.1 nm, 269.1 nm, 270.9 nm, 275.4 nm, 303.9 nm and 326.9 nm, which makes germanium a strong candidate to be used as a temperature sensor.

All spectra are strongly dominated by the neutral hydrogen line, Hα, at 656.3 nm which is produced from the dissociation of the metal hydrides under intense laser beam. Some argon and nitrogen emission lines in the far end of the visible region are also observed.

Quantitative measurements of Sn, As, Sb, Pb and Ge were performed at their most sensitive wavelengths of 284.0 nm, 278.0 nm, 259.8 nm, 405.8 nm and 265.1 nm, respectively.
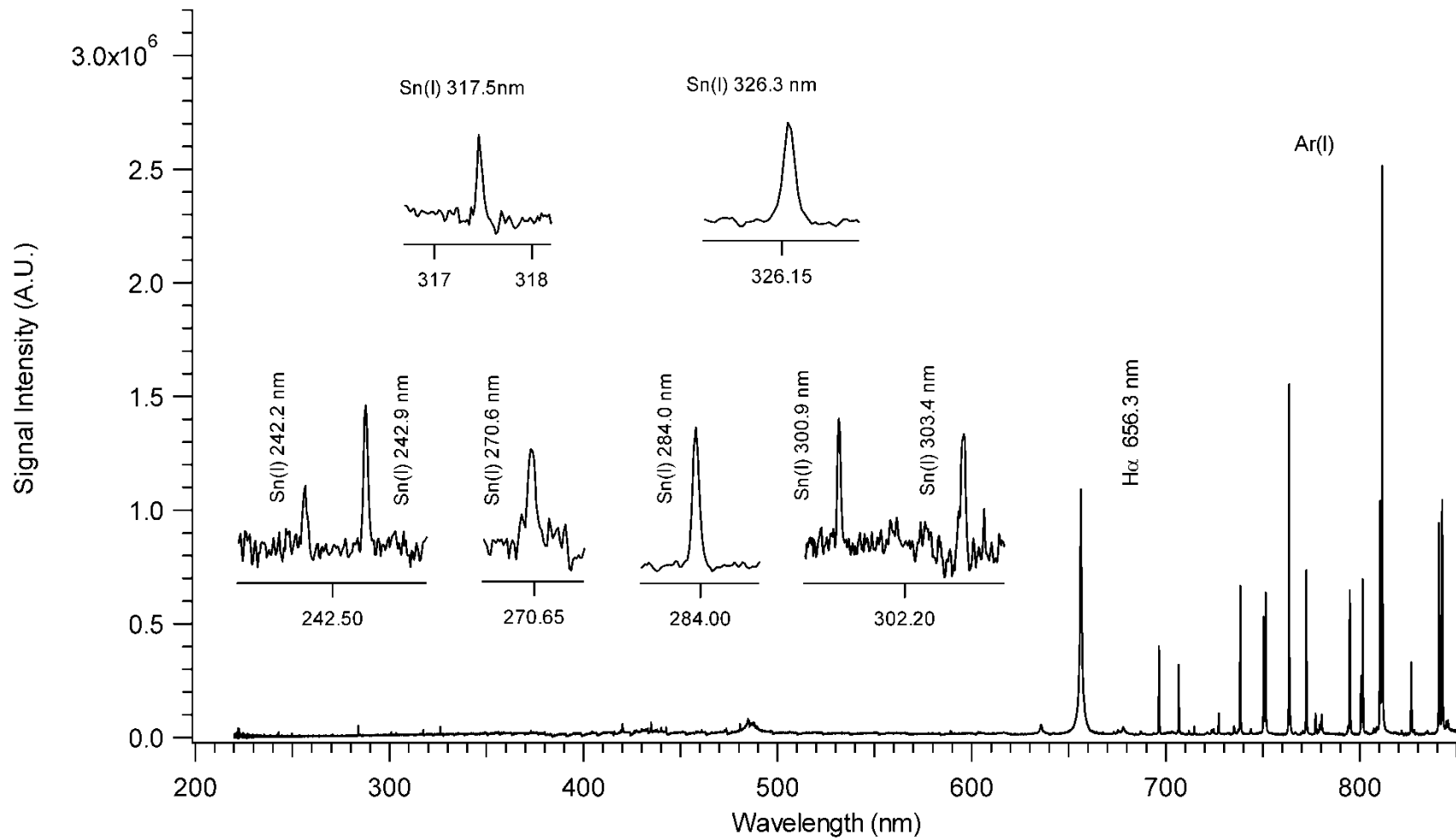
Figure 3.13. Representative HG-LIBS spectrum recorded from SnH_4 plasma under optimum experimental conditions. Spectrum recorded from 20.0 mg L^{-1} Sn.
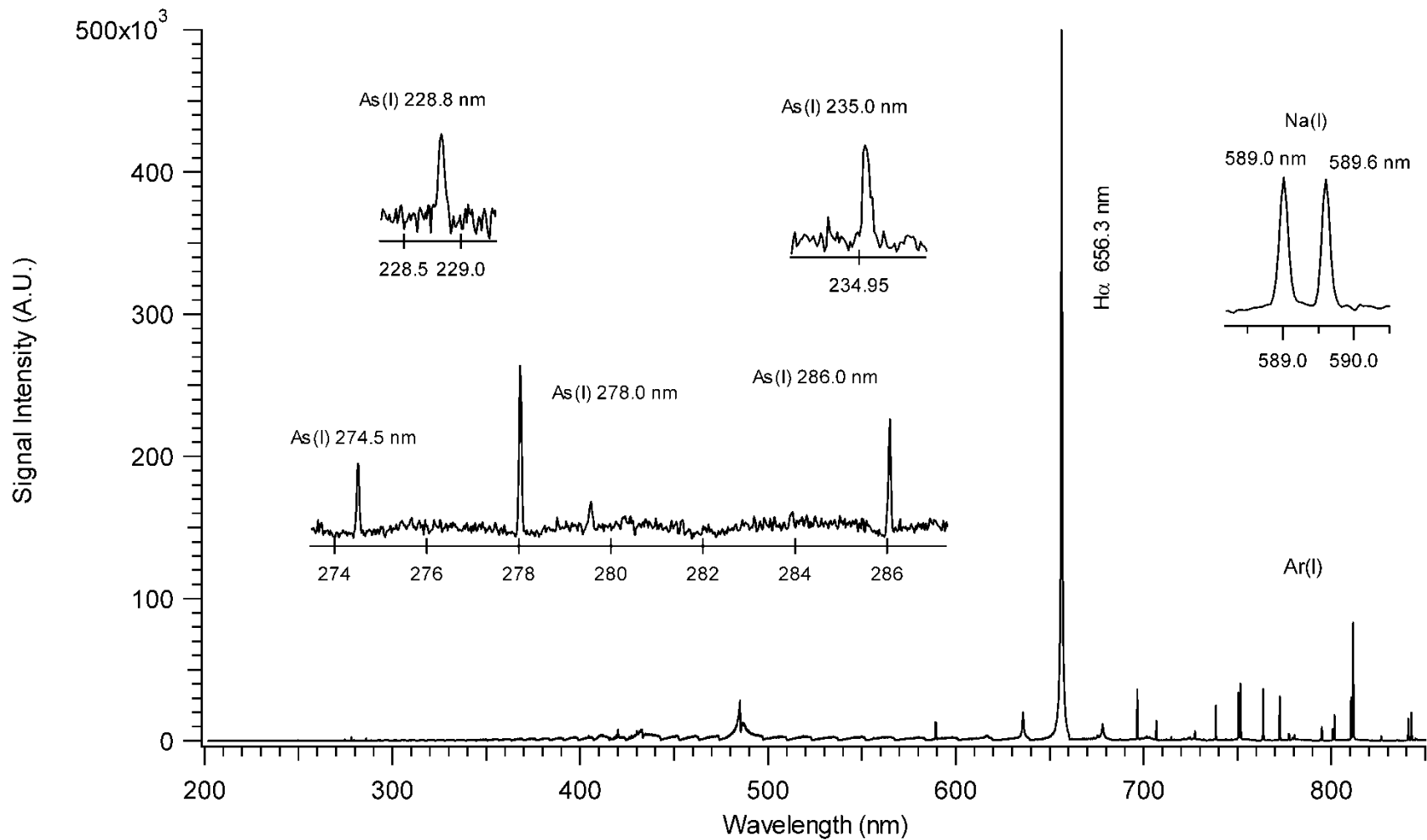
Figure 3.14. Representative HG-LIBS spectrum recorded from AsH₃ plasma under optimum experimental conditions. Spectrum recorded from 40.0 mg L⁻¹As.
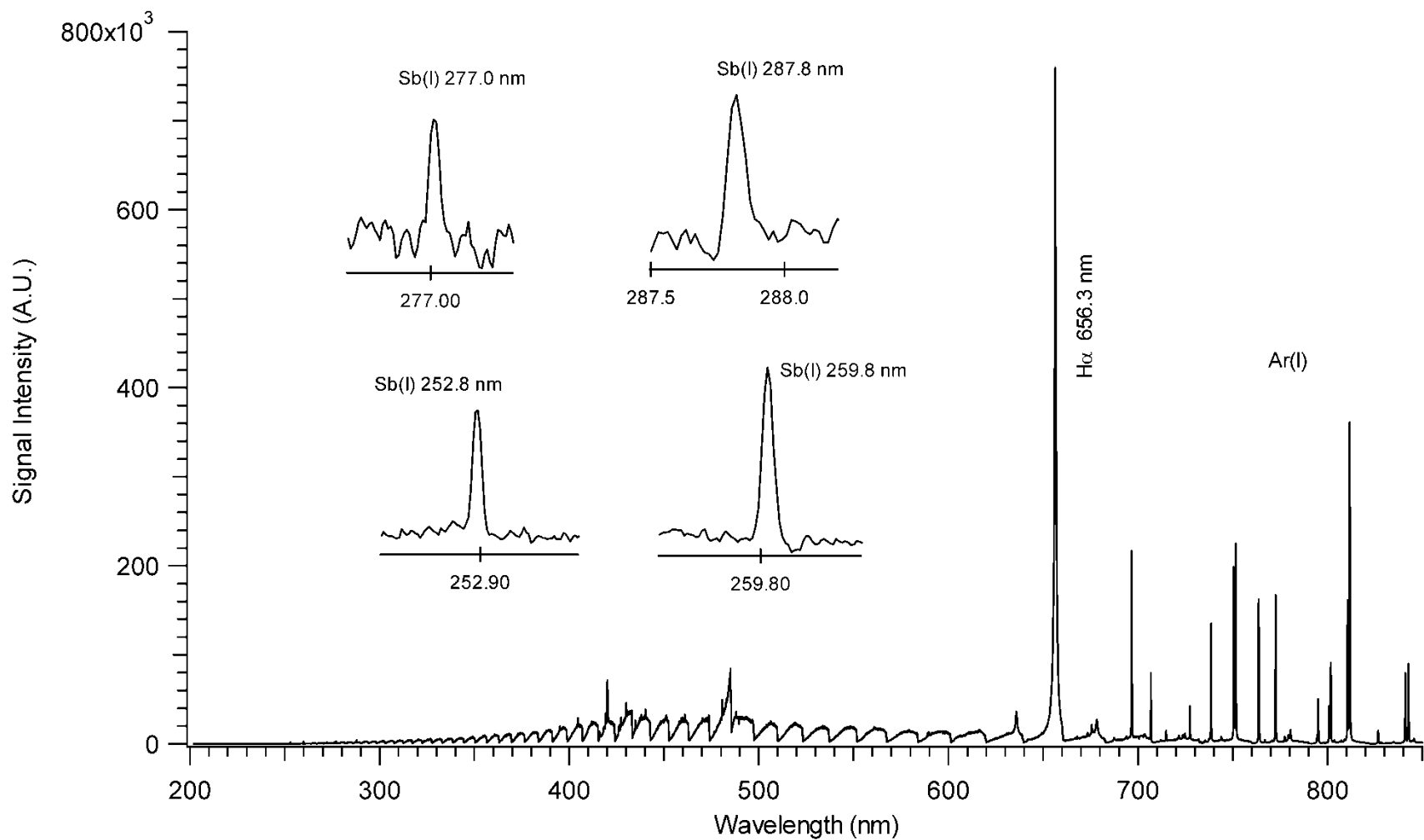
Figure 3.15. Representative HG-LIBS spectrum recorded from SbH$_3$ plasma under optimum experimental conditions. Spectrum recorded from 50.0 mg L^{-1} Sb.
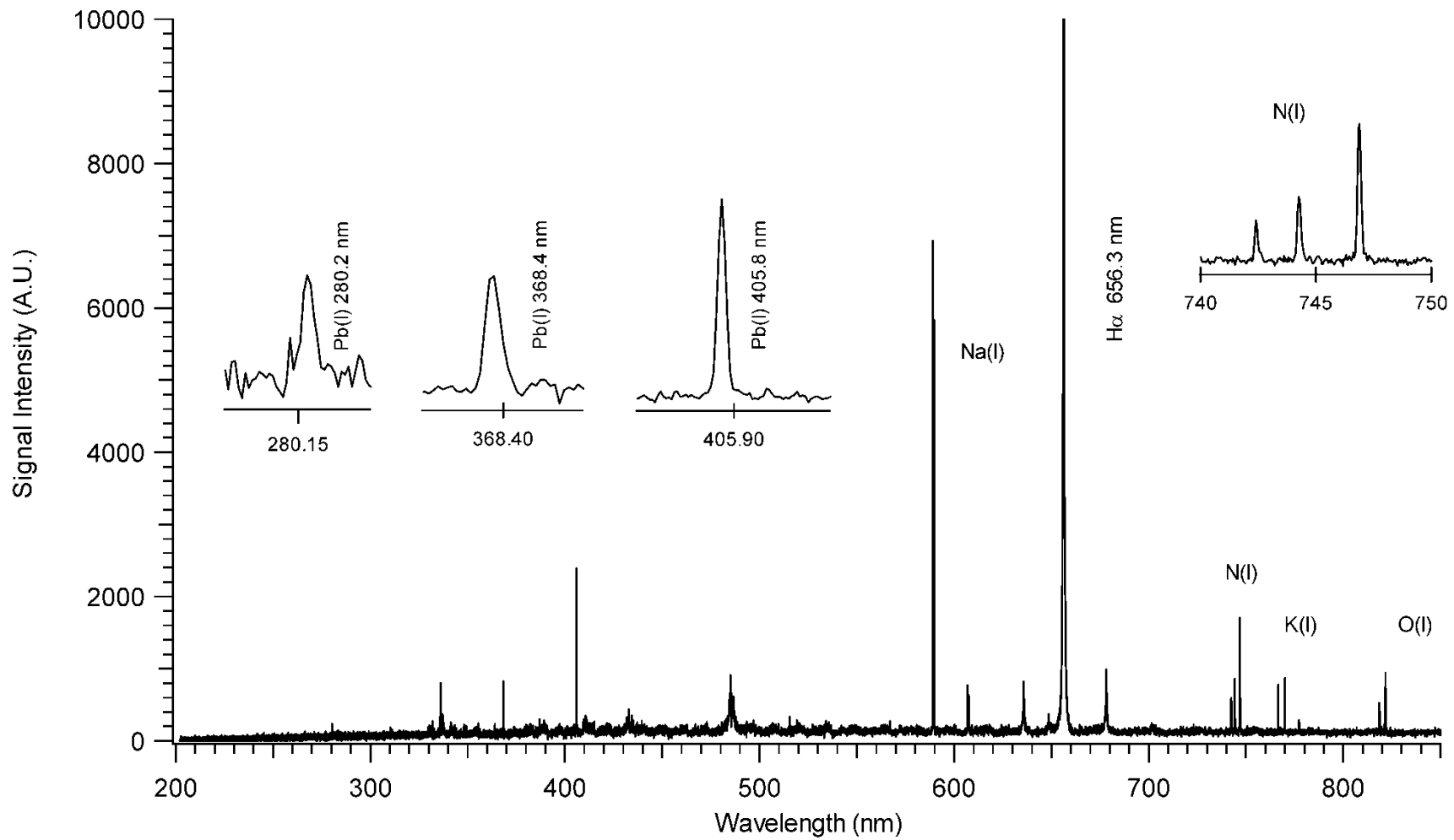
Figure 3.16. Representative HG-LIBS spectrum recorded from PbH$_4$ plasma under optimum experimental conditions. Spectrum recorded from 50.0 mg L^{-1} Pb.
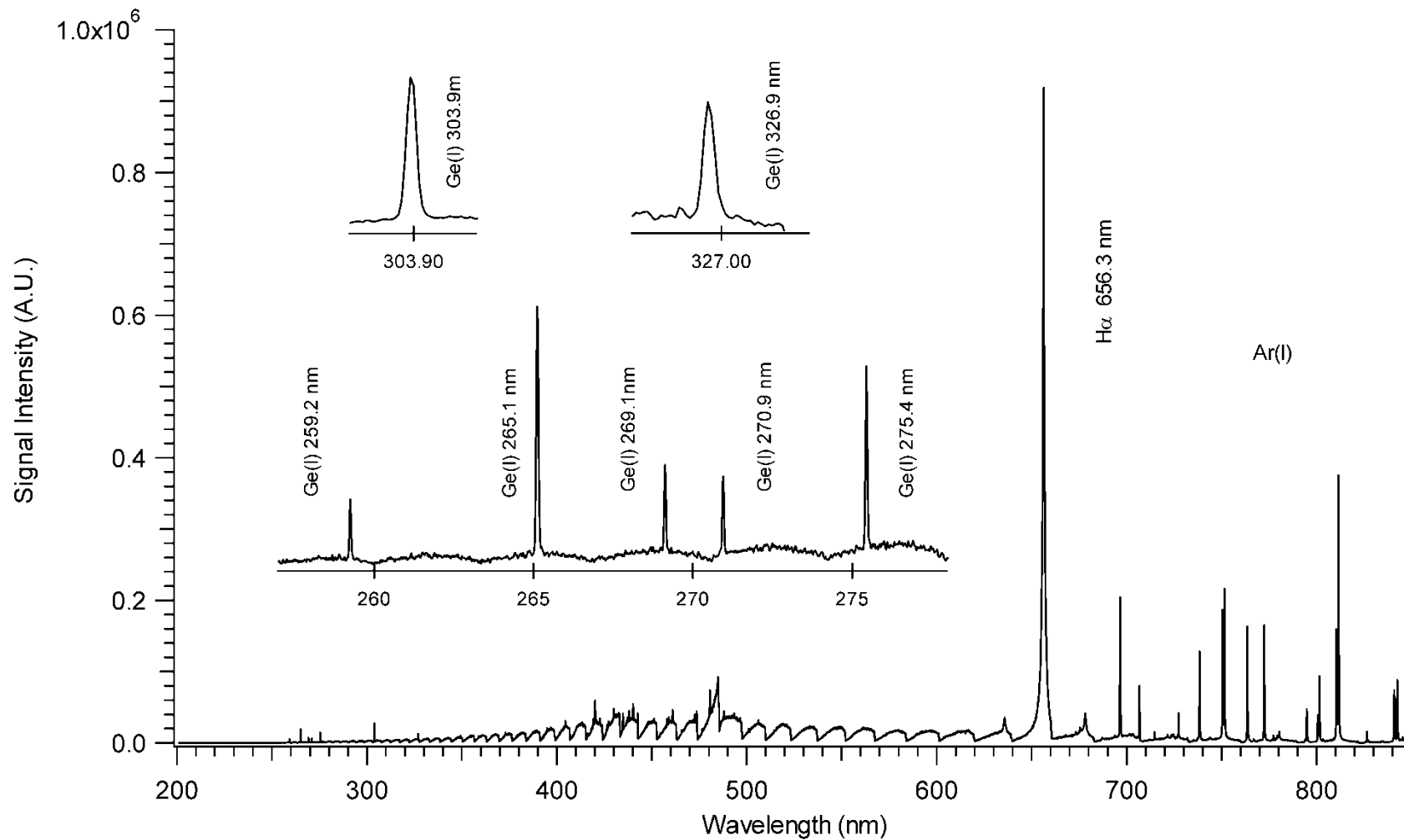
Figure 3.17. Representative HG-LIBS spectrum recorded from GeH₄ plasma under optimum experimental conditions. Spectrum recorded from 50.0 mg L⁻¹ Ge.

3.3. Calibration Graphs

In order to determine the applicability of the HG-LIBS technique for quantitative analysis of tin, arsenic, antimony, lead and germanium present in aqueous environments, calibration graphs were constructed and detection limits were determined.

Single standard solutions of Sn, As, Sb, Pb and Ge were prepared from their stock solution by appropriate dilution and acidified with hydrochloric acid to desired acid concentration. LIBS plasma emission from different analyte concentrations was collected under optimal experimental and chemical conditions listed in Table 3.2. In order to avoid contamination, system has been washed between samplings of different concentrations with continuously flowing $NaBH_4$ and acid solutions until no analyte signal was observed.

Calibration graphs were constructed using the most sensitive neutral emission lines of Sn (284.0 nm), As (278.0 nm), Sb (259.8 nm), Pb (405.8 nm) and Ge (265.1 nm) and are shown in Figure 3.18(a-f). Data points in graphs represent average of 10 replicate measurements each from the accumulation of 10 single laser shots and error bars are from the standard deviations of those measurements. As it can be seen from the figure, for all elements linear response with respect to analyte concentration was obtained with linear regression constants, R^2, close to 0.99.

Calibration graph of tin were constructed under both nitrogen and argon environment as seen in Figure 3.18 (a-b). Under nitrogen environment the graph is linear from 2.0 mg L^{-1} to 75.0 mg L^{-1} with a regression constant of $R^2 = 0.9955$ while under argon environment this linearity is limited up to 20.0 mg L^{-1} with $R^2 = 0.9953$. At higher concentration deviation from linearity was observed under argon environment. The deviation from linearity can be explained by self-absorption of 284.0 nm line.

Calibration plot of arsenic using 278.0 nm emission line at a concentration range of 5-40 mg L^{-1} resulted with a regression constant of $R^2=0.9989$ (Figure 3.18(c)).

Calibration curve of antimony was obtained from 2.5, 5.0, 10.0, 20.0, 30.0, 40.0 and 50.0 mg L^{-1} Sb^{3+} solutions (Figure 3.18(d)). It was observed that the graph was linear up to 50.0 mg L^{-1} with a regression constant of 0.9877.

Figure 3.18(e) indicates the calibration graph of lead under nitrogen environment. At a concentration range from 2.0 mg L^{-1} to 40.0 mg L^{-1} Pb a linear correlation was seen with R^2=0.9931.

In the case of germanium, Figure 3.18(f), the plot shows a deviation from linearity after 20.0 mg L^{-1} Ge concentration and regression constant value drops from 0.9978 to 0.9770 when the concentration range is extended to 50.0 mg L^{-1}, indicating a loss of sensitivity at high concentrations. This loss of sensitivity and hence deviation from linearity at high concentrations can be explained by self-absorption of resonance transition lines. In LIBS plasmas, self-absorption of the resonance lines is highly anticipated.

3.3.1. Analytical Figures of Merit

The analytical figures of merits including detection limit, dynamic range, precision and regression equation were calculated using net peak height of the emission signal under optimized conditions and are shown in Table 3.3.

Detection limit defined as the minimum concentration that can be detected at a known confidence level and is calculated from the formula (Ingle and Crouch, 1998),

$$DL = \frac{3\sigma}{m} \tag{3.1}$$

Where, DL is the detection limit, σ denotes the standard deviation of the background for the lowest observable concentration and m denotes the slope of the calibration curve (Ingle and Crouch, 1998).

The detection limit was calculated to be 0.3 mg L^{-1} for tin under nitrogen environment and under argon environment a detection limit of 0.2 mg L^{-1} at a concentration range from 0.5 mg L^{-1} to 20.0 mg L^{-1} using the line at 284.0 nm. Although an increase in signal intensity and a better detection limit was observed under argon atmosphere, due to an increase in background level as well as signal intensity, this enhancement in detection limit is not as expected.

Similarly using the $3\sigma/m$ method, a detection limit of 1.1 mg L^{-1}, 1.0 mg L^{-1}, 1.3 mg L^{-1} and 0.3 mg L^{-1} was obtained for arsenic, antimony, lead and germanium,

respectively. Detection limits obtained for As, and Sb in this thesis study are comparable with the ones given in the literature (Simeonsson and Williamson, 2011) by HG-LIBS method. A detection limit of 0.7 mg L^{-1} for arsenic and 0.2 mg L^{-1} for antimony were reported by Simeonsson *et al.* These results do not include optimization studies and are based on PMT type detection that could provide higher quantum efficiencies at the wavelengths of interest and larger detection area compared to ICCD type detectors. To the best of our knowledge, there is no record in the literature based on HG-LIBS detection of Sn, Pb and Ge, however, there are several reports on the determination of Sn and Pb in aqueous solutions based on direct liquids analysis by LIBS. Fichet and co-workers reported a detection limit of 100 mg L^{-1} Sn by the method of bulk liquid analysis (Fichet *et al.*, 2001). In this study, the detection limit obtained for tin (0.2 mg L^{-1}) corresponds to 500 times enhancement compared to the study performed by Fichet and co-workers (Fichet *et al.*, 2001). Same group reported an LOD of 100 mg L^{-1} Pb. In other study, Samek *et al.,* obtained a detection limit of 40 mg L^{-1} Pb using liquid-jet technique (Samek *et al.*, 2000). In previous work that has been performed by our research group (Aras *et al.*, 2012), a detection limit of 13.6 mg L^{-1} Pb was obtained from a LIBS system that utilize an ultrasonic nebulizer to produce sub-micron size aerosols. An LOD value of 1.3 mg L^{-1} Pb obtained in this study by the HG-LIBS technique, presents 10 times enhancement compared to that of by ultrasonic nebulization sample introduction system. Result also shows 30 and 77 times enhancement in LOD values compared to direct analysis of liquid samples by LIBS on liquid-jet and in bulk water, respectively.

Dynamic range of the HG-LIBS system is about two orders of magnitude extending from 0.5 to 50.0 mg L^{-1} and 0.5 to 20.0 mg L^{-1} for germanium and tin under argon environment, respectively.

The precision of the HG-LIBS system is given in terms of % RSD for ten replicate measurements at 20.0 mg L^{-1} concentration level and ranged between 4.9% and 17.5%. The precision of laser-induced plasma measurements depends largely on shot to shot reproducibility of the laser pulses, however, homogeneity and complexity of the sample has also considerable influence on the formation and evolution of the plasma and its dynamics. LIBS technique usually has low precision and accuracy with a typical RSD value in the range of 5–20%.
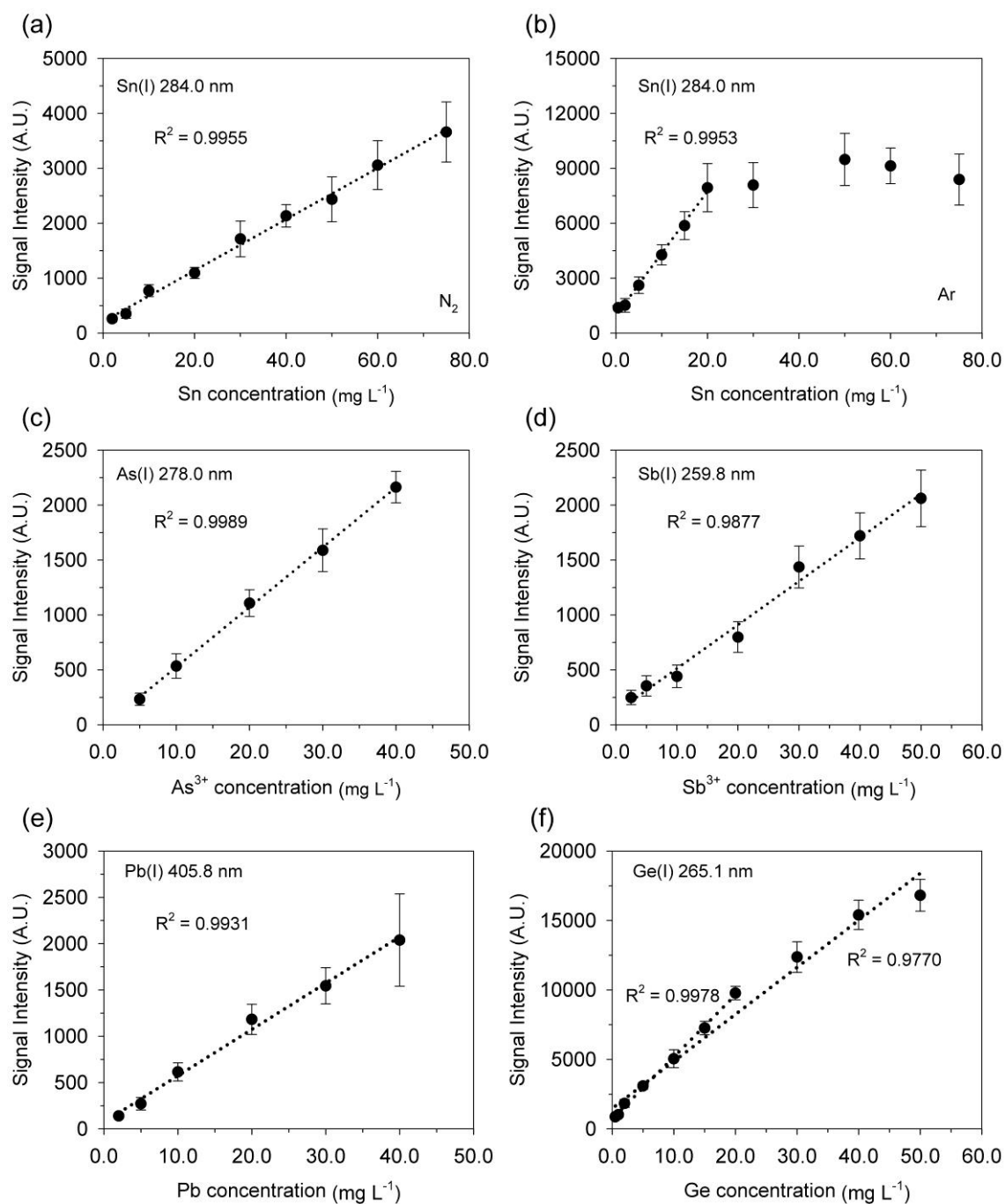
Figure 3.18. Calibration graphs for (a) Sn(I) 284.0 nm under N_2, (b) Sn(I) 284.0 nm under Ar, (c) As(I) 278.0 nm, (d) Sb(I) 259.8 nm, (e) Pb(I) 405.8 nm and (f) Ge (I) 265.1 nm emission lines under optimum instrumental and chemical conditions.

Table 3.3. Analytical figures of merit for HG-LIBS system.

Parameter	Sn		As
Carrier gas	Nitrogen	Argon	Argon
Spectral line	284.0 nm	284.0 nm	278.0 nm
Linear range	2.0 - 75.0 mg L^{-1}	0.5 - 20.0 mg L^{-1}	5.0 - 40.0 mg L^{-1}
Regression equation*	y = 46.601x + 208.11	y = 338.76x + 967.7	y = 54.506x - 19.254
Correlation coefficient, R^2	0.9955	0.9953	0.9989
Detection limit (3σ/m)	0.3 mg L^{-1}	0.2 mg L^{-1}	1.1 mg L^{-1}
Precision (%RSD.) at 20.0 mg L^{-1}, n=10	9.3%	16.6%	11.0%

Parameter	Sb	Pb	Ge
Carrier gas	Argon	Nitrogen	Argon
Spectral line	259.8 nm	405.8 nm	265.1 nm
Linear range	2.5 - 50.0 mg L^{-1}	2.0 - 50.0 mg L^{-1}	0.5 - 50.0 mg L^{-1}
Regression equation*	y = 39.683x + 115.597	y = 49.991x + 73.681	y = 446.088x + 718.195
Correlation coefficient, R^2	0.9877	0.9931	0.9978 (0.5-20.0 mg L^{-1}) 0.9770 (0.5-50.0 mg L^{-1})
Detection limit (3σ/m)	1.0 mg L^{-1}	1.3 mg L^{-1}	0.2 mg L^{-1}
Precision (%RSD.) at 20.0 mg L^{-1}, n=10	17.5%	13.7%	4.9%

*Emission intensity in terms of net peak height versus concentration (mg L^{-1})

3.3.2. Applications on Real Water Samples

The applicability of the HG-LIBS method for quantitative analysis of Sn, As, Sb, Pb and Ge in environmental samples was evaluated using real water samples, River Water Reference Material for trace metals, SLRS-4, tap water and drinking water provided from a local market. Method validation was performed using spiking experiments since the concentration of elements present in real samples are at low μgL^{-1} (ppb) level which are below than the detection limit of the HG-LIBS. For this purpose, bottled water, tap water, and river water standard (SLRS-4) were spiked with single standard solution of 5.0 mg L^{-1} concentrations for Ge and 10.0 mg L^{-1} concentrations for Sn, As, Sb and Pb to achieve desired final concentration. Then, the analyte content was determined under optimum chemical and experimental conditions, and recoveries were calculated. Water samples were also tested for Sn, As, Sb, Pb and Ge content by HG-LIBS but no detectable signal was observed before spiking.

Percent recovery results obtained from the average of ten replicate measurements are provided in Table 3.4. In general, for all types of water samples, recovery values within ±20% standard deviation were obtained. Sb was among the best, with recoveries higher than 98%. In the case of tin over 90% recoveries for all types of real water samples being 91.4%, 94.1% and 96.4% for river, tap and drinking water samples, respectively. Arsenic presents recoveries higher than 80% for all water samples studied. For lead, higher than 100% recoveries obtained for all types of water samples could be due to non-equilibrated reaction medium from the addition of $K_3[Fe(CN)_6]$, since standards and samples were prepared at the same time and the calibration standards were analyzed prior to the samples. Therefore, samples have more time for the reaction to be completed. Germanium has shown recoveries of 100.3% and 90.5% and 123.9% for river, tap and drinking water, respectively.

Relatively worse precision values obtained from this work could be attributed to inhomogeneity of the plasma and possible matrix effect through chemical hydride generation process, which could be a subject to a more detailed study.

Table 3.4. Recovery results from the real water samples spiked with a single element standard solutions* (n=10).

| | %Recovery ± SD | | | | |
	Sn	As	Sb	Pb	Ge
River water, SLRS-4	91.4±10.0	80.9±12.9	98.3±14.6	128.9±18.9	100.3±9.5
Tap water, Urla municipal water	94.1±16.3	84.2±4.0	98.9±15.3	129.7±11.1	90.5±13.5
Drinking water, Spring water, Aydın	96.4±12.1	100.9±19.4	100.1±10.8	108.9±15.6	123.9±7.8

* No detectable Sn, As, Sb, Pb and Ge signal before spiking by HG-LIBS system. 5.0 mg L^{-1} Ge and 10.0 mg L^{-1} Sn, As, Sb and Pb were used for spiking real water samples.

3.4. Signal Observation from Bismuth, Selenium and Tellurium

In addition to tin, arsenic, antimony, lead and germanium elements signal observation studies from other hydride forming elements namely bismuth, selenium and tellurium were performed under both nitrogen and argon environment. No analytical signal could be detected from selenium and tellurium hydrides. Bismuth signal could be detected; however the obtained signal was not reproducible. The experimental details of these studies can be found in the following parts.

3.4.1. Bismuth

Some problems have been encountered during the observation of signal from bismuthine. When bismuth sample solution containing HCl or HNO_3 was reacted with $NaBH_4$, finely dispersed black precipitates was observed in GLS. A similar observation reported in the literature attributes this black precipitate as metallic bismuth, Bi° (D'Ulivo, *et al.*, 2006, D'Ulivo, *et al.*, 2007). This group suggests use of additives such

as $KMnO_4$ and $K_3Fe(CN)_6$ at a concentration up to 5 mM, to provide more efficient hydride generation at high concentration of bismuth (5-10 mg L^{-1}), by preventing the formation of $Bi°$ (D'Ulivo *et al.,* 2006). In other study of the same group the mechanism of bismuthine (BiH_3) generation in the presence of Fe(III), $KMnO_4$, $K_3Fe(CN)_6$, Mo(VI) and KSCN was investigated. It was suggested that these additives prevent the formation of $Bi°$ by formation of reaction intermediates. And these intermediates evolve towards the formation of bismuthine at elevated Bi(III)/$NaBH_4$ ratios (D'Ulivo *et al.,* 2007).

In this study acidified bismuth solutions (20.0 mg L^{-1} Bi in HCl or HNO_3) was prepared separately in the presence of Fe(III), KSCN or $K_3Fe(CN)_6$ and using these additives prevented the formation of black precipitate. The Bi HG-LIBS signal at 306.7 nm obtained in the presence of additives is provided in Figure 3.19. Signal obtained from 20.0 mg L^{-1} Bi (in 2.0% HCl) and 0.25% $NaBH_4$ (in 0.1% NaOH) solutions under argon atmosphere. In the presence of KSCN no Bi signal was observed however, in the presence of both Fe(III) and potassium ferrocyanide signal could be seen clearly (Figure 3.19). In the presence of Fe(III) both background and signal intensity of Bi is higher compared to $K_3Fe(CN)_6$. However both of the recorded signals were not reproducible. When the ten repetitive data were examined it was seen that the signal sometimes appeared and sometimes disappeared. Use of nitric acid instead of hydrochloric acid, did not make any improvement, similar results were obtained. Changing the reduction solution concentration from 0.25% to 5.0% did not provide any improvement.
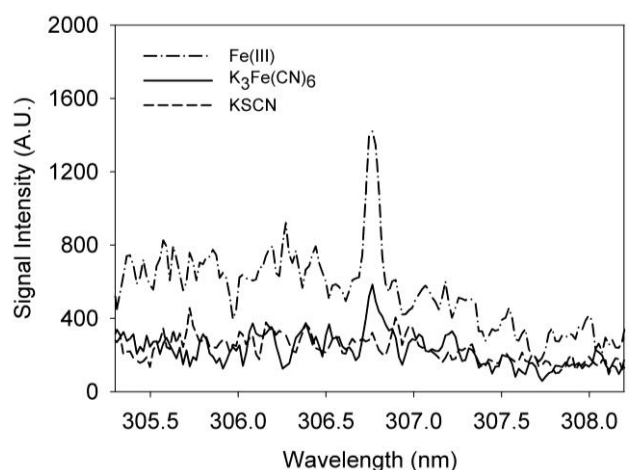
Figure 3.19. Effect of several additives on Bi signal at 306.7 nm. 20.0 mg L^{-1} Bi in 2.0% HCl, 0.01 M Fe(III), 0.8% $K_3Fe(CN)_6$, 0.01M KSCN, 0.25% $NaBH_4$ in 0.1% NaOH, LE: 100 mJ $pulse^{-1}$, t_d: 2 μs, t_g: 100 μs, carrier gas: 218 mL min^{-1} Ar

Up to now, the bismuth signal observation studies were performed by the direct addition of the additives in to the bismuth solutions. These acidified solutions and $NaBH_4$ were delivered to the T-junction by using the two arms of the peristaltic pump as seen in the Figure 2.2. In the above mentioned paper it is also pointed that not only the presence of additives but also the mixing sequence of them has important effect on the signal (D'Ulivo, 2007). The effect of mixing sequence was also investigated to provide reproducible signal. As suggested by the authors two type of mixing sequence was employed for Fe(III), which gives higher signal in our study. For this purpose one arm is added to the peristaltic pump and following sequences were employed (Figure 3.20).

In the first sequence the solution of 4.0×10^{-3} M Fe(III) containing 0.82 M HCl is allowed to react in a reaction coil with 0.8% $NaBH_4$ and then the resulting solution is mixed with the sample solution containing 20.0 mg L^{-1} Bi in 0.82 M HCl. In the second sequence sample solution and Fe(III) is allowed to react in a mixing coil and then the resulting solution is mixed with the reductant solution. Unfortunately, the signal is also very low and not reproducible in these conditions.

1st mixing sequence:
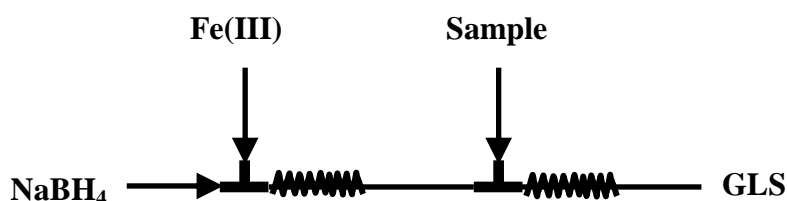
2nd mixing sequence:
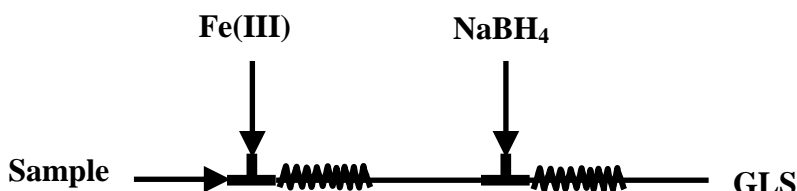
Figure 3.20. The mixing sequence for Bi analysis by HG-LIBS. 20.0 mg L^{-1} Bi in 0.82 M HCl, 4×10^{-3} M Fe(III) in 0.82 M HCl, 0.8% $NaBH_4$ in 0.4% NaOH. LE: 100 mJ pulse^{-1}, t_d: 2 μs, t_g: 100 μs, carrier gas: 218 mL min^{-1} Ar.

81

3.4.2. Selenium and Tellurium

By taking into consideration of the following reasons, the possible causes of non-observable selenium and tellurium signal were investigated with some modifications in experimental set-up and chemical conditions.

1- It is known that selenium hydride (H_2Se) and tellurium hydride (H_2Te) is a water soluble compound (Dedina and Tsalev, 2005) and there is a possibility of removal of the hydrides by the membrane dryer unit (MDU) during transportation of hydrides into the sample cell. In order to test whether selenium and tellurium hydride are removed with moisture while drying process, experiments were performed without membrane drying unit, however no signal could be detected.

2- With the possibility of having use of improper acid and reductant concentration, the range of acid and reductant concentrations were changed. A broad range of 1% to 5% HCl and 0.1% to 1% $NaBH_4$ solutions were used. The concentration of NaOH solution that was used for stabilization of sodium borohydride was prepared within the range of 0% - 1%. No signal could be detected under various chemical conditions.

3- It is also thought that, the reaction between sample and $NaBH_4$ may be not fully complete, so a reaction coil was added between pump and gas-liquid separator. This attempt also did not result with the observation of the signal.

3.5. Determination of Physical Plasma Parameters

The suitability of laser plasma for spectrochemical analysis can be determined by evaluation of its temperature and number of electron density. Plasma that is formed by laser pulses with nanosecond or femtosecond pulse duration begins to cool following the end of laser pulses. Plasma expands with the effect of the shock wave and grows over time. At the early stages of the plasma, ionic emission (II) is dominated and superimposed on background continuum due to the high level of electrons and ions. At later stages ions and electrons collide and neutral emission (I) appeared. Determination of plasma temperature and electron density plays an important role in describing the temporal and spatial evolution stages of the plasma.

It is known that the formation and evolution of plasma is strongly dependent on background gas type. Carrier gas type used in hydride transportation has also important effect on HG-LIBS signal intensity. In order to investigate the effect of carrier gas type on physical plasma parameters, temperature and electron density calculation of tin and germanium hydride plasma was performed under both nitrogen and argon environment. As indicated in part 3.1.2 germanium signal was suppressed to a great extent in the presence of nitrogen gas. To understand the possible reasons of observing higher germanium signal under argon atmosphere, temperature and electron density calculations were also evaluated in the presence of argon and nitrogen gas mixtures in different proportions.

In this study temperature calculations were performed using Boltzmann equation as described in part 1.1.3.1.1 and plasma electron density calculations were performed using Stark broadened H$_\alpha$ line at 656.3 nm.

3.5.1. Temperature and Electron Density Calculations in Tin Hydride Plasma

Temperature calculation of tin hydride plasma produced under argon atmosphere was performed using neutral emission Sn lines at 242.17 nm, 242.95 nm, 270.6 nm, 284.0 nm, 300.9 nm, 303.4 nm, and 317.5 nm which were clearly observed in Figure 3.13. Since in the presence of nitrogen gas the neutral emission line of Sn(I) at 242.17 nm, 242.95 nm and 270.6 nm could not be observed, the remaining Sn(I) lines was used for the temperature calculations of tin hydride plasma under nitrogen environment.

The tin lines intensity was expressed as peak area under curve. In order to investigate the best fitting model the Gauss, the Lorentz and the Voigt curves were used. The Gaussian curve dominates to close to the line center and the Lorentz in the wings. Voigt profiles depend on the relative strength of the two effects. Figure 3.21 shows the fitting curves for Sn(I) 284.0 nm line at argon environment. As seen from the figure the Sn(I) line was best fitted to Gaussian curve. Thus the intensities of all the Sn lines at each delay time were obtained from the peak area by fitting to a Gaussian function. Using these line intensities, a graph was constructed between *lnIλ⁄gA* and *E$_k$* (Equation 1.9). Figure 3.22 (a) and (b) shows a typical Boltzmann plot obtained at a delay time of 1.0 μs in the presence of argon and nitrogen, respectively. The slope of

this graph *(-1/kT)* was *1.5611* and *2.2345* which results in a temperature of 7440 K and 5208 K, respectively. Similarly, Boltzmann plots were constructed under argon and nitrogen atmosphere for several delay times and the temperatures corresponding to these delay times were calculated from their slopes. Spectroscopic data used for temperature calculations are listed in Appendix C.

The variation of the calculated temperatures from tin lines with respect to delay time is given in Figure 3.23. It can be seen that temperature of the plasma under argon environment is always higher than the one in N_2. The temperature stays nearly constant at around 7000 K in argon environment when delay time is changed from 0.3 μs to 10.0 μs. Similarly, in the presence of nitrogen at time interval from 0.3 μs to 8.0 μs temperature stayed constant around 5000 K.

It has also been observed that plasma emission is still exist at a delay time of 20 μs in the argon gas while no plasma emission is observed at delay times higher than 8.0 μs under nitrogen gas.
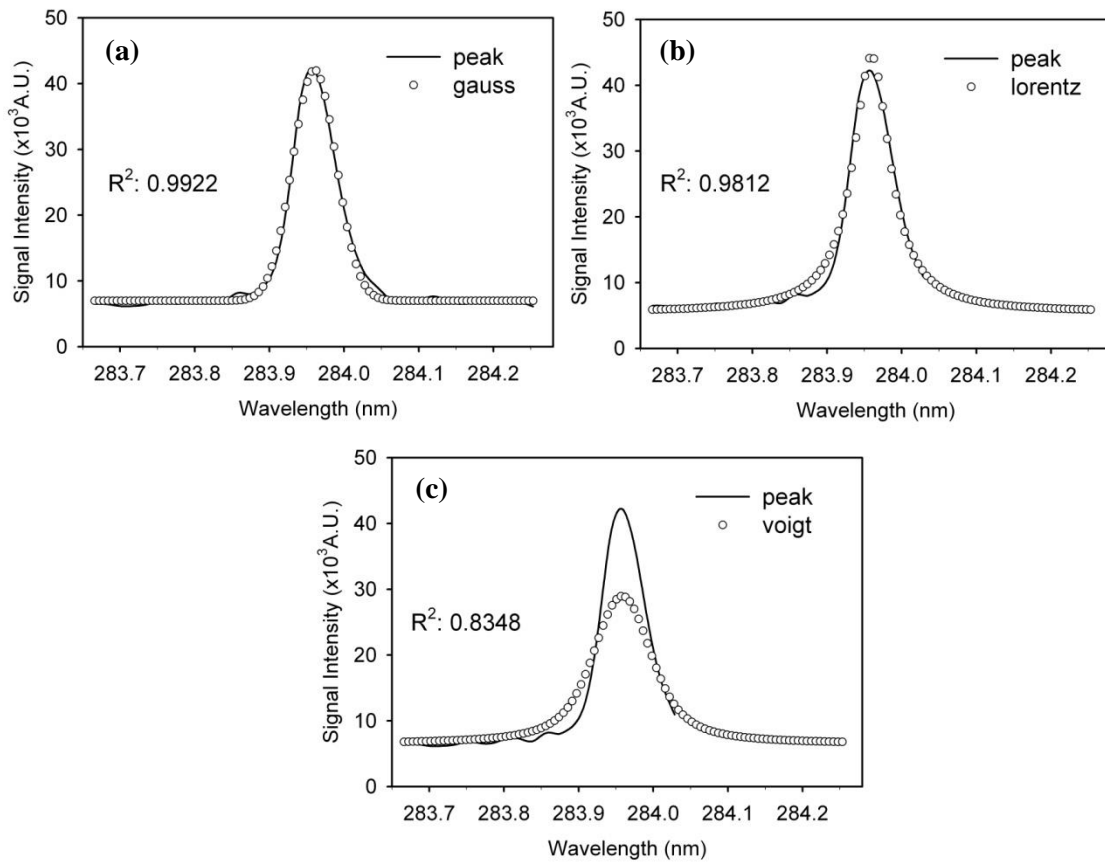
Figure 3.21. (a) Gauss (b) Voigt (c) Lorentz functions fitted to the experimental data for the Sn(I) 284.0 nm line under argon environment at a delay time of 1μs.
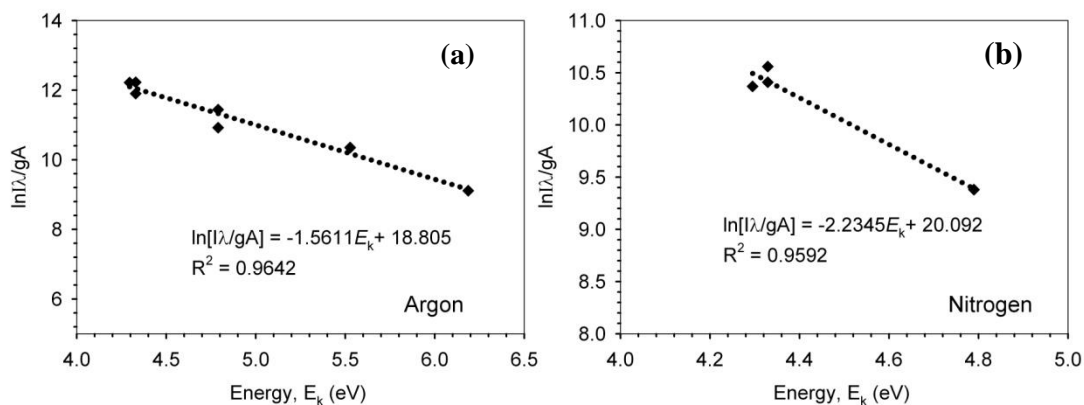
Figure 3.22. Typical Boltzmann plot that used for temperature calculation at a delay time of 1.0 μs obtained from Sn(I) lines under (a) argon and (b) nitrogen environment. (Gate width, t_g: 20 μs)
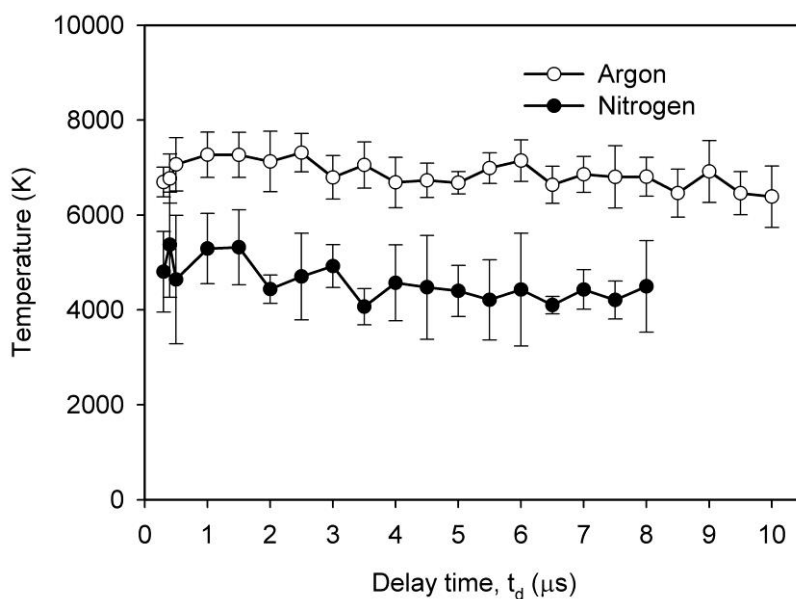
Figure 3.23. Temperature values calculated from neutral tin lines with respect to delay time. (30.0 mg L^{-1} Sn in 1.0% HCl, 1.0% $NaBH_4$ in 1.0% NaOH, 126.0 mL min^{-1} Ar or N_2, t_g 20 μs, LE: 100 mJ $pulse^{-1}$, n=7).

Tin hydride plasma temperatures under argon atmosphere were also evaluated from neutral Ar(I) lines. Again multiple lines Boltzmann equation was utilized by the help neutral emission lines of argon at 696.54 nm, 706.72 nm, 714.7 nm, 763.51 nm, 801.47 nm, 811.53 nm, 420.06 nm and 430.01 nm. The peak area of these lines were also calculated from Gaussian curve fitting method and using the spectroscopic data given in Appendix C, Boltzmann plot was constructed and finally temperature was calculated from the slope.

Figure 3.24 (a) shows a typical Boltzmann plot utilizing neutral argon lines at a delay time of 1.0 μs. From the slope temperature was determined to be 9013 K. At the same delay time the temperature was found to be 7440 K from tin lines. Obtaining different temperature values from different elements within the same plasma is an indication of non-uniform distribution of atomic species in the plasma.

Figure 3.26 (b) represent temperature values calculated from neutral argon lines and in that figure temperature values calculated from tin lines were also provided for the sake of comparison. At early stages of the plasma e.g. 0.3 μs temperature calculated from argon lines are higher than 12000 K whereas at late delay times temperature decreases up to 9000 K. Beside that lower temperature values are calculated from tin lines and there was no important change in temperature with respect to delay time.
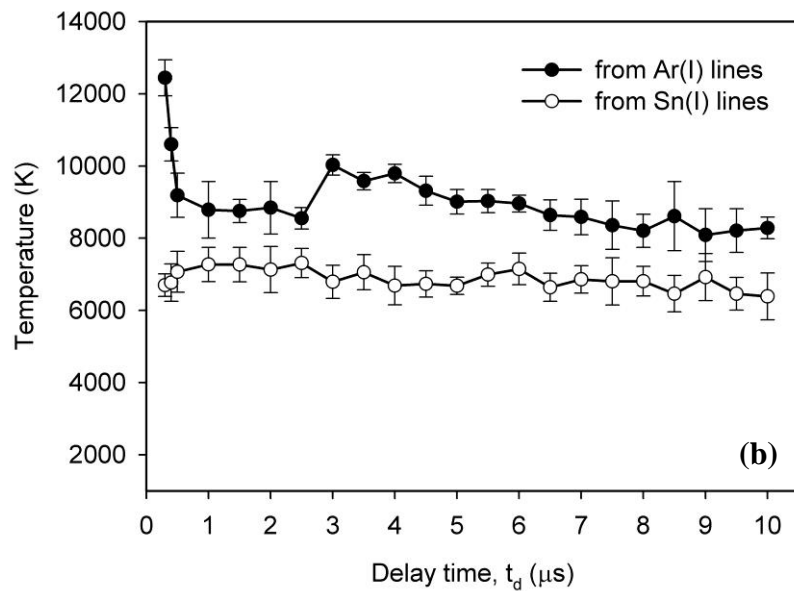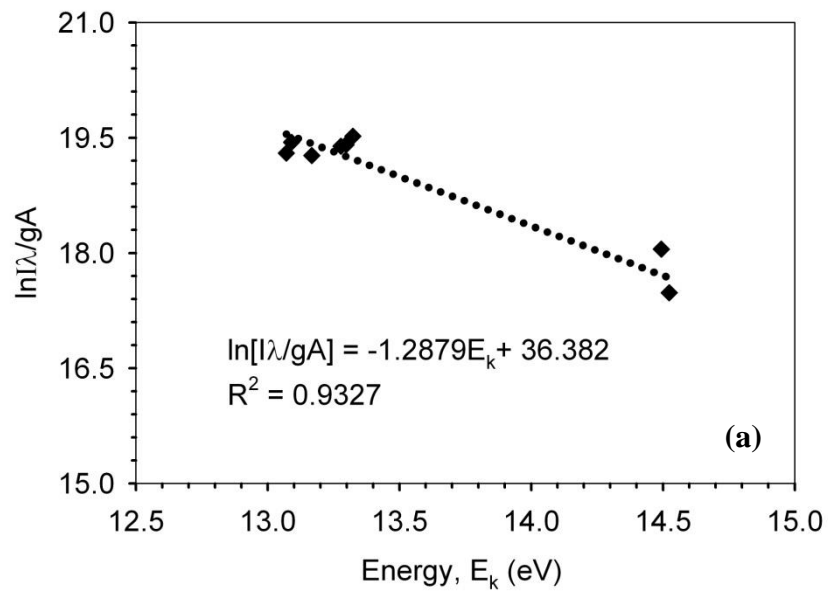
Figure 3.24. (a) Typical Boltzmann plot at a delay time of 1.0 μs obtained from argon lines. (b) Temperature values obtained from argon and tin lines with respect to delay time.

Plasma electron density (N_e) calculations were performed using Stark broadened H_α line at 656.3 nm by the following equation as also explained in part 1.1.3.2.2.

$$N_e \, (H_\alpha) = 8.02 \times 10^{12} \left(\Delta\lambda_{1/2} \, / \alpha_{1/2} \right)^{3/2} \, cm^{-3} \qquad (3.2)$$

Where; $\Delta\lambda_{1/2}$: FWHM of H_α in Å

         $\alpha_{1/2}$: Half width of the reduced Stark profiles in Å

$\alpha_{1/2}$, half width of the reduced Stark profiles in Å is a constant and tabulated for typical temperatures for the emission lines of the several elements (especially for hydrogen) in literature (Griem, 1974).

$\Delta\lambda_{1/2}$ is the width parameter value found by fitting the peak to a Lorentz function. Experimentally observed line width also consists of the instrumental width and should be corrected. The instrumental width of the spectrograph depends on slit widths, the grating dispersion and the dynamic behavior of the photon detector (Samek *et al.,* 2000). Calculated total line width is given by the following formula;

$$\Delta\lambda_{total} = \Delta\lambda_{line} + \Delta\lambda_{spectrometer} \qquad (3.3)$$

In order to find the instrumental broadening ($\Delta\lambda_{spectrometer}$), the emission line from Hg-Ar lamp at 253.7 nm was used. This line exhibited a Gaussian line profile with a FWHM value of 0.52 Å and was subtracted from the observed line width ($\Delta\lambda_{total}$) to obtain $\Delta\lambda_{1/2.}$

Figure 3.25 shows H line profile at various delay times. High number of electron density at early stages of the plasma, 0.5 μs, and results with a highly broadened line shape in contrast to the ones at later times. From 0.5 μs to 8.0 μs FWHM of H line decreases from 1.3 nm to 0.5 nm as the plasma cools down because of ion and electron recombination process.

Electron number density calculated from stark broadened H_α line with respect to delay time is provided in Figure 3.26. At early stages (specifically at 0.3 μs) the electron number density under argon environment was $2.07\pm0.05x10^{17}$ cm^{-3} and decreased exponentially to $2.0\pm0.2x10^{16}$ cm^{-3} at 15.0 μs delay time. In the case of nitrogen environment again exponential decrease was observed from $3.25\pm0.11x10^{17}$ cm^{-3} to

$0.8 \pm 0.1 \times 10^{16}$ cm^{-3}. Up to 1.0 µs number of electron density is higher in nitrogen however after 1.0 µs lower electron density values are obtained. Most important point is that, the decay of the plasma is faster in nitrogen compared to argon atmosphere. This explains why plasma emissions in argon environment are more stable and long lived.

The existence of LTE was investigated using McWhirter equation (Equation 1.3). The upper energy level of the 242.2 nm Sn line that used in temperature calculations in the presence of argon is 8613 cm^{-1} (1.07 eV) and the lower energy level is 49894 cm^{-1} (6.20 eV) (NIST database). Therefore ΔE value equals 5.13 eV. The critical N$_e$ value was found to be 1.7×10^{16} cm^{-3} at a delay time of 15.0 µs where the plasma temperature is 6050 K. As seen from the Figure 3.28 for all delay times LTE validity was established. In the case of nitrogen environment ΔE for the Sn(I) line at 284.0 nm is 4.37 eV results in a critical Ne values of 8.8×10^{15} cm^{-3}.
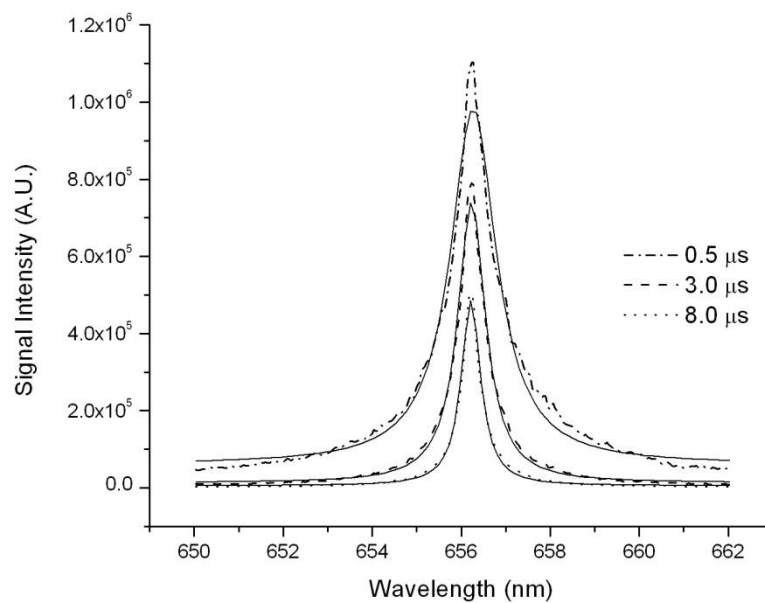
Figure 3.25. Lorentz function (solid) fitted to the experimental data (dashed) for the stark broadened H$_\alpha$ line at 656.3 nm under argon with respect to delay time.
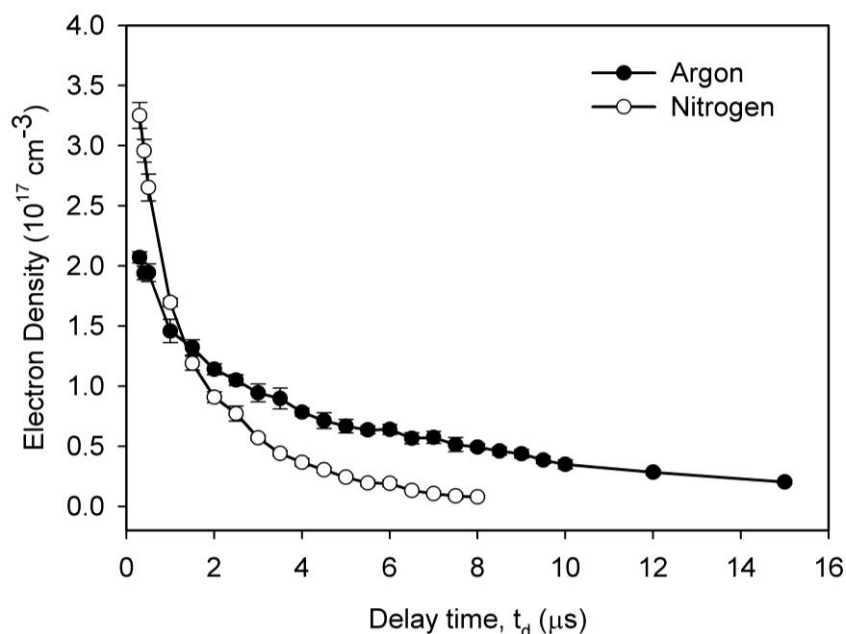
Figure 3.26. Tin hydride plasma electron density calculated from Stark broadened H_α line from tin hydride plasma under argon and nitrogen atmosphere with respect to delay time.

3.5.2. Temperature and Electron Density Calculations in Germanium Hydride Plasma

Since optimization studies of germanium signal were performed under argon gas, optimum laser energy and delay time should also be determined in the presence of nitrogen gas.

First of all, the optimum laser pulse energy for observing the signal for both flowing gases was investigated. For this purpose Ge signal under optimized chemical conditions were recorded as a function of laser energy ranging from 80 mJ to 200 mJ. Variation of the Ge signal intensity with respect to laser pulse energy for both Ar and N_2 is shown on the same graph (Figure 3.27). As seen from the figure that, germanium signal under argon environment is always higher than the one under nitrogen environment, with a maximum at 130 mJ per pulse, for all pulse energies studied. Although, only Ge(I) signal at 265.1 nm is provided in this figure, the same observations are also valid for the other emission lines of Ge(I) at different wavelengths.
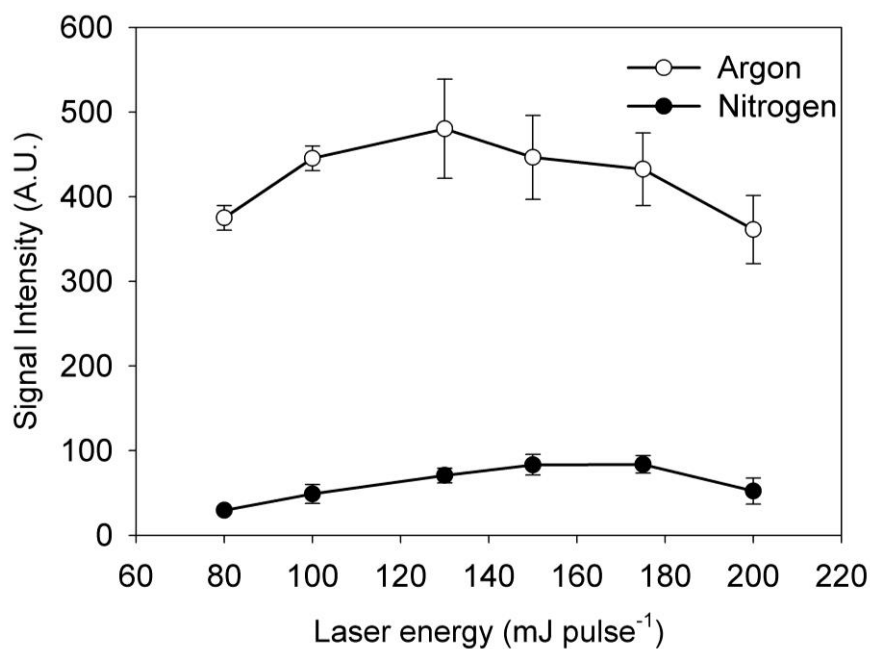
Figure 3.27. Effect of laser energy on Ge signal at 265.1 nm recorded under Ar and N_2 gas. t_d: 1 μs, t_g: 100 μs, carrier gas 126 mL min^{-1} argon or nitrogen gas.

In order to check if the signal is still low in nitrogen environment at other delay times, germanium hydride plasma emission with respect to delay time was also recorded under both argon and nitrogen atmosphere by using laser energy of 130 mJ pulse^{-1} and gate width of 100 μs. Variation of Ge(I) signal intensity with respect to delay time for both gases is given in Figure 3.28. Here, signal intensity from the germanium line at 265.1 nm in terms of peak area calculated by curve fitting method was utilized. Again at each delay times Ge signal is higher under argon atmosphere.
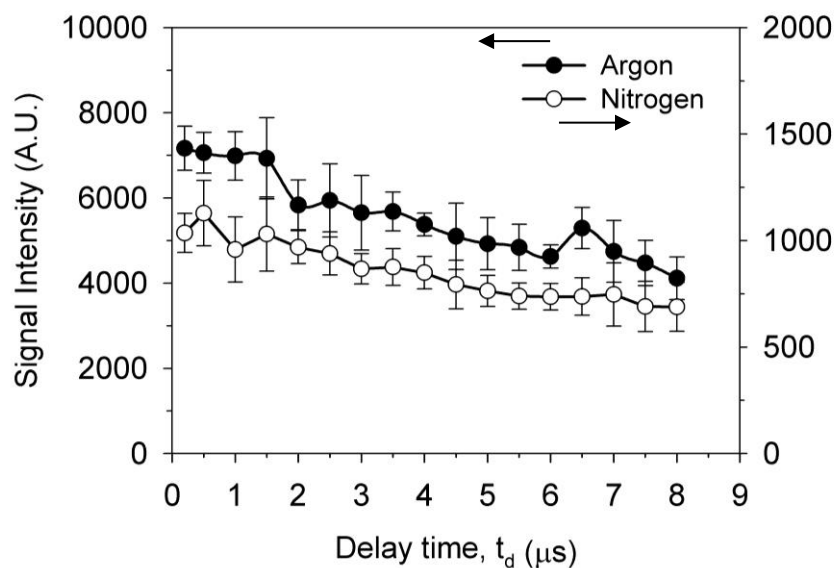
Figure 3.28. Effect of delay time and on Ge LIBS signal under argon and nitrogen gas. (126 mL min^{-1} argon or N_2).

After verifying that at a broad range of laser energies and delay times, germanium signal under argon atmosphere always higher than that of nitrogen, characterization of the hydride plasmas in terms of determining the magnitudes of the temperature and electron density under different flowing gases were performed.

Temperature calculation of germanium hydride plasma under argon and nitrogen carrier gas was also performed using multiple lines Boltzmann method (Equation 1.9). The neutral emission line of Ge at 259.25 nm, 265.1 nm, 269.1 nm, 270.96 nm, 275.45 nm, 303.9 nm, and 326.3 nm (Figure 3.17) were used in temperature calculations. The Gaussian function was used to calculate peak area under curve to find intensities of these lines.

A typical Boltzmann plot from germanium lines obtained at a delay time of 1 μs under argon and nitrogen can be seen in Figure 3.29 (a) and (b), respectively. From the slope of this graph the plasma temperature under argon and nitrogen gas was found to be 10517 K and 7985 K, respectively. When these two graphs are considered (Figure 3.29), it is seen that there was a large difference in signal line intensity corresponding to the same upper level energy. This difference gives rise to error in temperature calculations. This error is commonly encountered in Boltzmann graph because of difficulties in obtaining accurate and suitable spectroscopic constants.
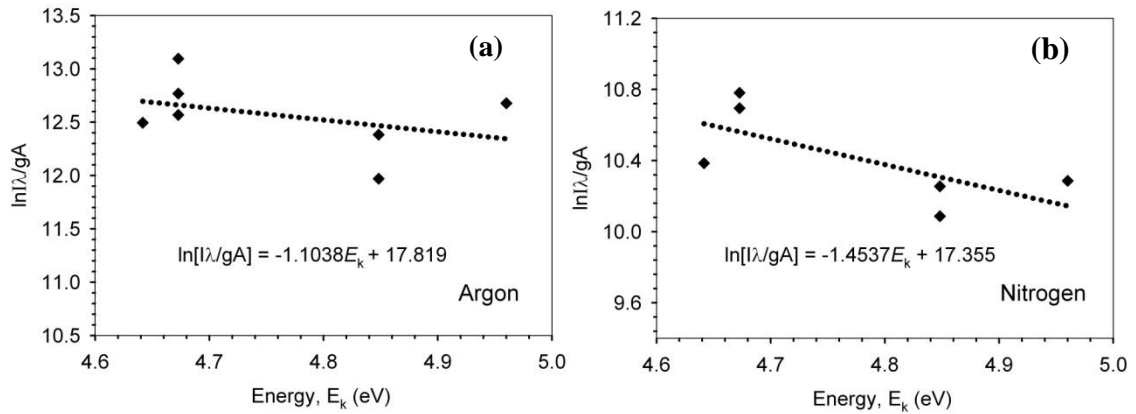
Figure 3.29. Typical Boltzmann plot that used for temperature calculation at a delay time of 1 μs obtained from Ge(I) lines under (a) argon and (b) nitrogen environment.(t_g: 100 μs)

Similar to temperature calculation of tin hydride plasma, from the intensities of germanium lines at various delay time Boltzmann plots were constructed and temperature values are calculated using the slopes of these plots. Spectroscopic data used for germanium lines is provided in Appendix C.

Figure 3.30 shows the temporal variation of plasma temperature in the presence of argon and nitrogen as carrier gases. it has been found that Ar atmosphere has relatively higher temperatures than the ones in N_2 atmosphere, especially at late delay times. Between 0.2 μs and 8 μs s time interval, plasma temperature that ranges from 10500 K to 8500 K in argon environment and 9832 K to 5216 K in N_2 environment were obtained. Also, the plasma temperature variation with respect to delay time in Ar is more stable than the one in N_2 atmosphere.
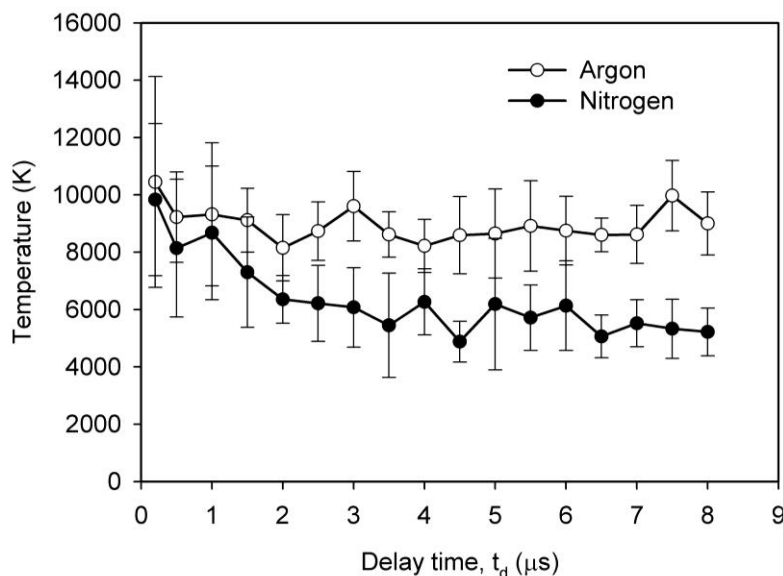
Figure 3.30. Temperature values calculated from neutral germanium lines with respect to delay time (20.0 mg L^{-1} Ge in 1.0% HCl, 0.2% NaBH$_4$ in 0.2% NaOH, 126.0 mL min^{-1} Ar or N$_2$, t$_g$: 100 µs, LE: 100 mJ pulse^{-1}, n=7).

The higher temperature of LIBS plasma under argon environment with respect to other gases such as air, nitrogen, and helium also reported widely in the literature (Aguilera and Aragon, 1999, Kim *et al.,* 1997; Iida, 1989; Harilal *et al.*, 1998). Kim *et al.* reported that, thermal properties of argon gas with a smaller conductivity and specific heat with respect to the corresponding air values result in a higher temperature leading to stronger line emission. In the case of our study the higher temperature values under argon may give rise to higher signal intensity of germanium.

The results for the temperatures under argon environment at some delays are listed in Table 3.5. Temperature results under similar experimental conditions from the literature study by Simeonsson and Williamson and are also provided in the table and compared with our work. The results of this study obtained from Sn(I), Ge(I) and Ar(I) lines are consistent with the HG-LIBS plasma temperatures presented by Simeonsson and Williamson, through As(I) and Ar(I) line emission measurements.

Table 3.5. Temperature values at some delays under argon atmosphere

Delay time (μs)	Temperature (K)				
	This work			(Simeonsson and Williamson, 2011)*	
	Ar(I)	Sn(I)	Ge(I)	As(I)	Ar(I)
2	8842 ± 728	7130 ± 640	8154 ± 1158	7600 ± 1400	-
3	10028 ± 284	6793 ± 453	9605 ± 1211	7000 ± 1300	-
4	9792 ±254	6687 ± 532	8221 ± 927	7000 ± 1300	8800 ± 1200
5	9007 ±338	6681 ± 237	8649 ± 1554	7900 ± 2500	8600 ± 800
6	8959 ±234	7148 ± 438	8752 ± 1194	6600 ± 1300	8700 ± 600
7	8586 ±493	6858 ± 378	8620 ± 1012	8900 ± 1700	8000 ± 500
8	8205 ±459	6808 ± 408	9002 ± 1098	7200 ± 1400	8400 ± 100

*These data are rough estimation extracted from the graph given by the authors.

Figure 3.31 shows the number of electron density in germanium hydride plasma that is calculated from stark broadened H_α line under Ar and N_2 with respect to delay time. Electron number density under argon environment decreased exponentially from $1.52 \pm 0.17 \times 10^{17}$ cm^{-3} to $2.9 \pm 0.4 \times 10^{16}$ cm^{-3} within the range of 0.2 μs - 8.0 μs delay time. Exponential decrease was also observed in nitrogen environment from $2.27 \pm 0.10 \times 10^{17}$ cm^{-3} to $1.7 \pm 0.1 \times 10^{16}$ cm^{-3}. Up to 3.0 μs plasma electron density in N_2 is higher than Ar while after three microseconds an opposite case was observed. As in the case of tin hydride plasma the faster decrease in electron density was also observed under N_2 environment.

McWhirter's criterion was also utilized in order to check for the LTE validity. The energy difference between upper and lower levels for the germanium line at 259.25 nm is 4.79 eV. At a delay time of 8.0 μs critical electron density is 1.7×10^{16} and 1.3×10^{16} under argon (T: 9002 K) and nitrogen environment (T: 5217 K); respectively. Therefore as seen in Figure 3.31 at all delay times LTE validity was established.
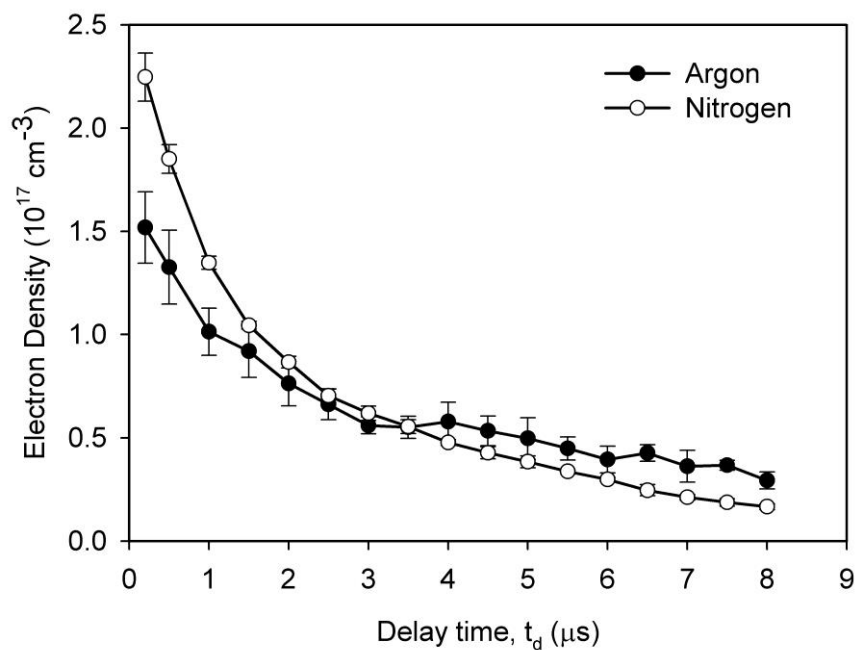
Figure 3.31. Germanium plasma electron density calculated from Stark broadened H_α line under argon and nitrogen atmosphere with respect to delay time.

3.5.3. The Effect of Gas Mixture on Temperature and Electron Density of Germanium Hydride Plasma

Since germanium signal decreases sharply in the presence of nitrogen, the signal variation was also investigated in the argon and nitrogen gas mixture in order to see how the signal is affected by the addition of nitrogen. For this purpose the relative amounts of argon and nitrogen were varied from pure argon to pure nitrogen by mixing of them in a total volume of 814 mL min^{-1}. Although the optimum flow rate was determined to be 126 mL min^{-1} from the optimization studies, 814 mL min^{-1} flow rate had to be used due to the limitation in flow meter. At such a high flow rate, the Ge signal was lower than the expected therefore; a solution of 50.0 mg L^{-1} Ge was used to compensate a decrease in signal intensity.

Variation of argon amount from 100% to 0% resulted in a decrease in germanium signal at 265.1 nm is given in Figure 3.32. From pure Ar to 80% Ar signal decreases slowly, after this point a sharp decrease in signal is observed.

As %Ar decreases not only the signal but also signal to noise ratio, S/N, also decreases (Table 3.5). Signal is defined as the background subtracted net signal height

96

and noise is defined as three times of the standard deviation of the background. Same behavior in S/N ratio values was observed for all other germanium lines.

Since some atomic emission line of germanium is diminished with the addition of nitrogen, temperature calculations were performed as a function of argon concentration using the two lines Boltzmann method as described earlier in equation 1.8. For temperature calculations the Ge(I) lines at 265.1 nm and 303.9 nm were used. Results are shown in Figure 3.33. The highest temperature was obtained for the condition in which pure argon was used. Only 10% addition of nitrogen resulted in a 50% decrease in the temperature however, conditions at which higher nitrogen concentrations were used the temperature did not change significantly.

The amount of energy absorbed by the hydride plasma was also studied in order to investigate the transmittance of the plasma in the presence of argon and nitrogen gas mixtures. For this purpose laser energy was measured before / after the plasma cell and energy absorbed by the plasma was calculated from the difference between them. The amount of energy absorbed by the quartz windows was corrected. This study was performed both in the presence and absence (only gas mixture) of germanium hydrides. The result of this study is provided in Figure 3.36. It was seen that as amount of argon increased amount of energy absorbed by the plasma also increased. This increase in amount of energy absorption in the presence of argon gas is an evidence of higher temperature values and enhanced emission signal intensities in the under argon environment. Another important outcome is that at the same composition in the presence of hydride, plasma absorbs more energy compared to in the absence of hydride.
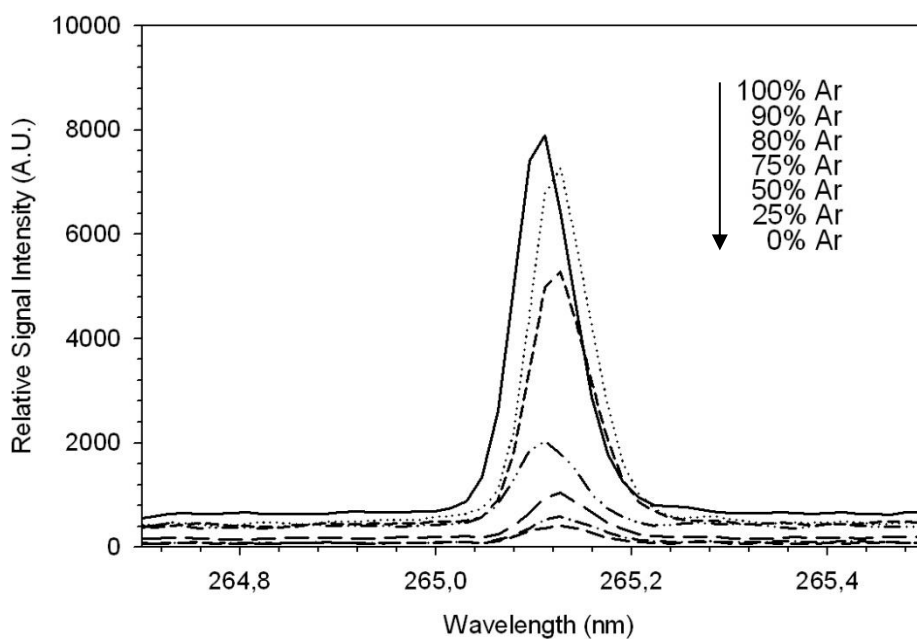
Figure 3.32. Ge line emision spectra at various concentration of argon in a balance with nitrogen. 50 mg L^{-1} Ge, LE: 100 mJ, t_d: 1.0 μs, t_g: 100 μs, total carrier gas flow rate is 814 mL min^{-1}.

Table 3.6. S/N ratio of Ge line at 265.1 nm at various concentration of argon in a balance with nitrogen.

Ar / N_2 (%)	S/N (265.1 nm Ge(I))
100/0	25.9 ± 4.2
90/10	31.3 ± 7.2
80/20	24.1 ± 9.9
75/25	8.4 ± 2.5
50/50	8.0 ± 2.2
25/75	5.5 ± 1.6
0/100	4.4 ± 1.2
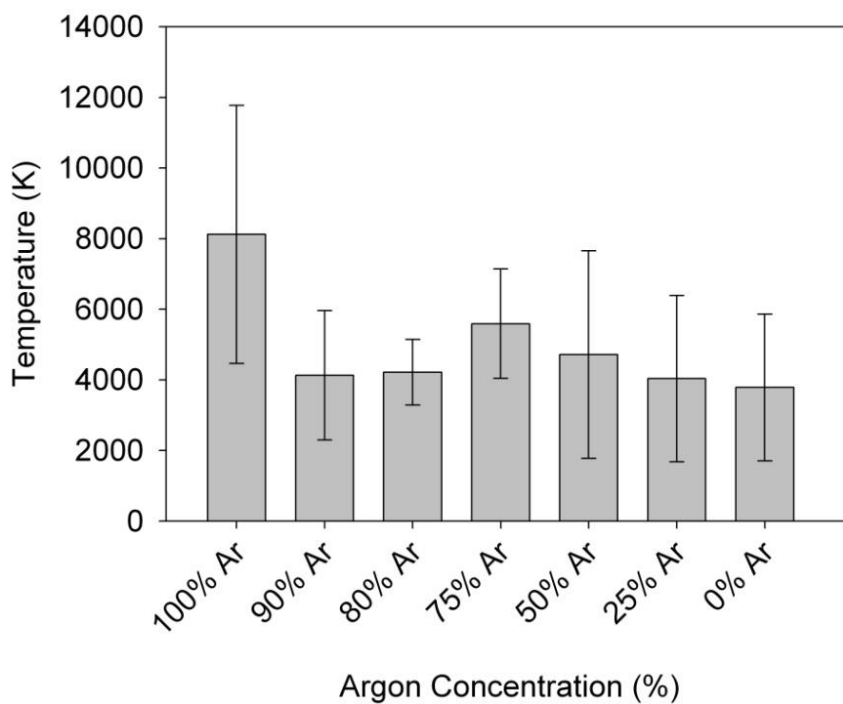
Figure 3.33. Temperature at various concentration of argon in a balance with nitrogen. 50.0 mg L^{-1} Ge, LE: 100 mJ, t_d: 1.0 μs, t_g: 100 μs, total flow of carrier gas: 814 mL min^{-1}.
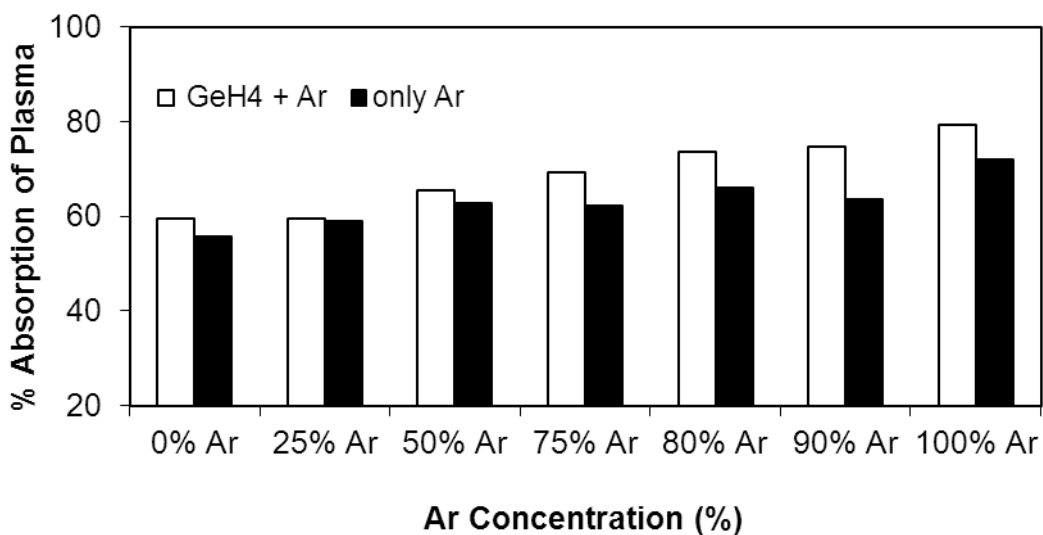
Figure 3.34. Energy absorption of plasma at various concentration of argon in a balance with nitrogen.

Increasing argon gas concentration with respect to nitrogen, Hα line intensity was also enhanced and the line width (FWHM) was decreased, as seen in Figure 3.37. The enhancement in hydrogen emission lines in the presence of pure helium is reported by Henry *et al.,* (Henry *et al.,* 2007).

Electron density of Ge plasma under Ar and N_2 gas mixture was obtained from the Stark broadened Hα line as is done previously. Generally at high N_2 amounts higher electron number density is observed, (Figure 3.38). From 0% to 25% Ar electron density does not change much; however, N_e starts to decrease drastically from 50% to 100% argon compositions.
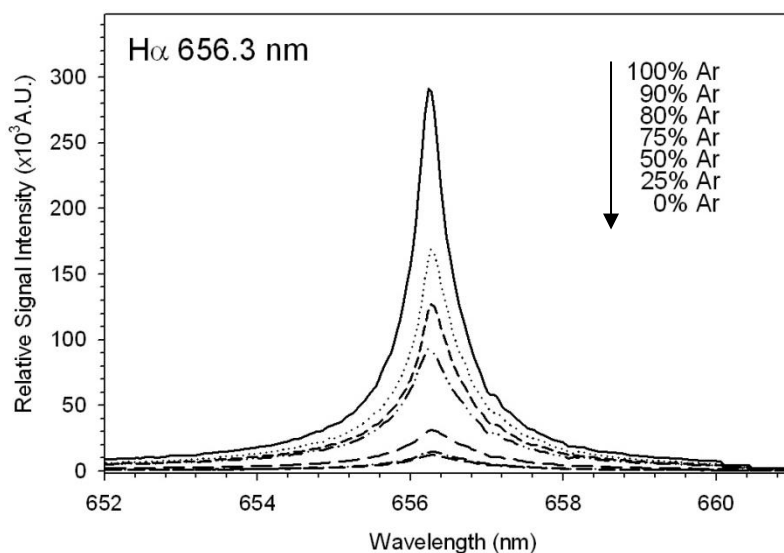
Figure 3.35. Hα line emission spectra at various concentration of argon in a balance with nitrogen. 50.0 mg L^{-1} Ge, LE: 100 mJ, t_d: 1 μs, t_g: 100 μs, total flow of carrier gas: 814 mL min^{-1}.
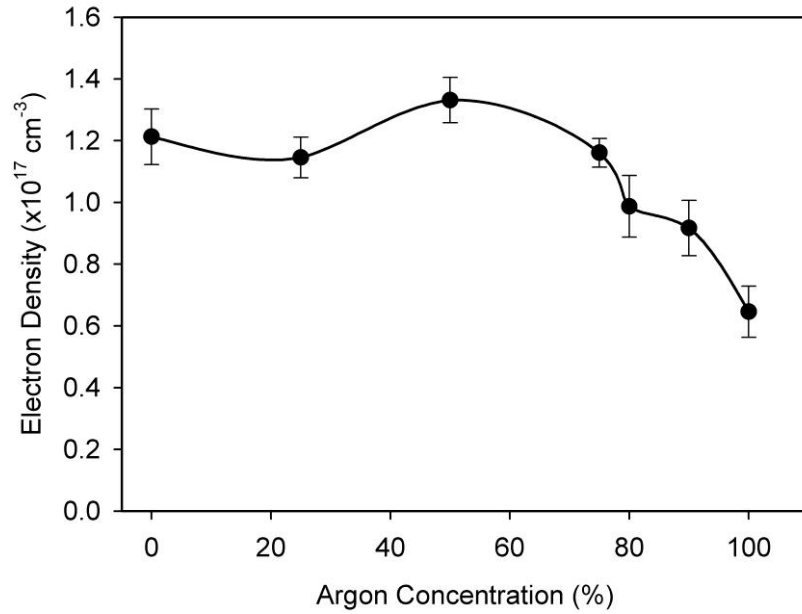
Figure 3.36. Electron density at various concentration of argon in a balance with nitrogen. 50.0 mg L^{-1} Ge, LE: 100 mJ, t$_d$: 1 μs, t$_g$: 100 μs, total flow of carrier gas: 814 m L min^{-1}.

The increase in electron number density as the nitrogen gas added can be explained by Penning ionization similar to observations made by Henry *et al.,* (Henry *et al.,* 2007). In their study, as the nitrogen content is increased the helium emission lines are eliminated as the metastable helium atoms are quenched to the ground state. They pointed out the Penning ionization (3.4) in which the metastable state of helium collide with molecular nitrogen and following ionization occurs;

$$He_M \ + \ N_2 \ \longrightarrow \ He \ + \ N^+_2 \ + \ e^- \qquad (3.4)$$
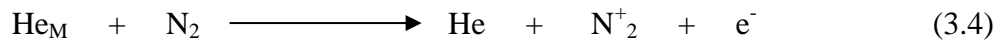
According to this ionization mechanism as the amount of nitrogen is increased the number of electron density also increases. After interpretation of the results obtained from germanium hydride, the atomic process occurred in the plasma can be explained by the following mechanisms.

i) The increase in electron density in the presence of nitrogen in a balance with argon can be explained as result of Penning ionization (Figure 3.36).

$$Ar_M \ + \ N_2 \ \longrightarrow \ Ar \ + \ N^+_2 \ + \ e^- \qquad (3.5)$$

ii) Similar mechanism between metastable Ar atoms and Ge atoms can be also written. In that process metastable argon atoms collide with germanium atoms and return to the ground state by losing some of its energy while germanium atoms ionize.

$$Ar_M \quad + \quad Ge \quad \longrightarrow \quad Ar \quad + \quad Ge^+ \quad + \quad e^- \qquad (3.6)$$
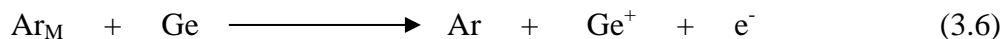
A decrease in argon emission line intensity in the presence of germanium hydride can be a proof for the proposed mechanism (Figure 3.37).

iii) Lastly, the collision between metastable argon atoms and germanium atoms brings about excitation of germanium atoms while argon atoms return to the ground state.

$$Ar_M \quad + \quad Ge \quad \longrightarrow \quad Ar \quad + \quad Ge^* \qquad (3.7)$$

Then, excited germanium atoms return to the ground state and an emission occurs. An increase in germanium signal with increasing of amount of argon supports this mechanism.

$$Ge^* \longrightarrow \quad Ge \quad + \quad h\nu \qquad (3.8)$$
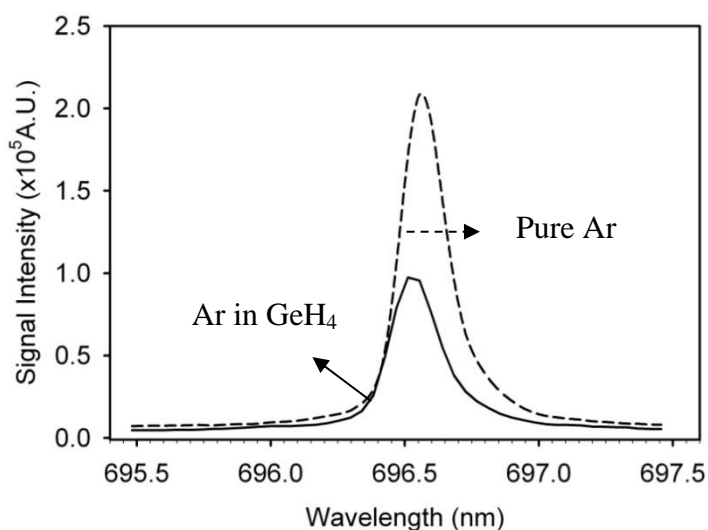
Figure 3.37. Ar line emission spectra at 696.54 nm under pure argon and in the presence of hydrides. (Dashed lines represents Ar signal from pure argon and solid line represents Ar signal in the presence of GeH_4).

CHAPTER 4

CONCLUSION

In this thesis study, continuous flow hydride generation sample introduction system has been coupled to a laser-induced breakdown spectrometry. In this technique chemically produced hydrides are transported to the sample/plasma cell by a stream of carrier gas and interacted with high power pulsed laser beam to produce plasma. Plasma emission has been collected with a suitable optics and directed to echelle spectrograph that contains an ICCD detector. Design, construction and optimization studies of the HG-LIBS system have been described for analysis of tin, arsenic, antimony, lead and germanium in aqueous environment.

In order to optimize plasma emission signal for each element, laser energy, delay time and gate width parameters have been investigated. In addition to instrumental conditions, some chemical parameters including reductant/acid concentration and flow rate, sample and carrier gas flow rate and the presence of pre-oxidizing or reducing agent that affect the efficiency of hydride generation and transportation have also been systematically studied.

Effect of ambient gas type, argon and nitrogen, has also been examined. It was seen that arsenic signal could be observed only in argon gas while tin, antimony, lead and germanium signal was observed under both argon and nitrogen environment. In the presence of argon gas strong enhancement in Sn(I), Ge(I) and Sb(I) is observed, however, Pb(I) signal intensity does not affected by the carrier gas type. No analytical line could be observed from selenium and tellurium under studied conditions. Bismuth signal could be detected however, it was not reproducible.

Under optimized conditions calibration graphs were constructed for Sn, As, Sb, Pb and Ge and their detection limits have been determined. Dynamic range of the HG-LIBS system is about two orders of magnitude and the precision of the HG-LIBS system is ranged between 4.9% and 17.5%. An LOD value of 0.2 mg L^{-1}, 1.1 mg L^{-1}, 1.0 mg L^{-1}, 1.3 mg L^{-1} and 0.2 mg L^{-1} were obtained for Sn, As, Sb, Pb and Ge, respectively. To the best of our knowledge, there is no record in the literature based on HG-LIBS detection of Sn, Pb and Ge. Detection limits obtained for As and Sb are

comparable with the ones in literature obtained by HG-LIBS method. Results show 500 and 77 times enhancement for tin and lead respectively, compared to direct analysis of liquid samples by LIBS.

The applicability of the HG-LIBS system to real samples has been investigated through spiking experiments. Recoveries higher than 90% for antimony and tin has been obtained for all water types including tap water, drinking water and Reference River water standard.

Temperature and electron number density calculations of tin and germanium plasma has been performed under nitrogen and argon atmosphere. Temperature calculations were performed through Boltzmann equation by utilizing neutral tin and germanium lines. Plasma electron density values were calculated from the Stark broadened $H\alpha$ line profiles. Compared to nitrogen higher temperature values are obtained in the presence of argon gas at all delay times. Although nitrogen provides higher initial electron number density values, faster decay is observed compared to argon. Argon environment leads to more stable and long lived plasma emissions. The intensity enhancement in Ge emission lines in the presence of argon attributed to Penning ionization process.

Detection limits for Sn, As, Sb, Pb and Ge are at low ppm (mg L^{-1}) level. Although substantial enhancement in detection limits has been obtained by HG-LIBS method with respect to direct liquid analysis by LIBS, they are still higher than other atomic spectrometric techniques that utilize hydride generation sample introduction. However the proposed system can be helpful for development of a portable LIBS sensor for on-line monitoring of environmental pollutants especially for arsenic and lead.

REFERENCES

Aguilera, J. A., and C. Aragon. 1999. A Comparison of the Temperatures and Electron Densities of Laser-Produced Plasmas Obtained in Air, Argon, and Helium at Atmospheric Pressure. *Applied Physics A*. 69 (1):S475-S478.

Alp, O., and N. Ertaş. 2010. Determination of Tin by on Situ Trapping of Stannane on a Resistively Heated Iridium Treated Tungsten Coil Surface and Interference Studies. *Talanta*. 81 (1):516-520.

Anzano, J., and R. Lasheras. 2009. Strategies for the Identification of Urinary Calculus by Laser Induced Breakdown Spectroscopy. *Talanta*. 79 (2):352-360.

Andor Technology, 2013. Echelle Spectrographs. *http://www.andor.com/learning-academy/echelle-spectrographs-the-properties-of-high-resolution-echelle-spectrographs* (accessed, April 19th 2013).

Aragon, C., J. Bengoechea, and J. A. Aguilera. 2001. Influence of the Optical Depth on Spectral Line Emission from Laser-Induced Plasmas. *Spectrochimica Acta Part B: Atomic Spectroscopy*. 56 (6):619-628.

Aras, N., S. Unal Yesiller, D. A. Ates, and S. Yalcin. 2012. Ultrasonic Nebulization-Sample Introduction System for Quantitative Analysis of Liquid Samples by Laser-Induced Breakdown Spectroscopy. *Spectrochimica Acta Part B:Atomic Spectroscopy*. 74-75:87-94.

Archontaki, H. A., and S. R. Crouch. 1988. Evaluation of an Isolated Droplet Sample Introduction System for Laser-Induced Breakdown Spectroscopy. *Applied spectroscopy*. 42 (5):741-746.

Babushok, V. I., F. C. DeLucia Jr, J. L. Gottfried, C. A. Munson, and A. W. Miziolek. 2006. Double Pulse Laser Ablation and Plasma: Laser Induced Breakdown Spectroscopy Signal Enhancement. *Spectrochimica Acta Part B: Atomic Spectroscopy*. 61 (9):999-1014.

Barrette, L., and S. Turmel. 2001. On-line Iron-Ore Slurry Monitoring for Real-Time Process Control of Pellet Making Processes using Laser-Induced Breakdown Spectroscopy: Graphitic vs. Total Carbon Detection. *Spectrochimica Acta Part B: Atomic Spectroscopy*. 56 (6):715-723.

Bauer, H. E., F. Leis, and K. Niemax. 1998. Laser Induced Breakdown Spectrometry with An Echelle Spectrometer and Intensified Charge Coupled Device Detection. *Spectrochimica Acta Part B: Atomic Spectroscopy*. 53 (13):1815-1825.

Bekefi, G. 1976. *Principles of Laser Plasmas*. New York: John Wiley & Sons, Inc.

Berkkan, A., and N. Ertas. 2004. Determination of Lead in Dialysis Concentrates using Flow Injection Hydride Generation Atomic Absorption Spectrometry. *Talanta*. 64 (2):423-427.

Berman, L. M., and P. J. Wolf. 1998. Laser-Induced Breakdown Spectroscopy of Liquids: Aqueous Solutions of Nickel and Chlorinated Hydrocarbons. *Applied Spectrosopy*. 52 (3):438-443.

Bogaerts, A., Z. Chen, and D. Bleiner. 2006. Laser Ablation of Copper in Different Background Gases: Comparative Study by Numerical Modeling and Experiments. *Journal of Analytical Atomic Spectrometry*. 21 (4):384-395.

Braman, R. S., C. C. Foreback, and L. L. Justen. 1972. Direct Volatilization Spectral Emission Type Detection System for Nanogram Amounts of Arsenic and Antimony. *Analytical Chemistry*. 44 (13):2195-2199.

Brindle, I. D., R. McLaughlin, and N. Tangtreamjitmun. 1998. Determination of Lead in Calcium Carbonate by Flow-Injection Hydride Generation with DC Plasma Atomic Emission Detection. *Spectrochimica Acta Part B: Atomic Spectroscopy*. 53 (6-8):1121-1129.

Broekaert, J. A. C., R. Pereiro, T. K. Starn, and G. M. Hieftje. 1993. A Gas-Sampling Glow-Discharge Coupled to Hydride Generation for the Atomic Spectrometric Determination of Arsenic. *Spectrochimica Acta Part B: Atomic Spectroscopy*. 48 (10):1207-1220.

Brysbaert, A., K. Melessanaki, and D. Anglos. 2006. Pigment Analysis in Bronze Age Aegean and Eastern Mediterranean Painted Plaster by Laser-Induced Breakdown Spectroscopy (LIBS). *Journal of Archaeological Science*. 33 (8):1095-1104.

Burakov, V. S., N. V. Tarasenko, M. I. Nedelko, V. A. Kononov, N. N. Vasilev, and S. N. Isakov. 2009. Analysis of Lead and Sulfur in Environmental Samples by Double Pulse Laser Induced Breakdown Spectroscopy. *Spectrochimica Acta Part B: Atomic Spectroscopy*. 64 (2):141-146.

Cáceres, J. O., J. Tornero López, H. H. Telle, and A. González Ureña. 2001. Quantitative Analysis of Trace Metal Ions in Ice using Laser-Induced Breakdown Spectroscopy. *Spectrochimica Acta Part B: Atomic Spectroscopy*. 56 (6):831-838.

Cahoon, E. M., and J. R. Almirall. 2012. Quantitative Analysis of Liquids from Aerosols and Microdrops Using Laser Induced Breakdown Spectroscopy. *Analytical Chemistry*. 84 (5):2239-2244.

Carranza, J. E., and D. W. Hahn. 2002. Sampling Statistics and Considerations for Single-Shot Analysis using Laser-Induced Breakdown Spectroscopy. *Spectrochimica Acta Part B: Atomic Spectroscopy*. 57 (4):779-790.

Carrion, N., M. Murillo, E. Montiel, and D. Diaz. 2003. Development of a Direct Hydride Generation Nebulizer for the Determination of Selenium by Inductively Coupled Plasma Optical Emission Spectrometry. *Spectrochimica Acta Part B: Atomic Spectroscopy*. 58 (8):1375-1389.

Cava-Montesinos, P., M. L. Cervera, A. Pastor, and M. de la Guardia. 2003. Hydride Generation Atomic Fluorescence Spectrometric Determination of Ultratraces of Selenium and Tellurium in Cow Milk. *Analytica Chimica Acta*. 481 (2):291-300.

Chari, S. 2008. *Hydride Generation and Laser Spectroscopy Techniques for Trace Analytical Measurements of Antimony and Selenium. MSc Thesis*, Youngstown State University, USA.

Chen, H. W., I. D. Brindle, and X. C. Le. 1992. Prereduction of Arsenic(V) to Arsenic(III), Enhancement of the Signal, and Reduction of Interferences by L-Cysteine in the Determination of Arsenic by Hydride Generation. *Analytical Chemistry*. 64 (6):667-672.

Chen, S. Y., Z. F. Zhang, H. M. Yu, W. Q. Liu, and M. Sun. 2002. Determination of Trace Lead by Hydride Generation-Inductively Coupled Plasma-Mass Spectrometry. *Analytica Chimica Acta*. 463 (2):177-188.

Chen, Z., H. Li, M. Liu, and R. Li. 2008. Fast and Sensitive Trace Metal Analysis in Aqueous Solutions by Laser-Induced Breakdown Spectroscopy using Wood Slice Substrates. *Spectrochimica Acta Part B: Atomic Spectroscopy*. 63 (1):64-68.

Cremers, D. A., M. J. Ferris, and M. Davies. 1996. Transportable Laser-Induced Breakdown Spectroscopy (LIBS) Instrument for Field-Based Soil Analysis. Paper read at SPIE's 1996 International Symposium on Optical Science, Engineering, and Instrumentation.

Cremers, D. A., and L. J. Radziemski. 1987. "Laser Plasma for Chemical Analysis." In *Laser Spectroscopy and Its Applications*, edited by L. J. Radziemski, R. W. Solarz and J. A Paisner. New York: Marcel Dekker, Inc.

Cremers, D. A., and L. J. Radziemski. 2006. *Handbook of Laser-Induced Breakdown Spectroscopy*. England: John Wiley & Sons, Inc.

Cremers, D. A., L. J. Radziemski, and T. R. Loree. 1984. Spectrochemical Analysis of Liquids Using the Laser Spark. *Applied Spectroscopy*. 38 (5):721-729.

Cristoforetti, G., S. Legnaioli, V. Palleschi, A. Salvetti, and E. Tognoni. 2004. Influence of Ambient Gas Pressure on Laser-Induced Breakdown Spectroscopy Technique in the Parallel Double-Pulse Configuration. *Spectrochimica Acta Part B: Atomic Spectroscopy*. 59 (12):1907-1917.

Cristoforetti, G., S. Legnaioli, V. Palleschi, A. Salvetti, and E. Tognoni. 2005. Characterization of a Collinear Double Pulse Laser-Induced Plasma at Several Ambient Gas Pressures by Spectrally-and Time-Resolved Imaging. *Applied Physics B*. 80 (4-5):559-568.

Cunat, J., F. J. Fortes, and J. J. Laserna. 2009. Real Time and in Situ Determination of Lead in Road Sediments using a Man-Portable Laser-Induced Breakdown Spectroscopy Analyzer. *Analytica Chimica Acta*. 633 (1):38-42.

D'Ulivo, A., S. S. T. Battistini, E. Pitzalis, R. Zamboni, Z. Mester, and R. E. Sturgeon. 2007. Effect of Additives on the Chemical vapour Generation of Bismuthane by Tetrahydroborate (III) Derivatization. *Analytical and Bioanalytical Chemistry*. 388 (4):783-791.

D'Ulivo, A., L. Lampugnani, G. Pellegrini, and R. Zamboni. 1995. Determination of Antimony by Continuous Hydride Generation Coupled with Nondispersive Atomic Fluorescence Detection. *Journal of Analytical Atomic Spectrometry*. 10 (11):969-974.

D'Ulivo, A., Z. Mester, J. Meija, and R. E. Sturgeon. 2006. Gas Chromatography–Mass Spectrometry Study of Hydrogen–Deuterium Exchange Reactions of Volatile Hydrides Of As, Sb, Bi, Ge And Sn on Aqueous Media. *Spectrochimica Acta Part B: Atomic Spectroscopy*. 61 (7):778-787.

D'Ulivo, A., M. Onor, R. Spiniello, and E. Pitzalis. 2008. Mechanisms Involved in Chemical Vapor Generation by Aqueous Tetrahydroborate (III) Derivatization: Role of Hexacyanoferrate (III) in Plumbane Generation. *Spectrochimica Acta Part B: Atomic Spectroscopy*. 63 (8):835-842.

De Giacomo, A., M. Dell'Aglio, and O. De Pascale. 2004. Single Pulse-Laser Induced Breakdown Spectroscopy in Aqueous Solution. *Applied Physics A-Materials Science & Processing*. 79 (4-6):1035-1038.

De Giacomo, A., M. Dell'Aglio, R. Gaudiuso, S. Amoruso, and O. De Pascale. 2012. Effects of the Background Environment on Formation, Evolution and Emission Spectra of Laser-Induced Plasmas. *Spectrochimica Acta Part B: Atomic Spectroscopy*. 78:1-19.

De Giacomo, A., M. Dell'Aglio, F. Colao, R. Fantoni, and V. Lazic. 2005. Double-pulse LIBS in Bulk Water and on Submerged Bronze Samples. *Applied Surface Science*. 247 (1):157-162.

De Lima, G. C., A. C. Do Lago, A. A. Chaves, P. S. Fadini, and P. O. Luccas. 2013. Determination of Selenium using Atomically Imprinted Polymer (AIP) and Hydride Generation Atomic Absorption Spectrometry. *Analytica Chimica Acta*. 768:35-40.

Dedina, J. 1982. Interference of Volatile Hydride-Forming Elements in Selenium Determination by Atomic Absorption Spectrometry with Hydride Generation. *Analytical Chemistry*. 54 (12):2097-2102.

Dedina, J., and D. L. Tsalev. 1995. *Hydride Generation Atomic Absorption Spectrometry*. Vol. 130. England: John Wiley & Sons.

Deng, F., R. Z. Dong, K. Yu, X. B. Luo, X. M. Tu, S. L. Luo, and L. X. Yang. 2013. Determination of Trace Total Inorganic Arsenic by Hydride Generation Atomic Fluorescence Spectrometry after Solid Phase Extraction-Preconcentration on Aluminium Hydroxide Gel. *Microchimica Acta*. 180 (5-6):509-515.

Díaz Pace, D. M., C. A. D'Angelo, D. Bertuccelli, and G. Bertuccelli. 2006. Analysis of Heavy Metals in Liquids using Laser Induced Breakdown Spectroscopy by Liquid-to-Solid Matrix Conversion. *Spectrochimica Acta Part B: Atomic Spectroscopy*. 61 (8):929-933.

Dockery, C. R., and S. R. Goode. 2003. Laser-Induced Breakdown Spectroscopy for the Detection of Gunshot Residues on the Hands of a shooter. *Applied Optics*. 42 (30):6153-6158.

Effenberger, A. J., and J. R. Scott. 2010. Effect of Atmospheric Conditions on LIBS Spectra. *Sensors*. 10 (5):4907-4925.

Ek, P., S. G. Hulden, and A. Ivaska. 1995. Sequential Injection-Analysis System for the Determination of Hydride-Forming Elements by Direct-Current Plasma-Atomic Emission-Spectrometry. *Journal of Analytical Atomic Spectrometry*. 10 (2):121-126.

El Sherbini, A. M., H. Hegazy, and Th. M. El Sherbini. 2006. Measurement of Electron Density utilizing the H alpha- Line from Laser Produced Plasma in Air. *Spectrochimica Acta Part B: Atomic Spectroscopy*. 61 (5):532-539.

Elci, L., Z. Arslan, and J. F. Tyson. 2009. Determination of Lead in Wine and Rum Samples by Flow Injection-Hydride Generation-Atomic Absorption Spectrometry. *Journal of Hazardous Materials*. 162 (2-3):880-885.

Erdem, N., and E. Henden. 2004. Inter-Element Interferences in the Determination of Arsenic and Antimony by Hydride Generation Atomic Absorption Spectrometry with a Quartz Tube Atomizer. *Analytica Chimica Acta*. 505 (1):59-65.

Essien, Marcelino, Leon J Radziemski, and Joseph Sneddon. 1988. Detection of Cadmium, Lead and Zinc in Aerosols by Laser-Induced Breakdown Spectrometry. *Journal of Anaytical Aomic Spectrometry*. 3 (7):985-988.

Etxebarria, N., R. Antolin, G. Borge, T. Posada, and J. C. Raposo. 2005. Optimisation of Flow-Injection-Hydride Generation Inductively Coupled Plasma Spectrometric Determination of Selenium in Electrolytic Manganese. *Talanta*. 65 (5):1209-1214.

Fantoni, R., L. Caneve, F. Colao, L. Fornarini, V. Lazic, and V. Spizzichino. 2006. "Laser Induced Breakdown Spectroscopy (LIBS) - The Process, applications to Artwork and Environment." In *Advances in Spectroscopy for Lasers and Sensing*, edited by B. DiBartolo and O. Forte, 229-254. Nethreland: Springer.

Farias, S., R. E. Rodriguez, A. Ledesma, D. A. Batistoni, and P. Smichowski. 2002. Assessment of Acid Media Effects on the Determination of Tin by Hydride Generation-Inductively Coupled Plasma Atomic Emission Spectrometry. *Microchemical Journal*. 73 (1-2):79-88.

Feng, X.J ., and B. Fu. 1998. Determination of Arsenic, Antimony, Selenium, Tellurium and Bismuth in Nickel Metal by Hydride Generation Atomic Fluorescence Spectrometry. *Analytica Chimica Acta*. 371 (1):109-113.

Feng, Y.-L., H. Narasaki, H.-Y. Chen, and L.-C. Tian. 1999. Speciation of Antimony (III) and Antimony (V) using Hydride Generation Inductively Coupled Plasma Atomic Emission Spectrometry Combined with the Rate of Pre-Reduction of Antimony. *Analytica Chimica Acta*. 386 (3):297-304.

Fichet, P., P. Mauchien, and C. Moulin. 1999. Determination of Impurities in Uranium and Plutonium Dioxides by Laser-Induced Breakdown Spectroscopy. *Applied Spectroscopy*. 53 (9):1111-1117.

Fichet, P., P. Mauchien, J. F. Wagner, and C. Moulin. 2001. Quantitative Elemental Determination in Water and Oil by Laser Induced Breakdown Spectroscopy. *Analytica Chimica Acta*. 429 (2):269-278.

Fisher, B. T., H. A. Johnsen, S. G. Buckley, and D. W. Hahn. 2001. Temporal Gating for the Optimization of Laser-Induced Breakdown Spectroscopy Detection and Analysis of Toxic Metals. *Applied Spectroscopy*. 55 (10):1312-1319.

Fornieles, A. C., A. G. de Torres, E. I. V. Alonso, and J. M. C. Pavon. 2013. Determination of Antimony, Bismuth and Tin in Natural Waters by Flow Injection Solid Phase Extraction Coupled with Online Hydride Generation Inductively Coupled Plasma Mass Spectrometry. *Journal of Analytical Atomic Spectrometry*. 28 (3):364-372.

Fortes, F. J., J. Moros, P. Lucena, L. M. Cabalin, and J. J. Laserna. 2013. Laser-Induced Breakdown Spectroscopy. *Analytical Chemistry*. 85 (2):640-669.

Garcia-Ayuso, L. E., J. Amador-Hernandez, J. M. Fernandez-Romero, and M. D. L. de Castro. 2002. Characterization of Jewellery Products by Laser-Induced Breakdown Spectroscopy. *Analytica Chimica Acta*. 457 (2):247-256.

Garrelie, F., C. Champeaux, and A. Catherinot. 1999. Expansion Dynamics of the Plasma Plume Created by Laser Ablation in a Background Gas. *Applied Physics A*. 69 (1):S55-S58.

Gaudiuso, R., M. Dell'Aglio, O. De Pascale, G. S. Senesi, and A. De Giacomo. 2010. Laser Induced Breakdown Spectroscopy for Elemental Analysis in Environmental, Cultural Heritage and Space Applications: A Review of Methods and Results. *Sensors*. 10 (8):7434-7468.

Giakoumaki, A., K. Melessanaki, and D. Anglos. 2007. Laser-Induced Breakdown Spectroscopy (LIBS) in Archaeological Science-Applications and Prospects. *Analytical and Bioanalytical Chemistry*. 387 (3):749-760.

Gottfried, J. L., F. C. De Lucia, C. A. Munson, and A. W. Miziolek. 2009. Laser-Induced Breakdown Spectroscopy for Detection of Explosives Residues: A Review of Recent Advances, Challenges, and Future Prospects. *Analytical and Bioanalytical Chemistry*. 395 (2):283-300.

Gottfried, J. L., F. C. De Lucia Jr., C. A. Munson, and A. W. Miziolek. 2007. Double-Pulse Standoff Laser-Induced Breakdown Spectroscopy for Versatile Hazardous Materials Detection. *Spectrochimica Acta Part B: Atomic Spectroscopy*. 62 (12):1405-1411.

Griem, H. R. 1964. *Plasma Spectroscopy*. New York: McGraw-Hill Book Company.

Griem, H. R. 1974. *Spectral Line Broadening by Plasmas*. New York: Academic Press Inc.

Groh, S., P. K. Diwakar, C. C. Garcia, A. Murtazin, D. W. Hahn, and K. Niemax. 2010. 100% Efficient Sub-Nanoliter Sample Introduction in Laser-Induced Breakdown Spectroscopy and Inductively Coupled Plasma Spectrometry: Implications for Ultralow Sample Volumes. *Analytical Chemistry*. 82 (6):2568-2573.

Gruber, J., J. Heitz, H. Strasser, D. Bäuerle, and N. Ramaseder. 2001. Rapid in-situ Analysis of Liquid Steel By Laser-Induced Breakdown Spectroscopy. *Spectrochimica Acta Part B: Atomic Spectroscopy*. 56 (6):685-693.

Hall, G. E. M., A. I. MacLaurin, J. C. Pelchat, and G. Gauthier. 1997. Comparison of the Techniques of Atomic Absorption Spectrometry and Inductively Coupled Plasma Mass Spectrometry in the Determination of Bi, Se and Te by Hydride Generation. *Chemical Geology*. 137 (1-2):79-89.

Harilal, S. S, B. OShay, Y. Tao, and M. S Tillack. 2006. Ambient Gas Effects on the Dynamics of Laser-Produced Tin Plume Expansion. *Journal of Applied Physics*. 99 (8):083303-083303-10.

Harilal, S. S., C. V. Bindhu, V. P. N. Nampoori, and C. P. G. Vallabhan. 1998. Influence of Ambient Gas on the Temperature and Density of Laser Produced Carbon Plasma. *Applied Physics Letters*. 72 (2):167-169.

Harmon, R. S., F. C. DeLucia, A. LaPointe, R. J. Winkel, and A. W. Miziolek. 2006. LIBS for Landmine Detection and Discrimination. *Analytical and Bioanalytical Chemistry*. 385 (6):1140-1148.

Henden, E., Y. Islek, M. Kavas, N. Aksuner, O. Yayayuruk, T. D. Ciftci, and R. Ilktac. 2011. A study of Mechanism of Nickel Interferences in Hydride Generation Atomic Absorption Spectrometric Determination of Arsenic and Antimony. *Spectrochimica Acta Part B: Atomic Spectroscopy*. 66 (11-12):793-798.

Henry, C. A., P. K. Diwakar, and D W Hahn. 2007. Investigation of helium Addition for Laser-Induced Plasma Spectroscopy of Pure Gas Phase Systems: Analyte Interactions and Signal Enhancement. *Spectrochimica Acta Part B: Atomic Spectroscopy*. 62 (12):1390-1398.

Ho, W. F., C.W. Ng, and N. H. Cheung. 1997. Spectrochemical Analysis of Liquids using Laser-Induced Plasma Emissions: Effects of Laser Wavelength. *Applied Spectroscopy*. 51 (1):87-91.

Holak, W. 1969. Gas-Sampling Technique for Arsenic Determination by Atomic Absorption Spectrophotometry. *Analytical Chemistry*. 41 (12):1712-1713.

Hosick, T. J., R. L. Ingamells, and S. D. Machemer. 2002. Determination of Tin In Soil by Continuous Hydride Generation and Inductively Coupled Plasma Mass Spectrometry. *Analytica Chimica Acta*. 456 (2):263-269.

Huang, J. S., and K. C. Lin. 2005. Laser-Induced Breakdown Spectroscopy of Liquid Droplets: Correlation Analysis with Plasma-Induced Current versus Continuum Background. *Journal of Analytical Atomic Spectrometry*. 20 (1):53-59.

Huang, J. S., H. T. Liu, and K. C. Lin. 2007. Laser-Induced Breakdown Spectroscopy in Analysis of Al^{3+} Liquid Droplets: On-Line Preconcentration by use of Flow-Injection Manifold. *Analytica Chimica Acta*. 581 (2):303-308.

Iida, Y. 1989. Atomic Emission Characteristics of Laser-Induced Plasmas in an Argon Atmosphere at Reduced Pressure. *Applied Spectroscopy*. 43 (2):229-234.

Iida, Y. 1990. Effects of Atmosphere on Laser Vaporization and Excitation Processes of Solid Samples. *Spectrochimica Acta Part B: Atomic Spectroscopy*. 45 (12):1353-1367.

Ingle, J. D., and S. R. Crouch. 1988. *Spectrochemical Analysis*. New Jersey, USA: Prentice Hall.

Jin, K., Y. Shibata, and M. Morita. 1991. Determination of Germanium Species by Hydride Generation Inductively Coupled Argon Plasma Mass-Spectrometry. *Analytical Chemistry*. 63 (10):986-989.

Kagawa, K., M. Ohtani, S. Yokoi, and S. Nakajima. 1984. Characteristics of the Plasma Induced by the Bombardment of N_2 Laser Pulse at Low Pressures. *Spectrochimica Acta Part B: Atomic Spectroscopy*. 39 (4):525-536.

Karadjova, I. B., L. Lampugnani, A. D'Ulivo, M. Onor, and D. L. Tsalev. 2007. Determination of Lead in Wine by Hydride Generation Atomic Fluorescence Spectrometry in the Presence of Hexacyanoferrate(III). *Analytical and Bioanalytical Chemistry*. 388 (4):801-807.

Karadjova, I. B., L. Lampugnani, M. Onor, A. D'Ulivo, and D. L. Tsalev. 2005. Continuous Flow Hydride Generation-Atomic Fluorescence Spectrometric Determination and Speciation of Arsenic in Wine. *Spectrochimica Acta Part B: Atomic Spectroscopy*. 60 (6):816-823.

Kasem, M. A., R. E. Russo, and M. A. Harith. 2011. Influence of Biological Degradation and Environmental Effects on the Interpretation of Archeological Bone Samples with Laser-Induced Breakdown Spectroscopy. *Journal of Analytical Atomic Spectrometry*. 26 (9):1733-1739.

Kilinc, E., and F. Aydin. 2012. Optimization of Continuous Flow Hydride Generation Inductively Coupled Plasma Optical Emission Spectrometry for Sensitivity Improvement of Bismuth. *Analytical Letters*. 45 (17):2623-2636.

Kim, D. E., K. J. Yoo, H. K. Park, K. J. Oh, and D. W. Kim. 1997. Quantitative Analysis of Aluminum Impurities in Zinc Alloy by Laser-Induced Breakdown Spectroscopy. *Applied Spectroscopy*. 51 (1):22-29.

Klein, S., J. Hildenhagen, K. Dickmann, T. Stratoudaki, and V. Zafiropulos. 2000. LIBS-spectroscopy for monitoring and control of the laser cleaning process of stone and medieval glass. *Journal of Cultural Heritage*. 1:S287-S292.

Knight, A. K., N. L. Scherbarth, D. A. Cremers, and M. J. Ferris. 2000. Characterization of Laser-Induced Breakdown Spectroscopy (LIBS) for Application to Space Exploration. *Applied Spectroscopy*. 54 (3):331-340.

Knopp, R., F. J. Scherbaum, and J. I. Kim. 1996. Laser Induced Breakdown Spectroscopy (LIBS) as an Analytical Tool for the Detection of Metal Ions in Aqueous Solutions. *Fresenius Journal of Analytical Chemistry*. 355 (1):16-20.

Koch, S., W. Garen, M. Muller, and W. Neu. 2004. Detection of Chromium in Liquids by Laser Induced Breakdown Spectroscopy (LIBS). *Applied Physics: Materials Science & Processing*. 79 (4-6):1071-1073.

Korkmaz, D. K., N. Ertas, and O. Y. Ataman. 2002. A Novel Silica Trap for Lead Determination by Hydride Generation Atomic Absorption Spectrometry. *Spectrochimica Acta Part B: Atomic Spectroscopy*. 57 (3):571-580.

Krachler, M., H. Emons, C. Barbante, G. Cozzi, P. Cescon, and W. Shotyk. 2002. Inter-Method Comparison for the Determination of Antimony and Arsenic in Peat Samples. *Analytica Chimica Acta*. 458 (2):387-396.

Kratzer, J., and J. Dedina. 2008. Stibine and Bismuthine Trapping in Quartz Tube Atomizers for Atomic Absorption Spectrometry - Method optimization and Analytical Applications. *Spectrochimica Acta Part B: Atomic Spectroscopy*. 63 (8):843-849.

Kratzer, J., B. Docekal, U. Heitmann, and J. Dedina. 2011. Spectral Interferences of Oxygen and Water Molecules in Hydride Generation Atomic Absorption Spectrometry with Quartz Atomizers: Comparison of Preconcentration and On-Line Atomization Modes for As and Se Determination. *Journal of Analytical Atomic Spectrometry*. 26 (11):2230-2237.

Kula, I., Y. Arslan, S. Bakirdere, and O. Y. Ataman. 2008. A Novel Analytical System Involving Hydride Generation and Gold-Coated W-Coil Trapping Atomic Absorption Spectrometry for Selenium Determination at ng l^{-1} Level. *Spectrochimica Acta Part B: Atomic Spectroscopy*. 63 (8):856-860.

Kumar, A. R., and P. Riyazuddin. 2010. Chemical Interferences in Hydride-Generation Atomic Spectrometry. *Trac-Trends in Analytical Chemistry*. 29 (2):166-176.

Kunati, S. R. 2008. *Trace Measurements of Tellurium, Tin and Other Metals by Atomic and Laser Spectroscopy Techniques. MSc Thesis*, Youngstown State University, USA.

Kurniawan, H, W. Setia Budi, M. M. Suliyanti, A. M. Marpaung, and K. Kagawa. 1997. Characteristics of a Laser Plasma Induced by Irradiation of a Normal-Oscillation Yag Laser at Low Pressures. *Journal of Physics D: Applied Physics*. 30 (24):3335.

Lajunen, L. H. J., and P. Perämäki. 2004. *Spectrochemical Analysis By Atomic Absorption And Emission*. 2nd Edition ed. Cambridge, UK: The Royal Society of Chemistry.

Lasue, J., R. C. Wiens, T. F. Stepinski, O. Forni, S. M. Clegg, S. Maurice, and Team ChemCam. 2011. Nonlinear Mapping Technique for Data Visualization and Clustering Assessment of LIBS Data: Application to Chemcam Data. *Analytical and Bioanalytical Chemistry*. 400 (10):3247-3260.

Le, X. C., X. F. Li, V. Lai, M. Ma, S. Yalcin, and J. Feldmann. 1998. Simultaneous Speciation of Selenium and Arsenic using Elevated Temperature Liquid Chromatography Separation with Inductively Coupled Plasma Mass Spectrometry Detection. *Spectrochimica Acta Part B: Atomic Spectroscopy*. 53 (6):899-909.

Lee, Y-Ill., K. Song, and J. Sneddon. 1997. "Laser Induced Plasmas for Analytical Atomic Spectroscopy." In *Lasers in Analytical Atomic Spectroscopy*, edited by J. Sneddon, T. L. Thiem and Y-Ill. Lee. New York: Wiley-VCH, Inc.

Li, J. X., F. Lu, T. Umemura, and K. Tsunoda. 2000. Determination of Lead by Hydride Generation Inductively Coupled Plasma Mass Spectrometry. *Analytica Chimica Acta*. 419 (1):65-72.

Li, Z.-X., and Y. Guo. 2005. Simultaneous Determination of Trace Arsenic, Antimony, Bismuth and Selenium in Biological Samples by Hydride Generation-Four-Channel Atomic Fluorescence Spectrometry. *Talanta*. 65 (5):1318-1325.

Lichte, F. E., and R. K. Skogerboe, 1972. Emission Spectrometric Determination of Arsenic. *Analytical Chemistry*. 44 (8):1480-1482.

Lindén, J., C. Knappe, M. Richter, and M. Aldén. 2012. Limitations of ICCD Detectors and Optimized 2D Phosphor Thermometry. *Measurement Science and Technology*. 23 (3):035201.

Masson, P., D. Orignac, and T. Prunet. 2005. Optimization of Selenium Determination in Plant Samples by Hydride Generation and Axial View Inductively Coupled Plasma Atomic Emission Spectrometry. *Analytica Chimica Acta*. 545 (1):79-84.

Mateo, M. P., V. Pinon, D. Anglos, and G. Nicolas. 2012. Effect of Ambient Conditions on Ultraviolet Femtosecond Pulse Laser Induced Breakdown Spectra. *Spectrochimica Acta Part B: Atomic Spectroscopy*. 74-75:18-23.

Matusiewicz, H., and M. Slachcinski. 2006. Simultaneous Determination of Hydride Forming and Hg in Sonicate Slurries of Biological and Elements (As, Sb, Se, Sn) Environmental Reference Materials by Hydride Generation Microwave Induced Plasma Optical Emission Spectrometry (SS-HG-MIP-OES). *Microchemical Journal*. 82 (1):78-85.

Michel, A. P. M. 2010. Review: Applications of Single-Shot Laser-Induced Breakdown Spectroscopy. *Spectrochimica Acta Part B: Atomic Spectroscopy*. 65 (3):185-191.

Miziolek, A. W., V. Palleschi, and I. Schechter. 2006. *Laser-Induced Breakdown Spectroscopy (LIBS) Fundemantels and Applications*. United Kingdom: Cambridge University Press.

Moreda-Pineiro, J., C. Moscoso-Perez, P. Lopez-Mahia, S. Muniategui-Lorenzo, E. Fernandez-Fernandez, and D. Prada-Rodriguez. 2001. Multivariate Optimisation of Hydride Generation Procedures for Single Element Determinations of As, Cd, Sb and Se in Natural Waters by Electrothermal Atomic Absorption Spectrometry. *Talanta*. 53 (4):871-883.

Mosier-Boss, P. A., and S. H. Lieberman. 2005. Detection of Lead Derived from Automotive Scrap Residue using a Direct Push Fiber-Optic Laser-Induced Breakdown Spectroscopy Metal Sensor. *Applied Spectroscopy*. 59 (12):1445-1456.

Musil, S., and J. Dedina. 2013. A sapphire Tube Atomizer for on-line Atomization and in situ Collection of Bismuthine for Atomic Absorption Spectrometry. *Journal of Analytical Atomic Spectrometry*. 28 (4):593-600.

Narsito, A. J., and S. J. Santosa. 1990. Study of Processes in the Hydride Generation Atomic-Absorption Spectrometry of Antimony, Arsenic and Selenium. *Analytica Chimica Acta*. 237 (1):189-199.

Ni, Z. M., and H. Bin. 1995. Determination of Germanium in Environmental-Samples by Electrothermal Atomic-Absorption Spectrometry with Continuous-Flow Hydride Generation in Dilute Perchloric-Acid Solution. *Journal of Analytical Atomic Spectrometry*. 10 (10):747-751.

Niedzielski, P., M. Siepak, and J. Siepak. 2002. Comparison of Modifiers for Determination of Arsenic, Antimony and Selenium by Atomic Absorption Spectrometry with Atomization in Graphite Tube or Hydride Generation and In-Situ Preconcentration in Graphite Tube. *Microchemical Journal*. 72 (2):137-145.

Novotny, P., and J. Kratzer. 2013. Hydride Generation - in-Atomizer Collection of Pb in a Quartz Trap-and-Atomizer Device for Atomic Absorption Spectrometry - an Interference Study. *Spectrochimica Acta Part B: Atomic Spectroscopy*. 79-80:77-81.

Orellana-Velado, N. G., M. Fernandez, R. Pereiro, and A. Sanz-Medel. 2001. Arsenic and Antimony Determination by On-Line Flow Hydride Generation-Glow Discharge-Optical Emission Detection. *Spectrochimica Acta Part B: Atomic Spectroscopy*. 56 (1):113-122.

Panne, U., R. E. Neuhauser, M. Theisen, H. Fink, and R. Niessner. 2001. Analysis of Heavy Metal Aerosols on Filters by Laser-Induced Plasma Spectroscopy. *Spectrochimica Acta Part B: Atomic Spectroscopy*. 56 (6):839-850.

Park, H. S., S. H. Nam, and S. M. Park. 2005. Time-Resolved Optical Emission Studies on the Laser Ablation of a Graphite Target: The Effects of Ambient Gases. *Journal of Applied Physics*. 97 (11).

Pereiro, R., M. Wu, J. A. C. Broekaert, and G. M. Hieftje. 1994. Direct Coupling of Continuous Hydride Generation with Microwave Plasma Torch Atomic-Emission Spectrometry for the Determination of Arsenic, Antimony and Tin. *Spectrochimica Acta Part B: Atomic Spectroscopy*. 49 (1):59-73.

Pohl, P. 2004. Hydride Generation - Recent Advances in Atomic Emission Spectrometry. *Trac-Trends in Analytical Chemistry*. 23 (2):87-101.

Pohl, P., and P. Jamroz. 2011. Recent Achievements in Chemical Hydride Generation Inductively Coupled and Microwave Induced Plasmas with Optical Emission Spectrometry Detection. *Journal of Analytical Atomic Spectrometry*. 26 (7):1317-1337.

Pohl, P., and W. Zyrnicki. 2002. Study of Chemical and Spectral Interferences in the Simultaneous Determination of As, Bi, Sb, Se And Sn By Hydride Generation Inductively Coupled Plasma Atomic Emission Spectrometry. *Analytica Chimica Acta*. 468 (1):71-79.

Pu, X. Y., and N. H. Cheung. 2003. ArF Laser Induced Plasma Spectroscopy of Lead Ions in Aqueous Solutions: Plume Reheating with a Second Nd: YAG Laser Pulse. *Applied Spectroscopy*. 57 (5):588-590.

Radziemski, L. J., T. R. Loree, D. A. Cremers, and N. M. Hoffman. 1983. Time-Resolved Laser-Induced Breakdown Spectrometry of Aerosols. *Analytical Chemistry*. 55 (8):1246-1252.

Rai, N. K., and A. K. Rai. 2008. LIBS—an Efficient Approach for the Determination of Cr in Industrial Wastewater. *Journal of Hazardous Materials*. 150 (3):835-838.

Reyes, M. N. M., M. L. Cervera, and M. de la Guardia. 2009. Determination of Total Sb, Se, Te, and Bi and Evaluation of their Inorganic Species in Garlic by Hydride-Generation-Atomic-Fluorescence Spectrometry. *Analytical and Bioanalytical Chemistry*. 394 (6):1557-1562.

Rifai, K., S. Laville, F. Vidal, M. Sabsabi, and M. Chaker. 2012. Quantitative Analysis of Metallic Traces in Water-Based Liquids by UV-IR Double-Pulse Laser-Induced Breakdown Spectroscopy. *Journal of Analytical Atomic Spectrometry*. 27 (2):276-283.

Robbins, W. B., J. A. Caruso, and F. L. Fricke. 1979. Determination of Germanium, Arsenic, Selenium, Tin and Antimony in Complex Samples By Hydride Generation - Microwave-Induced Plasma Atomic-Emission Spectrometry. *Analyst*. 104 (1234):35-40.

Rusak, D. A., B. C. Castle, B. W. Smith, and J. D. Winefordner. 1997. Fundamentals and Applications of Laser-Induced Breakdown Spectroscopy. *Critical Reviews in Analytical Chemistry*. 27 (4):257-290.

Salle, B., D. A. Cremers, S. Maurice, and R. C. Wiens. 2005. Laser-Induced Breakdown Spectroscopy for Space Exploration Applications: Influence of the Ambient Pressure on the Calibration Curves Prepared from Soil and Clay Samples. *Spectrochimica Acta Part B: Atomic Spectroscopy*. 60 (4):479-490.

Samek, O., D. C. S. Beddows, J. Kaiser, S. V. Kukhlevsky, M. Liska, H. H. Telle, and J. Young. 2000. Application of Laser-Induced Breakdown Spectroscopy to in Situ Analysis of Liquid Samples. *Optical Engineering*. 39 (8):2248-2262.

Sarkar, A., S. K Aggarwal, K. Sasibhusan, and D. Alamelu. 2010. Determination of sub-ppm Levels of Boron in Ground Water Samples by Laser Induced Breakdown Spectroscopy. *Microchimica Acta*. 168 (1-2):65-69.

Sasaki, Y., and K. Wagatsuma. 2009. Temporal Variations in the Excitation Temperature of a Laser-induced Argon Plasma Estimated with Copper Emission Lines. *Analytical Sciences*. 25 (4):481-485.

Senesi, G. S., M. Dell'Aglio, R. Gaudiuso, A. De Giacomo, C. Zaccone, O. De Pascale, T. M. Miano, and M. Capitelli. 2009. Heavy Metal Concentrations in Soils as Determined by Laser-Induced Breakdown Spectroscopy (LIBS), with Special Emphasis on Chromium. *Environmental Research*. 109 (4):413-420.

Simeonsson, J. B., and A. W. Miziolek. 1993. Time-Resolved Emission Studies of ArF-Laser-Produced Microplasmas. *Applied Optics*. 32 (6):939-947.

Simeonsson, J. B., and L. J. Williamson. 2011. Characterization of Laser Induced Breakdown Plasmas used for Measurements of Arsenic, Antimony and Selenium Hydrides. *Spectrochimica Acta Part B: Atomic Spectroscopy*. 66 (9):754-760.

Singh, J. P., and S. N. Thakur. 2007. *Laser-Induced Breakdown Spectroscopy*: Elsevier Science.

Singh, J. P., H. Zhang, F.-Y. Yueh, and K. P. Carney. 1996. Investigation of the Effects of Atmospheric Conditions on the Quantification of Metal Hydrides using Laser-Induced Breakdown Spectroscopy. *Applied Spectroscopy*. 50 (6):764-773.

Skoog, D. A., F. J. Holler, and S. R. Crouch. 2007. *Principles of Instrumental Analysis*. Canada: Thomson, Brooks/Cole.

Sneddon, J., and Y. I. Lee. 1999. Novel and Recent Applications of Elemental Determination by Laser-Induced Breakdown Spectrometry. *Analytical Letters*. 32 (11):2143-2162.

Song, K., Y. I. Lee, and J. Sneddon. 1997. Applications of Laser-Induced Breakdown Spectrometry. *Applied Spectroscopy Reviews*. 32 (3):183-235.

St-Onge, L., E. Kwong, M. Sabsabi, and E. B. Vadas. 2002. Quantitative Analysis of Pharmaceutical Products by Laser-Induced Breakdown Spectroscopy. *Spectrochimica Acta Part B: Atomic Spectroscopy*. 57 (7):1131-1140.

Taschuk, M. T., Y. Y. Tsui, and R. Fedosejevs. 2006. Detection and Mapping of Latent Fingerprints by Laser-Induced Breakdown Spectroscopy. *Applied Spectroscopy*. 60 (11):1322-1327.

Telle, H. H., A. G. Urena, and R. J. Donovan. 2007. *Laser Chemistry: Spectroscopy, Dynamics and Applications*. England: John Wiley & Sons Ltd.

Thompson, M., B. Pahlavanpour, and S. J. Walton. 1978. Simultaneous Determination of Trace Concentrations of Arsenic, Antimony, Bismuth, Selenium and Tellurium in Aqueous-Solution by Introduction of Gaseous Hydrides into an Inductively Coupled Plasma Source for Emission Spectrometry Part 1. Preliminary Studies. *Analyst*. 103 (1227):568-579.

Tsalev, D. L., P. B. Mandjukov, and D. L. Draganova. 1992. Optimization Study of Plumbane Generation and Preconcentration in Hydride Generation-Graphite Furnace Atomic-Absorption Spectrometry. *Spectroscopy Letters*. 25 (7):943-957.

Tyson, J. F., R. I. Ellis, G. Carnrick, and F. Fernandez. 2000. Flow Injection Hydride Generation Electrothermal Atomic Absorption Spectrometry with in-Atomizer Trapping for the Determination of Lead in Calcium Supplements. *Talanta*. 52 (3):403-410.

Vinas, P., I. López-García, B. Merino-Merono, N. Campillo, and M. Hernández-Córdoba. 2004. Liquid Chromatography-Hydride Generation-Atomic Absorption Spectrometry for the Speciation of Tin in Seafoods. *Journal of Environmental Monitoring*. 6 (4):262-266.

Werheit, P., C. Fricke-Begemann, M. Gesing, and R. Noll. 2011. Fast Single Piece Identification with a 3D Scanning LIBS for Aluminium Cast and Wrought Alloys Recycling. *Journal of Analytical Atomic Spectrometry*. 26 (11):2166-2174.

Weyl, G.M. 1989. *Physics of Laser-Induced Breakdown: An Update. In: Laser-Induced Plasmas and Applications*. New York: Marcel Dekker, Inc.

Yalçin, S., and X. C. Le. 1998. Low Pressure Chromatographic Separation of Inorganic Arsenic Species using Solid Phase Extraction Cartridges. *Talanta*. 47 (3):787-796.

Yalçin, Ş, D. R. Crosley, G. P. Smith, and G. W. Faris. 1999. Influence of Ambient Conditions on the Laser Air Spark. *Applied Physics B: Lasers and Optics*. 68 (1):121-130.

Yalçin, Ş., D. R. Crosley, G. P. Smith, and G. W. Faris. 1996. Spectroscopic Characterization of Laser-Produced Plasmas for in Situ Toxic Metal Monitoring. *Hazardous Waste and Hazardous Materials*. 13 (1):51-61.

Yaroshchyk, P., R. J. S. Morrison, D. Body, and B. L. Chadwick. 2005a. Quantitative Determination of Wear Metals in Engine Oils using Laser-Induced Breakdown Spectroscopy: A Comparison Between Liquid Jets and Static Liquids. *Spectrochimica Acta Part B: Atomic Spectroscopy*. 60 (7):986-992.

Yaroshchyk, P., R. J. S. Morrison, D. Body, and B. L. Chadwick. 2005b. Quantitative Determination of Wear Metals in Engine Oils using LIBS: The use of Paper Substrates and a Comparison Between Single-and Double-Pulse LIBS. *Spectrochimica Acta Part B: Atomic Spectroscopy*. 60 (11):1482-1485.

Yildirim, E., P. Akay, Y. Arslan, S. Bakirdere, and O. Y. Ataman. 2012. Tellurium Speciation Analysis using Hydride Generation in situ Trapping Electrothermal Atomic Absorption Spectrometry and Ruthenium or Palladium Modified Graphite Tubes. *Talanta*. 102:59-67.

Yilmaz, V., Z. Arslan, and L. Rose. 2013. Determination of Lead By Hydride Generation Inductively Coupled Plasma Mass Spectrometry (HG-ICP-MS): On-line Generation of Plumbane using Potassium Hexacyanomanganate(III). *Analytica Chimica Acta*. 761:18-26.

APPENDIX A

TIME RESOLUTION EXPERIMENTS FOR Sn UNDER NITROGEN ENVIRONMENT

Time resolution experiments was also performed for tin hydride plasma under nitrogen environment using 10.0 mg L^{-1} Sn (in 1.0% HCl) standard solution and 2.0% (w/v) $NaBH_4$ in 1.0% (w/v) NaOH. Stannane, SnH_4, plasma emission was collected with laser energy of 150 mJ at various delay time from 0.5 μs to 10.0 μs. For t_g measurements same procedure was applied by recording signal emission with respect to gate width between 0.05 ms – 3.0 ms.

Figure A1.(a) represents effect of delay time on neutral Sn signal at 284.0 nm. At early times of plasma, 0.5 μs, continuum emission dominates and at later times background emission decreases while the signal to background ratio increases.

Sn signal intensity with respect to detector gate time is provided in Figure A1.(b). As seen from figure signal increases as gate time increases. Optimum delay time and gate time were selected as 10 μs and 3 ms, respectively.
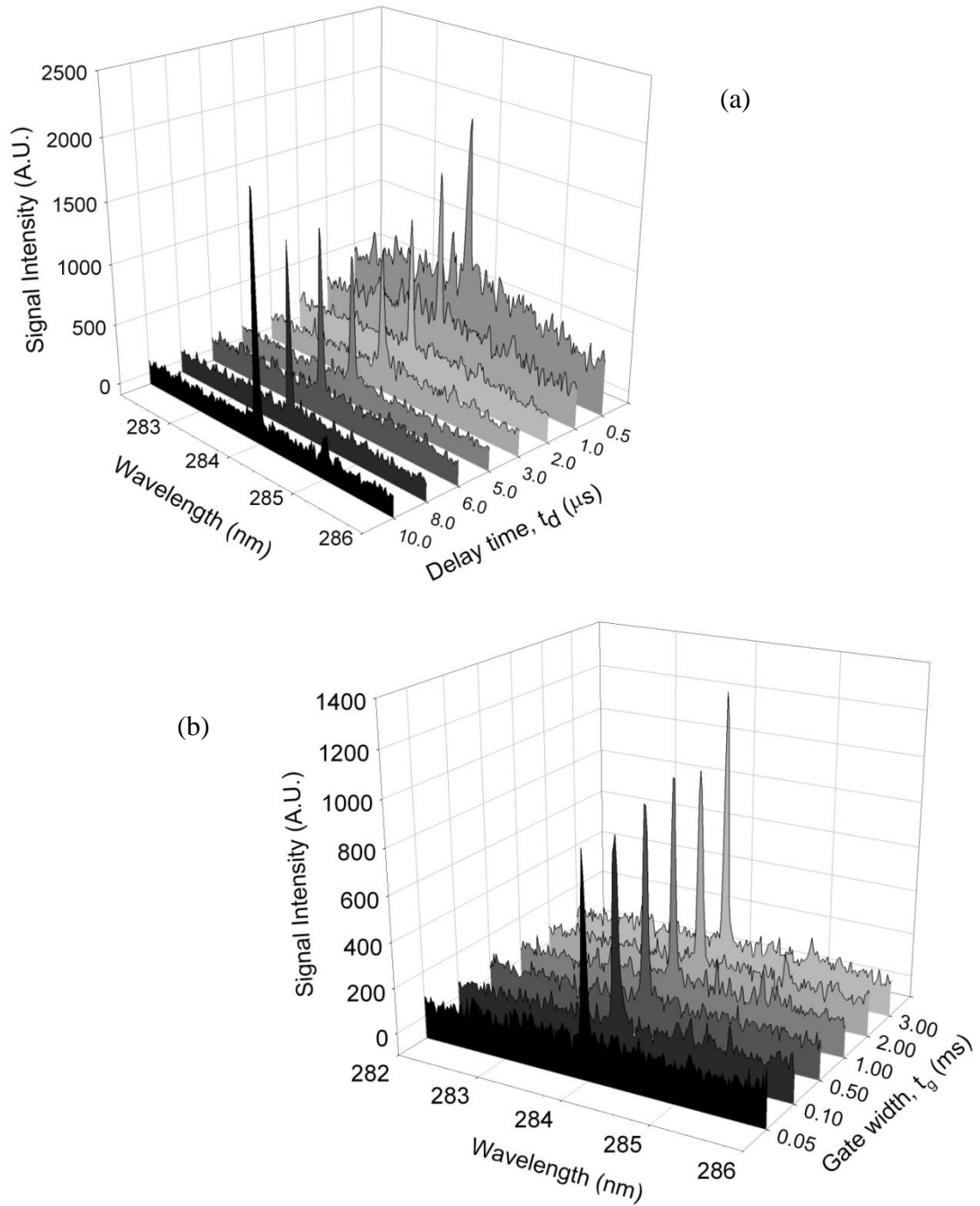
Figure A.1. Effect of (a) delay time and (t_g: 3.0 ms) (b) gate width (t_d: 10 µs) on Sn LIBS signal. (150 mJ pulse[-1], 10.0 mg L^{-1} Sn in 1.0% HCl, 2.0% (w/v) NaBH4 in 1.0% (w/v) NaOH and 155 mL min^{-1} carrier gas (N_2).

APPENDIX B

REPRESENTATIVE SPECTRA RECORDED FROM STANNANE PLASMA UNDER NITROGEN ENVIRONMENT

Figure B.1. Representative HG-LIBS spectrum recorded from SnH_4 plasma under argon environment. Spectrum recorded from 40.0 mg L^{-1} Sn under optimum experimental conditions.

APPENDIX C

SPECTROSCOPIC CONSTANTS THAT USED IN TEMPERATURE CALCULATIONS

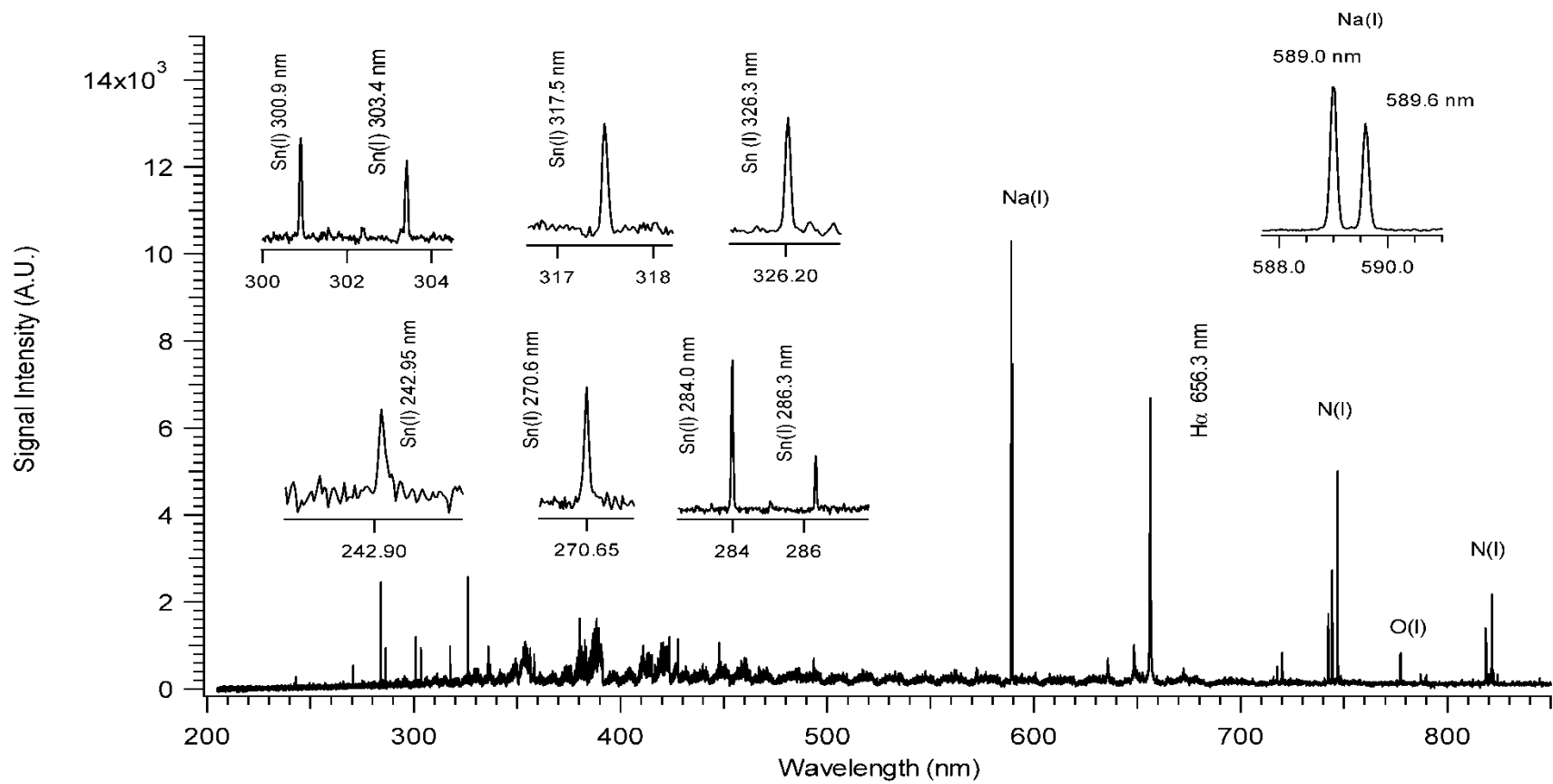Table C.1. Spectroscopic constants for Sn(I), Ar(I) and Ge(I) that used in temperature calculations (NIST database).

Element	Wavelength (nm)	E_i (cm^{-1})	E_k (cm^{-1})	g_k	A_{ki} (10^8 s^{-1})
Sn(I)	242.17	8612.955	49893.823	7	2.50
	242.95	3427.673	44576.006	7	1.50
	270.65	1691.806	38628.876	5	0.66
	283.99	3427.673	38628.876	5	1.70
	300.91	1691.806	34914.282	3	0.38
	303.41	1691.806	34640.758	1	2.00
	317.50	3427.673	34914.282	3	1.00
Ar(I)	696.54	93143.760	107496.4166	3	0.0639
	706.72	93143.7600	107289.7001	5	0.0380
	714.7	93143.7600	107131.7086	3	0.0063
	763.51	93143.7600	106237.5518	5	0.2450
	801.47	93143.7600	105617.2700	5	0.0928
	811.53	93143.7600	105462.7596	7	0.3310
	420.06	93143.7600	116942.7542	7	0.0097
	426.62	93750.5978	117183.5901	5	0.0031
	430.01	93750.5978	116999.3259	5	0.0057
Ge(I)	259.25	557.1341	39117.9021	5	0.60
	265.15	0.0000	37702.3054	5	1.6
	269.13	557.1341	37702.3054	3	0.47
	270.96	557.1341	37451.6893	1	2.08
	275.45	1409.9609	37702.3054	3	0.79
	303.91	7125.2989	40020.5604	3	2.04
	326.95	7125.2989	37702.3054	3	0.17

Semira ÜNAL YEŞİLLER

Date and Place of Birth: 01.03.1981, Hatay
Nationality: Turkish (TC)
E-mail: semireunal@yahoo.com

EDUCATION

[2007-2013]	**Ph.D.** (Faculty of Science, Department of Chemistry) **İzmir Institute of Technology** **Dissertation:** Design, construction and optimization studies of a hydride generation laser-induced breakdown spectrometric system, (HG-LIBS), for the determination of toxic elements in aqueous samples
[2004-2007]	**M.Sc.** (Faculty of Science, Department of Chemistry) **İzmir Institute of Technology** **Dissertation:** Preconcentration of rare earth elements (REEs) using silica gel modified with several functional groups
[2004-2005]	**Non-thesis M.Sc.** (Graduate School of Natural and Appl. Sci.) Department of Secondary School Sci. and Math. Education **Ege University** **Chemistry Teaching**
[1999-2003]	**B.Sc.** (Faculty of Science, Department of Chemistry), **Ege University**

ACADEMIC POSITIONS HELD

[2005-2013]	**Research Assistant** **İzmir Institute of Technology** Faculty of Science, Department of Chemistry, İzmir, Turkey **Assisted undergraduate courses:** General Chemistry, General Chemistry Laboratory I&II, Analytical Chemistry Laboratory I&II, Instrumental Analysis Laboratory

PUBLICATIONS

Ünal S., Yalçın Ş. (2010). "Development of a Continuous Flow Hydride Generation Laser-Induced Breakdown Spectroscopic System: Determination of Tin in Aqueous Environments" *Spectrochim. Acta B*, 65:750-757.

Karabelli D., Ünal S., Shahwan T., Eroğlu A.E. (2011). "Preparation and Characterization of Alumina-Supported Iron Nanoparticles and its Application for the Removal of Aqueous Cu^{2+} ions" *Chem. Eng. J.*, 168:979-984.

Aras N., Ünal Yeşiller S., Arıca Ateş D., Yalçın Ş. (2012). "Ultrasonic Nebulization-Sample Introduction System for Quantitative Analysis of Liquid Samples by Laser-Induced Breakdown Spectroscopy" *Spectrochim. Acta B*, 74-75:87-94.

Ünal Yeşiller S., Shahwan T., Eroğlu A.E. (2013). "Removal of Aqueous Rare Earth Elements (REEs) using Nano-iron Based Materials" *J. Ind. Eng. Chem.,* 19:898-907.

Ünal Yeşiller S., Yalçın Ş. (2013). "Optimization of Chemical and Instrumental parameters in Hydride Generation Laser-Induced Breakdown Spectrometry for the Determination of Arsenic, Antimony, Lead and Germanium in Aqueous Samples" *Anal. Chim. Acta*, 770:7-17.